

SR ISOTOPIC STUDY OF ULTRAMAFIC NODULES FROM NEOGENE ALKALINE
LAVAS OF BRITISH COLUMBIA, CANADA AND JOSEPHINE PERIDOTITE,
SOUTHWESTERN OREGON, U.S.A.

by

MIN } SUN

B. Sc. Peking University, 1982

A THESIS SUBMITTED IN PARTIAL FULFILMENT OF
THE REQUIREMENTS FOR THE DEGREE OF
MASTER OF SCIENCE

in

THE FACULTY OF GRADUATE STUDIES
Department of Geological Sciences

We accept this thesis as conforming
to the required standard

THE UNIVERSITY OF BRITISH COLUMBIA

August 1985

© Min Sun, 1985

In presenting this thesis in partial fulfilment of the requirements for an advanced degree at the The University of British Columbia, I agree that the Library shall make it freely available for reference and study. I further agree that permission for extensive copying of this thesis for scholarly purposes may be granted by the Head of my Department or by his or her representatives. It is understood that copying or publication of this thesis for financial gain shall not be allowed without my written permission.

Department of Geological Sciences

The University of British Columbia
2075 Wesbrook Place
Vancouver, Canada
V6T 1W5

Date: 29 August 1985

ABSTRACT

Twelve ultramafic nodules from Neogene alkaline lavas of British Columbia are Cr-diopside series peridotite. Nodules are depleted or undepleted with respect to Cr, Al, Ti and Na abundance per diopside or enstatite formula unit, and either Ti-metasomatised or unmetasomatised. Four samples from the Josephine Peridotite are even more depleted than the depleted nodules and lack Ti-metasomatism.

Pyroxene geothermobarometry (Mercier, 1980) was modified and used for clino- and ortho-pyroxene equilibrium temperature, pressure and depth calculations. Nodules came from a mantle depth of 30-50 km (936-1008°C, 9-15.5 kb). Josephine Peridotite came from a mantle depth of 30-65 km (1003-1042°C, 10-20 kb)

After establishing an average total Rb blank of 0.26 ng and Sr blank of 3.3 ng, Rb and Sr contents and Sr isotopic compositions of whole rock, acid-leached mineral separates (ol, cpx and opx) and acid leachate from the nodules, eleven host and associated whole rock basalts, and acid leached mineral separates (ol, cpx and opx) from the Josephine Peridotite have been analysed.

The host basalts have $^{87}\text{Sr}/^{86}\text{Sr}$ (0.70238-0.70289) similar to MORB, but very much higher Rb, Sr and $^{87}\text{Rb}/^{87}\text{Sr}$ ratios (12.7-62.1 ppm, 702-1514 ppm and 0.028-0.138, respectively). This is attributed to a low $^{87}\text{Sr}/^{86}\text{Sr}$ mantle with small degree of melting or melting after recent

metasomatism by a low $^{87}\text{Sr}/^{86}\text{Sr}$ fluid. Nodules occur only in ne normative alkali basalts and basanites.

Diopside is the main carrier of Rb and Sr (Rb = 0.125-3.47 ppm in nodules and 0.023-0.076 ppm in Josephine Peridotite, Sr = 9.3-239 ppm in nodules and 0.256-0.582 ppm in Josephine Peridotite), with low $^{87}\text{Sr}/^{86}\text{Sr}$ ratio (0.7022-0.7041 in nodules and 0.7054-0.7063 in Josephine Peridotite) and $^{87}\text{Rb}/^{86}\text{Sr}$ ratio (0.004-0.1 in nodules and 0.23-0.38 in Josephine Peridotite). Olivines contain the least Rb and Sr (Rb = 0.055-0.27 ppm in nodules and 0.084-0.102 ppm in Josephine Peridotite, Sr = 0.11-3.5 ppm in nodules and 0.153-0.305 ppm in Josephine Peridotite) and give the highest $^{87}\text{Sr}/^{86}\text{Sr}$ ratios (0.7036-0.7197 in nodules and 0.7089-0.7133 in Josephine Peridotite) and $^{87}\text{Rb}/^{86}\text{Sr}$ ratios (0.19-2.06 in nodules and 0.8-1.73 in Josephine Peridotite).

Nodules from Jacques Lake, depleted in Sr and undepleted in major elements, could be a MORB-source-type mantle. Other nodules represent somewhat less Sr-depleted mantle. Whole rock nodule data fall on or off the corresponding mineral isochrons. The latter phenomenon is due to relatively recent contamination with interstitial material having a high Rb/Sr ratio. "Synthetic" whole rocks, calculated from leached-mineral data, have higher $^{87}\text{Sr}/^{86}\text{Sr}$ ratios than host basalts. Together with the well defined mineral isochrons, this supports the conclusion that the nodules and host basalts are not cognate.

Equigranular nodules give a mid-Proterozoic mineral isochron date (1518-1537 Ma and $(^{87}\text{Sr}/^{86}\text{Sr})_0 = 0.70185$). Protogranular nodules give late Precambrian (645 Ma and $(^{87}\text{Sr}/^{86}\text{Sr})_0 = 0.7037$. early-mid Paleozoic (276-576 Ma and $(^{87}\text{Sr}/^{86}\text{Sr})_0 = 0.7024-0.7032$) and Mesozoic (104 Ma and $(^{87}\text{Sr}/^{86}\text{Sr})_0 = 0.7029$) isochron dates. Porphyroclastic nodules do not define reliable mineral isochrons, but also show evidence of old age (at least 560-790 Ma and $(^{87}\text{Sr}/^{86}\text{Sr})_0 = 0.7028-0.7030$).

Depleted Josephine Peridotite gives middle Paleozoic mineral isochron dates (366-441 Ma and $(^{87}\text{Sr}/^{86}\text{Sr})_0 = 0.7038-0.7041$), in conflict with the general view that the Josephine Peridotite was generated in Late Jurassic time. This implies that the ophiolite base does not necessarily have the same age as overlying volcanic rocks and dykes.

Table of Contents

ABSTRACT.....	ii
LIST OF FIGURES.....	vii
LIST OF TABLES.....	viii
ACKNOWLEDGEMENTS.....	ix
I. INTRODUCTION	1
General Statement.....	1
Ultramafic Nodules.....	2
Alpine Orogenic and Ophiolite Peridotite.....	9
II. GENERAL GEOLOGY.....	12
II-1. Ultramafic Nodules in British Columbia.....	12
Geological and Tectonic Setting.....	12
Previous Work.....	15
Samples Studied.....	20
(1). Jacques Lake.....	20
(2). Big Timothy Mountain.....	21
(3). Kettle River.....	24
(4). Lassie Lake.....	26
II-2. Josephine Peridotite of Southern Oregon.....	27
III. CHEMICAL MINERALOGY.....	30
Olivine.....	32
Clinopyroxene and Orthopyroxene.....	32
Spinel.....	39
Pressure and Temperature Estimates.....	39
IV. RB-SR ISOTOPE ANALYTICAL METHOD.....	46
IV-1. Sample Preparation.....	46
(1). Nodules.....	46
(2). Josephine Peridotite.....	47
IV-2. Chemical Procedures.....	48
(1). Laminar Flow Hood.....	48
(2). Reagents.....	49
(3). Rb and Sr Spikes.....	52
(4). Sample Dissolution.....	53
(5). Chemical Separation.....	54
(6). Mass Spectrometry.....	57
(7). Blanks.....	60
(8). Data reduction.....	65
(9). N.B.S. Standard SRM987 Measurements.....	67
(10). Isochron Calculation and Plot.....	67
V. Rb-Sr ISOTOPE RESULTS.....	69
V-1. Nodules and Host Basalts.....	69
V-2. Josephine Peridotite.....	70
VI. DISCUSSION.....	90
General Considerations.....	90
Basalts.....	91

Ultramafic Nodules.....	93
(1). Jacques Lake.....	94
(2). Big Timothy Mountain.....	95
(3). Kettle River.....	95
(4). Lassie Lake.....	97
Josephine Peridotite.....	98
Mantle Growth Curve.....	99
Summary.....	100
REFERENCES.....	102
APPENDIX 1. PROBE ANALYTICAL DATA OF NODULE MINERALS.....	116
APPENDIX 2. Fe ⁺⁺ and Fe ⁺⁺⁺ IN SPINEL CALCULATION.....	119
APPENDIX 3. PROBE ANALYTICAL DATA FOR JOSEPHINE PERIDOTITE PYROXENES.....	120
APPENDIX 4. CALCULATED TEMPERATURE, PRESSURE, DEPTH FROM J.V.ROSS.....	121
APPENDIX 5. PROGRAM "RBSR".....	122
APPENDIX 6. (a) PROGRAM "YORK".....	127
(b) PROGRAM "PLRBSR".....	131
APPENDIX 7. DUPLICATED RB-SR DATA.....	133

LIST OF FIGURES

Figure.....	Page
2-1. Location map of the Juan de Fuca Plate System.....	13
2-2. Crustal Structure of the southern Canadian Cordillera.....	14
2-3. Localities of ultramafic nodules in British Columbia.....	16
2-4. Sample classification based on modal mineralogy.....	22
2-5. Composition of clinopyroxene and orthopyroxene in ultramafic nodules from British Columbia.....	23
2-6. Generalized tectonic sketch map of the Josephine Peridotite.....	28
3-1. Ti-Cr plots of diopsides and enstatites.....	34
3-2. (a) $Cr/(Cr+Al) \times 100$ vs. Al plot of enstatites.....	36
(b) $Cr/(Cr+Al) \times 100$ vs. Al plot of diopsides.....	37
3-3. $Cr/(Cr+Al) \times 100$ vs. $Mg/(Mg+Fe) \times 100$ plot of diopsides and enstatites.....	38
3-4. (a) $Mg/(Mg+Fe) \times 100$ vs. Cr/Ti plot of enstatites.....	40
(b) $Mg/(Mg+Fe) \times 100$ vs. Cr/Ti plot of diopsides.....	41
3-5. $Mg/(Mg+Fe^{++}) \times 100$ vs. $Cr/(Cr+Al) \times 100$ plot of spinels.	42
4-1. Elution curves for Mg, Rb, Ca, Sr and Sm on large column.....	56
4-2. Elution curves for Rb, Ca and Sr on small columns...	58
4-3. (a) Total Rb blanks.....	63
(b) Total Sr blanks.....	64
5-1. JL1 mineral isochron.....	75
5-2. JL14 mineral isochron.....	76
5-3. JL15 mineral isochron.....	77
5-4. JL18 mineral isochron.....	78
5-5. BM11 mineral isochron.....	79
5-6. BM16 mineral isochron.....	80
5-7. BM55 mineral isochron.....	81
5-8. KR1 mineral isochron.....	82
5-9. KR2 mineral isochron.....	83
5-10. KR35 mineral isochron..	84
5-11. LL1 mineral isochron..	85
5-12. LL14 mineral isochron	86
5-13. JM5 mineral isochron.....	87
5-14. JM14 mineral isochron.....	88
5-15. JM15 mineral isochron.....	89
6-1. Earth evolution curves.....	101

LIST OF TABLES

Table.....	Page
2-1. Visual estimated modal mineralogy of the samples.....	22
2-2. Chemical compositions of the host and associated basalts.....	25
2-3. Concentrations of trace elements in host and associated basalts.....	26
3-1. Nodule mineral compositions.....	31
3-2. Josephine Peridotite pyroxene compositions.....	33
3-3. Comparison of pyroxenes of depleted and undepleted nodules and Josephine Peridotite.....	33
3-4. Calculated T, P, Depth.....	44
4-1. Reagent Blanks.....	51
4-2. Isotopic composition of N.B.S. Sr spike SRM-988.....	53
4-3. Total blanks.....	62
4-4. Comparison of total blanks with other labs.....	65
4-5. $^{87}\text{Sr}/^{86}\text{Sr}$ ratios of N.B.S. SRM-987.....	68
5-1. Rb-Sr data of host basalts.....	71
5-2. Rb-Sr isotope data of Jacques Lake nodules.....	71
5-3. Rb-Sr isotope data of Big Timothy Mountain.....	72
5-4. Rb-Sr isotope data of West Kettle River.....	72
5-5. Rb-Sr isotope data of Lassie Lake.....	73
5-6. Rb-Sr isotope data of Josephine Peridotite.....	73
5-7. Summary of mineral isochrons.....	74

Acknowledgements

I wish to express sincere appreciation to Dr. Richard Lee Armstrong, thesis supervisor, for his support, supervision, advice and encouragement throughout the study.

Many samples were obtained through the courtesy of Dr. J.V. Ross. Thanks are also due him for valuable discussion.

I would also like to thank K. Scott, S. Horsky, J. Knight and Dr. J. Rice, for assistance and guidance in the laboratory.

I am also grateful for help and discussions with Dr. R.L. Chase, Dr. P. Michael, Dr. J. Mortenson, Prof. R.G. Sun and other faculty members and students.

Finally, the inspiration from Institute of Geology, Academia Sinica, notably Prof. Molan E, Prof. Xinhua Zhou, Yang Yu and Juanjuan Xia, is also acknowledged.

Financial support was provided by a Canadian Natural Sciences and Engineering Research Council Operating Grant (67-8841) to R. L. Armstrong.

I. INTRODUCTION

This thesis examines Rb and Sr concentrations and Sr isotope composition of spinel peridotite from two different settings: nodules from Neogene alkali basalts of British Columbia and samples from the Mesozoic alpine ophiolitic Josephine Peridotite, southwestern Oregon.

General statement

Plate tectonics theory divides the lithosphere of the earth into several plates that overlie and move over the asthenosphere. Understanding plate tectonics and the earth's evolution depends to large degree on our knowledge of mantle chemistry, physical properties, history, and current temperature, pressure, and velocity structure. Present knowledge is based on geophysical data, the results of experiments on inferred mantle compositions under high temperature and high pressure (e.g. Kennedy and Ito, 1972; Ringwood, 1975), studies of lunar and meteoritic samples (e.g. Macdonald, 1959; Ringwood, 1962, 1975; Larimer, 1971; Gast, 1972), petrological, geochemical, isotopic, and experimental studies on basalts, and petrological, structural, geochemical, isotopic and experimental studies on natural mantle samples (alpine peridotite and ophiolite, nodules in kimberlite pipes, and nodules in alkali basalts).

These studies reveal that the mantle is typically a lherzolite (ol-opx-cpx±plagioclase, spinel, or garnet)

(Ringwood, 1975).

Ultramafic nodules

Early studies of ultramafic nodules from kimberlites led to the conclusion that they come from the mantle (Wagner, 1928). Early work on nodules in alkali basalts is reviewed by Ross et al. (1954), Forbes and Kuno (1965, 1967), Wyllie (1967) and Kuno (1969). Since the introduction of plate tectonics in the 1960's, numerous papers on nodules have been published. The study fields are diverse - including petrology and thermodynamics (e.g. Boyd, 1973; MacGregor, 1974; Wood, 1975; Mercier, 1976, 1980); rheology (e.g. Ross, 1983); trace elements (e.g. Griffin and Murthy, 1968; Basu and Murthy, 1977; Basu, 1978; Jagoutz et al., 1979) and Sr, Nd and Pb isotope geochemistry (e.g. Paul, 1971; Stueber and Ikramuddin, 1974; Burwell, 1975; O'Nions et al., 1977; Kramers, 1977; Menzies and Murthy, 1980; Stosch et al., 1980; Jagoutz et al., 1980; Cohen et al., 1984; Mengel et al., 1984; Betton and Givetta, 1984; Bielski-Zyskind et al., 1984). The ultramafic nodules in kimberlite pipes are mainly garnet lherzolite and eclogite and those in alkali basalts are dominantly spinel lherzolite (Ringwood, 1975).

The nodules of alkali basalts

Spinel lherzolite nodules have a simple mineralogy of olivine, orthopyroxene, clinopyroxene and spinel. Some workers are in favour of a cognate relationship of the

nodules with their host rock (e.g. O'Hara, 1967, 1968), i.e. they are cumulates from the ascending magma. Many others (Ross et al., 1954; Wilshire and Binns, 1961; Harris et al., 1967) agree that the nodules are samples of the mantle, accidentally caught up in the ascending basaltic magma. Partial melting of spinel lherzolite in the mantle may produce a silica undersaturated basalt and leave a more magnesian lherzolite, harzburgite or dunite as residue (Kushiro, 1969). Differences in the chemistry of lherzolite nodules may be due to original heterogeneity as well as different degrees or conditions of partial melting. Both cognate and accidental ultramafic nodules may coexist at the same locality.

Ross et al. (1954) emphasized the uniformity in mineralogy and chemistry of ultramafic nodules and suggested that these nodules were derived from a uniform mantle. Work by White (1966), Jackson (1968) and Kuno (1969) has shown that there are two main types of nodules in alkali basalt, a lherzolite series and a dunite - wehrlite - pyroxenite series, accompanied by a minority of eclogite and gabbro nodules. The second series was also named as black clinopyroxene type, black type, pyroxene suite and other less descriptive names (Wilshire and Shervais, 1975). The dunite - wehrlite - pyroxenite and gabbro suites are thought to be of cumulate origin and the spinel lherzolite suites and eclogite are thought to be mantle fragments (White, 1966).

From mineral chemistry, two sorts of ultramafic nodules, Al-augite and Cr-diopside, were distinguished. The Al-augite group is characterized by Al and Ti-rich augite, comparatively Fe-rich olivine and orthopyroxene, and Al-rich spinel, dominated by augite-rich varieties. The Cr-diopside group is characterized by Cr-rich clinopyroxene and spinel and by Mg-rich olivine and orthopyroxene, dominated by olivine - rich lherzolites (Wilshire and Shervais, 1975). The Al-augite group was ascribed by most workers to a cumulus process. Nevertheless metamorphic textures of olivine-rich members of this group were recognized by Jackson (1968), Trask (1969) and Fuster et al. (1970). These dunites were considered to be residues of partial melt that produced tholeiitic lavas (Jackson and Wright, 1970) or interpreted as Cr-diopside peridotite modified by partial melting and reaction (Wilshire and Shervais, 1975). On the other hand, the Cr-diopside group was considered by most workers to represent mantle material from which variable amounts of basaltic liquid have been removed. Within the Cr-diopside group, less deformed pyroxene-rich members are thought to represent segregation of melts like those of the Al-augite group.

From structural-fabric studies, three important textural groups have been recognized (Mercier and Nicolas, 1975):

(a). Protogranular: characterized by a coarse grain size (5-10 mm), with the curvilinear boundaries between the

principal minerals, olivine and orthopyroxene. The crystals have almost no elongation and the nodules seem to be devoid of any foliation or lineation. The diopside and spinel are much smaller (1mm) and the relationships between them are such that both minerals are always in direct contact with large enstatite grains. This texture is believed to represent minor modification of original magmatic texture by partial melting. The symplectitic spinel results from exsolution of more aluminous pyroxene. This could take place by the lowering of pressure during the upward migration of peridotite through the garnet/spinel facies boundary (Green, 1976). The nodules with this texture are interpreted as coming from a static part of the mantle (Ross, 1983).

(b). Porphyroclastic: characterized by large and elongated strained porphyroclasts of and small generally polygonal strain-free neoblasts of olivine and orthopyroxene. Hand specimens are marked by a foliation outlined by olivine and enstatite together with a spinel lineation. This texture is interpreted as characteristic of deformed mantle. (Ross, 1983).

(c). Equigranular: characterized by all the phases having almost the same shape and small size (1-2mm). The grain boundaries are typically straight and converge at 120° in triple points. This texture results from high temperature recrystallization and is interpreted to have formed in mantle levels that are both deformed and exceptionally hot. (Ross, 1983).

Since the 1970's, many studies of trace and rare earth elements and of Sr, Pb and Nd isotopes have been carried out on the ultramafic nodules. The work confirms that most Al-augite wehrlitic nodules represent cumulates, mostly cognate (a few represent accidentally acquired cumulates from an earlier magmatic event) and that most Cr-diopside lherzolite nodules are fragments of the upper mantle.

The lherzolite nodule whole-rock is generally not in equilibrium with the host basalt and the $^{87}\text{Sr}/^{86}\text{Sr}$ ratios are generally neither correlated with Sr concentrations nor with Rb/Sr ratios (e.g. Paul, 1971; Burwell, 1975; Mengel et al., 1984). The acid leach material has proven to be enriched in Rb and Sr and not in equilibrium with the nodule. (e.g. Griffin and Murthy, 1968; Basu and Murthy, 1977).

Acid washed mineral separates, clinopyroxene, orthopyroxene and olivine, have been analysed by several authors. The minerals are not in equilibrium with the host basalt and some mineral isochrons have been obtained. For example, Stueber et al. (1974) derived a mineral isochron, from Mt. Aldaz, Antarctica, giving a date of 610 ± 110 Ma with $(^{87}\text{Sr}/^{86}\text{Sr})_0 = 0.7020 \pm 0.0002$ and one from Kilbourne Hole, New Mexico, giving a date of 1270 ± 230 Ma with $(^{87}\text{Sr}/^{86}\text{Sr})_0 = 0.7024 \pm 0.0002$. In those cases the isochron ages are similar to the age of the underlying crustal basement and are consistent with the idea that continental lithosphere is being sampled. Basu and Murthy (1977) derived

a mineral isochron, from Baja California, giving a date of 3400 ± 300 Ma with $(^{87}\text{Sr}/^{86}\text{Sr})_0 = 0.70057 \pm 0.00004$, which is much older than any nearby crustal rocks. It is also reported some mineral separates do not define an isochron (e.g. Stuber et al., 1974; Polvé and Allègre, 1980).

The distinction between "depleted" and "undepleted" mantle is an important achievement in studies of the mantle. Incompatible elements will be enriched in the melts and depleted in the residues of partial melting. The "undepleted mantle" is the mantle that geochemically consistent with the Sm-Nd evolution of chondritic meteorites, and close to presumed "bulk earth" chemical and isotope composition for Rb-Sr and U-Pb and close to chondritic in many nonvolatile trace element abundances and ratios. The "depleted mantle" has relatively low concentrations of incompatible elements, compared to the "bulk earth".

Different elements have been selected as depletion/enrichment indicators by different authors. Ross (1983) adopted the Mercier (1976) chemical depletion criteria (evident on a Cr vs. Ti plot). Many authors use rare earth elements or isotopic ratios, i.e. undepleted mantle has undepleted rare earth pattern, $\epsilon_{\text{Nd}} \approx 0$ and $\epsilon_{\text{Sr}} \approx 0$ (i.e. $^{143}\text{Nd}/^{144}\text{Nd} = 0.51187$ and $^{87}\text{Sr}/^{86}\text{Sr} = 0.7045$, today, respectively). The depleted mantle has low concentration of LREE, $\epsilon_{\text{Nd}} \approx +10$ (Jacobson et al., 1984) and low $^{87}\text{Sr}/^{86}\text{Sr}$ (<0.7030).

A few spinel lherzolite nodules have undepleted character (e.g. "primitive nodules" of Jagoutz, 1979). Most lherzolite nodules have a depleted character.

The mantle depletion process is interpreted to occur by continuous or episodic accretion of the continental lithosphere (Allègre et al., 1982), or in terms of a multiple stage extraction of melt fraction (Jacobsen et al., 1984).

The "undepleted mantle" can be interpreted as resulting from an incompatible-element enrichment in the mantle after the previous separation of the crust and mantle, or as a "primitive/primordial" mantle.

The "enriched" mantle is interpreted to be a result of metasomatism in the mantle. The metasomatic fluid, enriched in incompatible elements, may be derived from subducted crust (e.g. Armstrong, 1968, 1981; Chase, 1981; Hofmann and White, 1982; Zindler et al., 1982; White and Hofmann, 1982; White and Patchett, 1984), or from a lower mantle plume source (e.g. Lupton, 1983; Vollmer, 1983).

The "primitive mantle" concept is supported by studies of isotopes of inert gases (e.g. Allègre et al., 1983; Lupton, 1983). Only the Hawaiian basalts simultaneously meet the Sr, Pb and Nd isotope and inert gas criteria for a "primitive" source (White, 1985). He, among the least reactive of gases and present only in trace quantities in air, is the most important indicator of a primitive source. Continental rocks are depleted in ^3He , but MORB glasses have

excess ^3He . No mechanism has been found that could produce the non-radiogenic $^3\text{He}/^4\text{He}$ ratios found in the earth's mantle. The detection of excess ^3He in the MORB samples can only be interpreted as evidence for the existence of "primitive" mantle He. In many cases its transfer to the surface may be uncoupled with the fluxes of other elements (White, 1985).

Alpine orogenic and ophiolite peridotite

The tectonic significance of alpine orogenic peridotite and ophiolite was recognized by Steinmann (1926 and 1927) in the European Alps. Alpine peridotites characteristically intruded close to the axes of maximum deformation along orogenic belts and island arcs. Intrusion has frequently been controlled by major faults with strike lengths up to several hundred miles, which almost certainly extend into the mantle. Steinmann (1927) originally proposed that peridotites represented ultramafic cumulates from submarine lava. Hess (1938) suggested that the alpine peridotites were the result of the direct injection of a primary ultramafic magma but such hypotheses are given little credence today. Based on the persistent association of alpine peridotites with orogenic andesite, it was also proposed that the peridotites represent the cumulate or residual portion of andesitic magmas brought to the surface by faulting (Hess, 1955; Osborn, 1969; Challis, 1969; Miyashiro, 1973).

Ophiolites consist of basal ultramafic layers from several hundred meters to several kilometers thick overlain by gabbroic and doleritic rocks which in turn grade upward into mafic pillow lavas and breccias, frequently associated with radiolarian cherts.

Hess emphasized the distinctions between alpine peridotites and ophiolites (Ringwood, 1975), but the trend of more recent and detailed studies has been to underline their affinities. Alpine peridotites are now regarded as nothing more than the basal zones of ophiolite complexes.

Impressed by the similarity of the ophiolitic sequence to the hypothetical vertical section of the ocean floor, many investigators proposed that ophiolites represent fragments of the ancient oceanic lithosphere (i.e. Davies, 1968 and 1971; Coleman, 1971). Some workers considered the peridotites to be formed by crystal setting from a basaltic magma during the formation of oceanic crust (Thayer, 1964, 1967, 1969; McTaggart, 1971). Others suggested the peridotites represent residual mantle material (e.g. Hess, 1964; Dickey, 1970). Alpine peridotites and ophiolites are in part tectonites, foliated and deformed at high temperature, but surrounding rocks are often of very low metamorphic grade. The basal ultramafic rocks are similar in petrology, mineralogy and structural features to nodules in alkali basalts.

Mainly because of the highly altered nature of the Alpine peridotites, there are fewer geochemical and isotopic

studies on them than on ultramafic nodules. However, study of a well-preserved Alpine peridotite has the advantage over nodules in that field relations between the various lithologies can be preserved, and this may aid in interpreting their origin.

All recent studies support the hypothesis that alpine - ophiolitic peridotites are fragments of the upper mantle (e.g. Polvé and Allègre, 1980). Geochemical and isotopic studies reveal that some are suitable to be depleted suboceanic mantle (e.g. Menzies and Murthy, 1978), they have the same ϵNd - ϵSr correlation line as oceanic basalts (Richard and Allègre, 1980). Many cannot be explained by simple single stage models of partial melting and (or) contamination. Thus the idea that the oceanic mantle is progressively more and more depleted and that it is mixed and recycled was proposed (Polvé and Allègre, 1980). Jacobson et al. (1984) postulated a multiple partial melting history for Trinity peridotite.

II. GENERAL GEOLOGY

II-1 Ultramafic nodules in British Columbia

Geological and tectonic setting

An important feature of the present tectonic situation off the west coast of Canada is the ridge - trench -transform triple junction between the Juan de Fuca, Pacific, and American lithospheric plates near the continental margin at approximately 51°N (Figure 2-1).

The Juan de Fuca plate is one of the last remnants of the Farallon plate, which converged with the western margin of North America over the last 150 million years. The collision of the Pacific - Farallon ridge with the American plate between 25 and 30 million years ago (Ma) led to the isolation of the Juan de Fuca plate at about 20 Ma. Since then its southern edge has migrated northward and there has been a reduction in spreading rate and clockwise ridge and plate rotation. For the period from 7 to 4 Ma, motion of Juan de Fuca plate relative to the America plate was to the northeast at about 6.0 cm/yr. Between 4 and 3 Ma, the Explorer plate broke off from Juan de Fuca plate and was overridden by the American plate. The Juan de Fuca plate continues to subduct to the northeast at about 4 cm/yr (Riddihough, 1984). The Juan de Fuca plate Benioff zone dips 15° eastward under Vancouver Island (Rodgers, 1983). Depth to Moho and to the low velocity zone are shown in Figure 2-2.

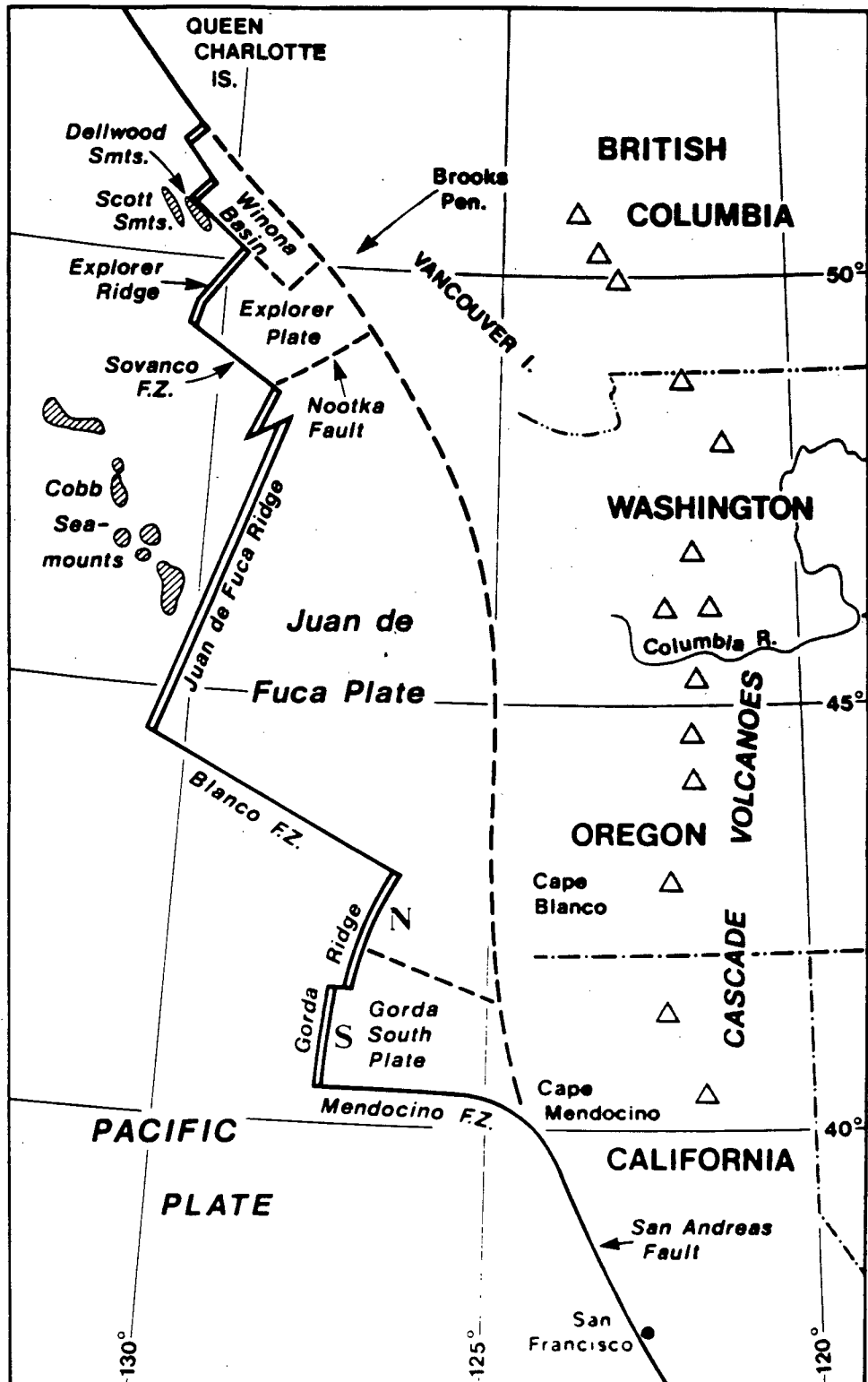


Fig 2-1. Location map of the Juan de Fuca plate system (from Riddiough, 1984).

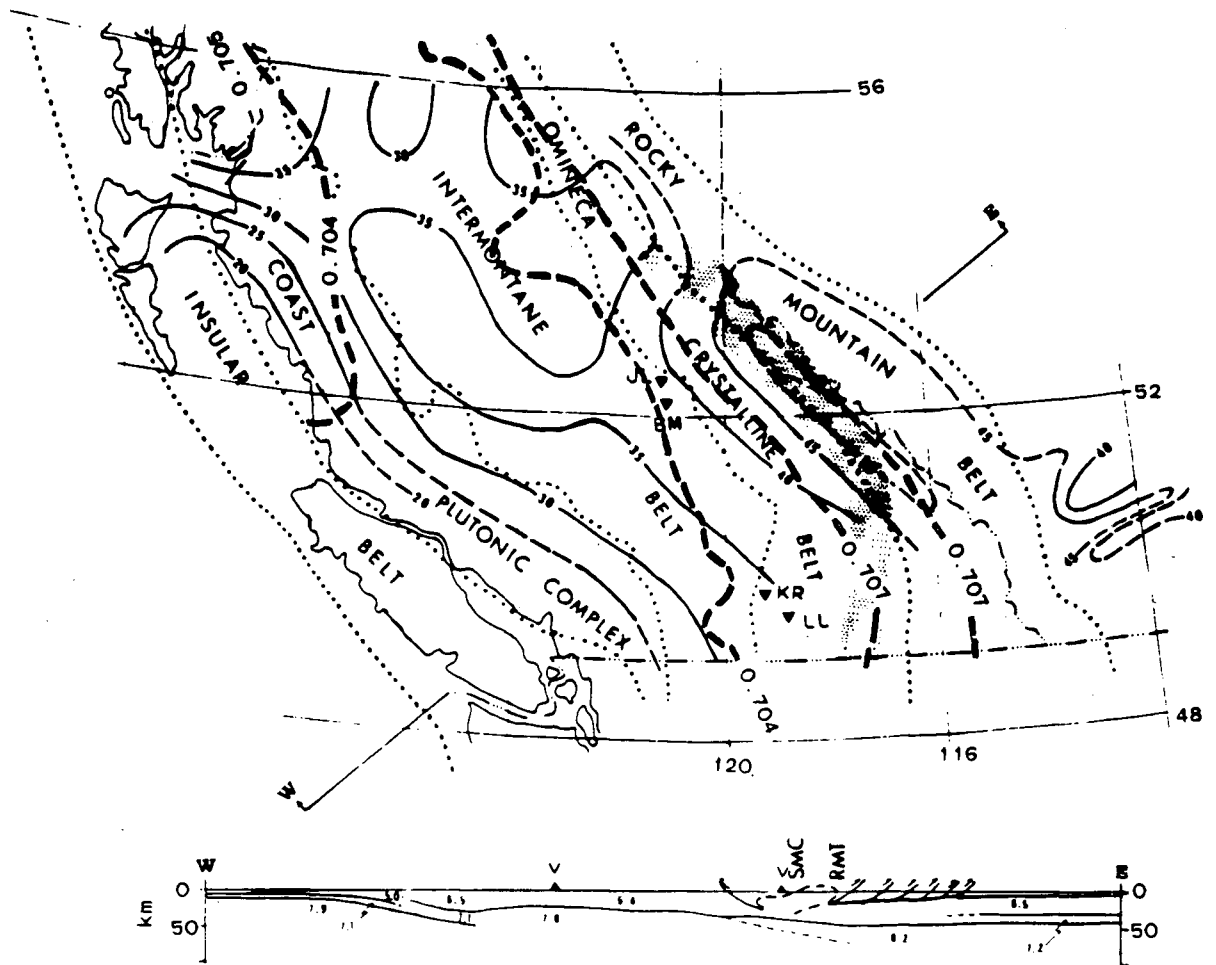


Fig. 2-2 Crustal structure of the southern Canadian Cordillera. Structure contours at 5 km intervals giving depth to the Moho. Stippled pattern shows zone of geomagnetic stations marking transition between highly conductive crust and upper mantle to the southwest, and less conductive crust and upper mantle to the northeast. Structure section W-E showing P-wave velocity in km/s. Quaternary and Recent volcanic rocks occur at the localities marked by solid triangles labelled "v". The thin-skinned thrust faults of the Rocky Mountain Belt are shown schematically east of the southern Rocky Mountain Trench (RMT), and the general outline of the deeply rooted Shuswap Metamorphic Complex (SMC) is shown schematically west of the Rocky Mountain Trench (from Monger and Price, 1979). $^{87}\text{Sr}/^{86}\text{Sr}$ contours of Mesozoic igneous rock are also shown (Armstrong, 1985, pers. comm.). Nodule sample localities are shown with inverted triangles: JL from Jacques Lake, BM from Big Timothy Mountain, KR from West Kettle River, LL from Lassie Lake.

Recent volcanic centers are largely confined to three belts (Figure 2-3). The Garibaldi Belt volcanic centers in southwestern British Columbia are the northern continuation of the Cascade arc and occur above the subducted Jan de Fuca plate. The E-W trending volcanic belt at approximately 52°N is the Anahim Belt, considered by Bevier et al. (1979) to be a hot spot trace. The Stikine Belt in northern British Columbia is thought to be rift related (Souther and Hickson, 1984).

Throughout the Intermontane Belt of British Columbia are isolated cinder cones and flows of alkalic olivine basalt erupted from Neogene through Recent time (Ross, 1983; W.H.Mathews unpublished data; Bevier, 1983). Many of these volcanic flows and cones contain peridotite nodules. Figure 2-3 shows the localities of basalts containing ultramafic nodules in British Columbia.

Previous work

Soregaroli (1968) described nodules from Big Timothy Mountain.

Littlejohn and Greenwood (1974) analysed the minerals of spinel lherzolite nodules from Jacques Lake, Castle Rock and Nicola Lake. Temperatures were calculated from distribution of iron and magnesium between spinel and olivine. They concluded that the lherzolite nodules of Castle Rock and Jacques Lake are probably from the upper mantle, whereas the Nicola Lake lherzolites are probably

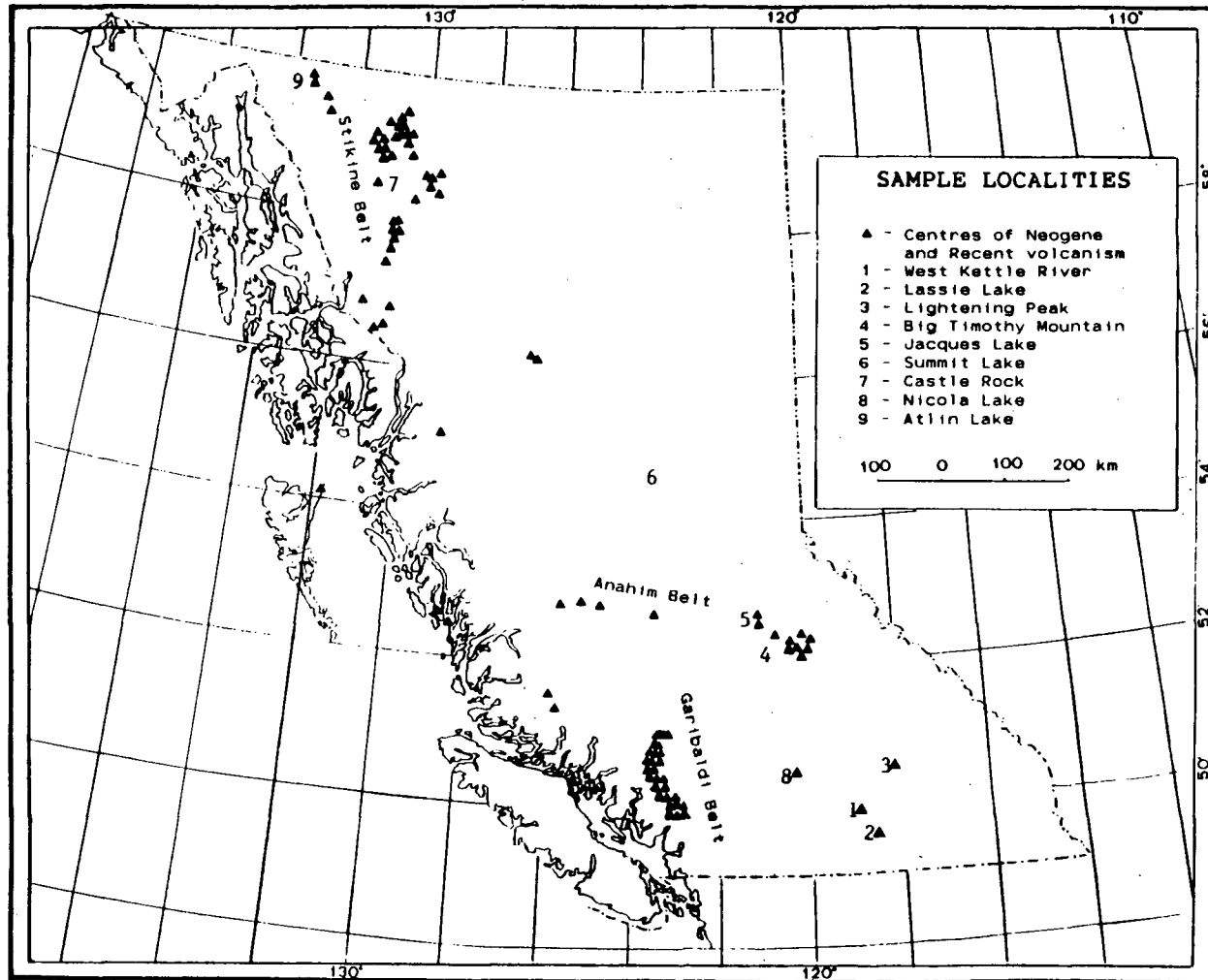


Fig. 2-3 Localities of ultramafic nodules in British Columbia, compiled from Farley (1979), Ross (1983), Littlejohn and Greenwood (1974), Nicholls et al. (1982).

crystal cumulates. They saw no evidence of regional chemical variations.

Fujii and Scarfe (1982) studied nodules from the West Kettle River. They concluded that the upper mantle beneath southern British Columbia is dominated by spinel lherzolite but contains some banding on a scale of centimetre to metres and that the chemical variations of constituent minerals within individual nodules of the chromian diopside series are small even when banding is present. Calculated equilibration temperatures, using the two-pyroxene geothermometer of Wells (1977), ranged between 920 and 980°C. Pressures of equilibration, based on published phase stability experiments, were inferred between 10 to 18 kbar (30-60 km).

Ross (1983) did numerous chemical and rheological analyses of nodules from West Kettle River, Lassie Lake, Lightning Peak, Big Timothy Mountain, Jacques Lake, Summit Lake, and Castle Rock. He presented geotherms and deviatoric stress vs. depth and strain rate/viscosity vs. depth profiles for all the above localities and postulated a dynamic model of the upper mantle beneath British Columbia.

Ross separated ultramafic nodules in British Columbia into the following six groups:

Al-augite (black clinopyroxene) series:

- (a). Mg-rich wehrlites. Metacumulates.
- (b). Fe-rich wehrlites. Cumulate.

Cr-diopside series (most abundant type)

Magmatic—

(c). Dark emerald-green diopside-bearing Ti-rich lherzolites.

Metamorphic, with bright emerald-green diopside—

(d). Depleted lherzolite, harzburgite and dunite.

(e). Undepleted lherzolite.

(f). Coarse-grained homogeneous websterite.

all with recrystallised magmatic textures with or without plastic deformation.

Brearley et al. (1984) studied nodules from the Summit Lake basanitoid flow. Their microprobe data on the mineral phases indicate that the nodules are generally well equilibrated. Calculated equilibration temperatures, using the two-pyroxene geothermometer of Wells (1977), ranged between 1080 to 1100°C. Pressures of equilibration, estimated from a Cordilleran geotherm, were between 10 to 20 kbar. The temperatures are somewhat higher than estimates from nodules of other localities. They concluded that either the Summit Lake suite represents samples from a deeper source region in the upper mantle or the Late Cenozoic geotherm varied in time and space.

Brearley and Scarfe (1984) studied pargasitic amphiboles in a chrome diopside - bearing spinel lherzolite trapped within an alkali basaltic lava flow at Lightning Peak. They indicated that the pargasite is in equilibrium with the other phases in spinel lherzolite and probably

crystallized within the spinel stability field of the upper mantle from a volatile-rich metasomatic fluid. The pargasite always shows evidence of melting. They interpreted the melting in the pargasite as caused by one of three processes: superheating by the host alkali basalt, decompression as the magma ascended, or in situ partial melting within the upper mantle. They concluded that the partial melting of amphibole-bearing spinel lherzolite provides a possible mechanism for the generation of late Cenozoic alkaline magmas of the Intermontane Belt of British Columbia.

Fieshinger and Nicholls (1977) described the ultramafic nodules in Kostal Lake and Takomkane Mountain (near Jacques Lake and Big Timothy Mountain) and Nicholls et al. (1982) described the ultramafic nodules in Castle Rock, Nicola Lake, Jacques Lake and Big Timothy Mountain in their basalt papers.

Maxwell (1976) analysed Rb and Sr isotopes in two nodules from Jacques Lake and one from Big Timothy Mountain, with poor data reproducibility. Differences of $^{87}\text{Rb}/^{86}\text{Sr}$ in reruns of the same mineral are about 30% and of $^{87}\text{Sr}/^{86}\text{Sr}$ are up to ± 0.003 for olivine and orthopyroxene and ± 0.001 for clinopyroxene. Maxwell attributed this to different batches of mineral separates used for repeat analyses, overleaching, spiking errors, and erratic lab contamination. One nodule from Jacques Lake gave a mineral isochron date of 2000 ± 100 Ma with $(^{87}\text{Sr}/^{86}\text{Sr})_0 = 0.7024 \pm 0.0001$. The other

Jacques Lake nodule and the Big Timothy Mountain nodule did not give reasonable mineral isochrons, but they show evidence of great age (4700 ± 2400 and 4400 ± 2500 Ma with $(^{87}\text{Sr}/^{86}\text{Sr})_0 = 0.7020-0.7006$, respectively. He concluded that the apparent isochron is due to in situ decay of ^{87}Rb and that the lower date represents a "mantle event". The cause of disequilibrium in other two nodules was unknown, but he thought metasomatism in the mantle may be a possible explanation. The new analyses suggest that his Rb analyses may have been too low because of overestimation of the Rb blank.

Samples studied

Samples for this study are from Jacques Lake, Big Timothy Mountain, West Kettle River and Lassie Lake. The chemical compositions of the host and associated basalts are shown in Tables 2-2 and 2-3.

(1). Jacques Lake (5 on Fig. 2-3) ($52^\circ 28.6' \text{N}$ $121^\circ 9.4' \text{W}$)

The Jacques Lake locality is a small cone of coarse basaltic tuff, Pleistocene in age (Campbell, 1978), 4 miles south of Quesnel Lake in central British Columbia. The lava adhering to nodule JL14 is sodic alkali olivine basalt series ankaramite (Armstrong, 1985, pers. comm.). Ultramafic nodules and fragments of other rocks are scattered throughout the tuff. The nodules are sub-rounded and range in size from 2 to 35 cm. Most are less than 15 cm in diameter (Littlejohn and Greenwood, 1974).

Four nodules from Jaques Lake (JL1, JL14, JL15 and JL18) were selected for this study. They fall in the lherzolite region in OL-OPX-CPX triangle (Figure 2-4; Table 2-1) and are all of protogranular texture. Olivine and orthopyroxene range up to 4 mm. Olivine forms an interlocking mosaic of equidimensional grains, nearly colorless to pale yellow in hand specimen and colorless in thin section. Kink bands are observed in most olivine grains. Orthopyroxene occurs as subhedral grains with perfect cleavage, dark brown in hand specimen and pale yellow in thin section. Clinopyroxene forms small anhedral grains, bright emerald green in hand specimen and pale green in thin section. New spongiform microcrystalline clinopyroxene, due to partial melting, occurs commonly around clinopyroxene grains. Spinels occur as irregularly-shaped grains inside or in contact with orthopyroxene, some subhedral spinel grains crystallized in intergranular partial melt.

Somewhat equigranular and porphyroclastic texture were found in JL15 and JL18, respectively.

The clinopyroxene is diopside and orthopyroxene is enstatite (Table 3-1, Figure 2-5).

(2). Big Timothy Mountain (4 on Fig. 2-3) ($52^{\circ}63'N$, $121^{\circ}9.4'W$)

Big Timothy Mountain, not far from Jaques Lake, is a cone (600 meters in diameter) of potassic series alkali (adhering to nodule BM11 and BM26) to picritic alkali

Table 2-1 Visual estimated modal mineralogy of the samples

Sample	Olivine	Opx	Cpx	Spinel
JL 1	56%	26%	16%	3%
JL 14	55%	24%	18%	3%
JL 15	56%	25%	15%	4%
JL 18	60%	20%	15%	5%
BM 11	70%	20%	8%	2%
BM 16	30%	40%	30%	5%
BM 55	30%	35%	30%	5%
KR 1	73%	14%	10%	3%
KR 2	60%	30%	5%	5%
KR 35	50%	30%	15%	5%
LL 1	60%	20%	15%	5%
LL 14	60%	30%	5%	5%
JM 2	56%	39%	4%	1%
JM 5	63%	31%	4%	2%
JM 15	38%	56%	4%	2%
JM 14	68%	26%	4%	2%

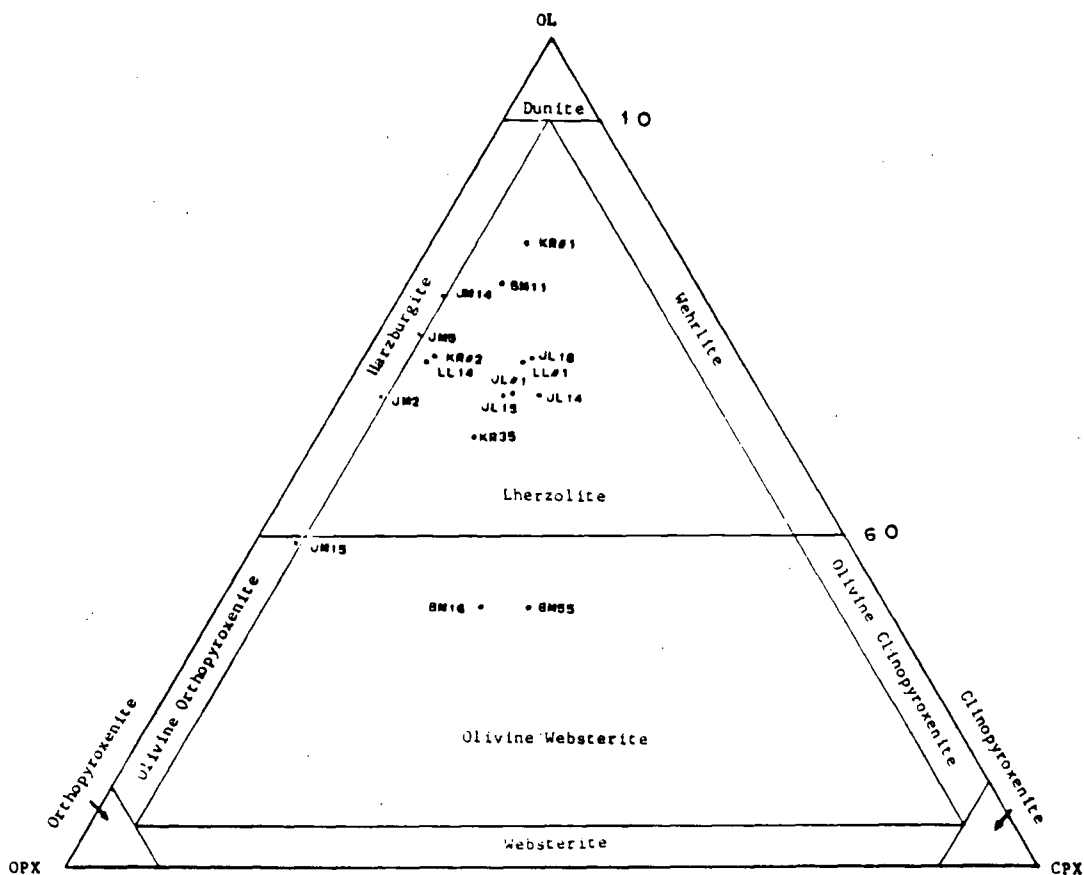


Fig 2-4 Sample classification based on modal mineralogy in terms of olivine, orthopyroxene and clinopyroxene.

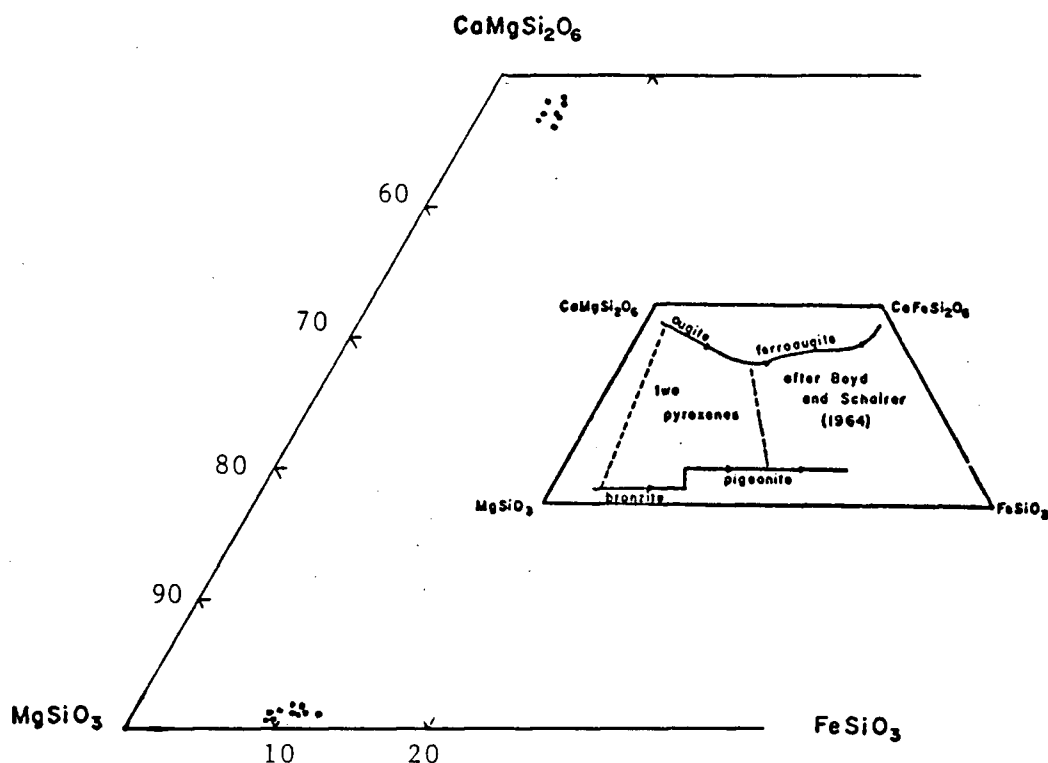


Fig 2-5 Composition of clinopyroxene and orthopyroxene in ultramafic nodules from British Columbia.

(adhering to nodule BM55) basalt or basanite (Armstrong, 1985, pers. comm.), Pleistocene in age (Campbell, 1978). The ultramafic nodules are round and subround, they range in size from 5 to 50 cm, and comprise from 1 to 25% of the lavas (Soregaroli, 1968).

Three nodules from this locality (BM11, BM16 and BM55) were selected for this study. BM11 is lherzolite and BM16 and BM55 are olivine websterite (Figure 2-4, Table 2-1).

BM11 and BM55 exhibit protogranular texture as observed at Jacques Lake. BM55 olivine displays spectacular kink bands in large grains.

BM16 exhibits equigranular texture. Olivine and orthopyroxene grains are less than 1.5 mm across, with 120°

triple junctions. Subhedral clinopyroxene and spinel are 0.5 mm across.

The clinopyroxene is diopside and orthopyroxene is enstatite (Table 3-1, Figure 2-5).

(3). West Kettle River (1 on Fig. 2-3) ($49^{\circ}46.9'N$, $119^{\circ}4.0'W$)

There are four lava flow layers found in West Kettle River field. The four layers are stacked concordantly. The lower three are each approximately 2 meters thick, the top layer is 11 meters thick. The flows are separated by rubbly horizons about 10 cm thick, but no weathering zones were observed, suggesting that the flows were erupted within a short time. Two K-Ar dates for nearby basalts are 2.8 ± 1.5 Ma (Church, 1980) and 4.2 ± 0.5 Ma (Boyle, 1980; Stevens et al., 1982). The three lower layers are calc-alkaline series subalkaline basalts, while the top layer is sodic alkali olivine basalt or basanite (Armstrong, 1985, pers. comm.) (Table 2-2). Ultramafic nodules were found only in the top layer. This layer shows well developed columnar joints with 50 cm average widths of columns. The nodules are sub-rounded and range in size from 2 to 25 cm.

The three nodules (KR1, KR2 and KR35) selected for this study are lherzolite (Figure 2-4, Table 2-1).

KR2 exhibits porphyroclastic texture. Elongated olivine and orthopyroxene give a foliation in hand specimen, and spinels are strung out parallel to that foliation in thin section. The [010] of olivine is oblique to the foliation by

Table 2-2 Chemical compositions of host and associated basalts (wt%)

	WKR1B	WKR2B	WKR3B	WKR4B	KR35B	KRB	LL1B	LL14B	JL14B	BM11B	BM26B	BM55B
SiO ₂	48.86	49.31	49.61	45.01	44.83	44.5	47.59	46.75	42.21	41.80	43.36	41.40
TiO ₂	2.35	2.22	2.17	2.94	2.57	3.12	2.36	2.33	2.58	3.19	3.16	3.16
Al ₂ O ₃	16.41	16.67	16.62	14.65	14.60	14.1	15.83	14.36	13.27	13.03	13.38	12.95
Fe ₂ O ₃ T	12.53	12.49	11.67	13.45	14.50		11.66	13.04	14.50	15.26	13.31	15.83
Fe ₂ O ₃						3.73						
FeO						8.52						
MnO	0.19	0.17	0.16	0.18	0.19	0.21	0.17	0.18	0.18	0.20	0.19	0.21
MgO	4.89	4.59	4.99	8.53	8.44	9.50	7.94	10.50	7.32	10.64	10.64	11.18
CaO	9.81	9.33	9.66	9.29	9.20	4.20	8.79	7.93	15.43	9.01	8.95	8.88
Na ₂ O	3.17	3.39	3.35	3.46	3.43	1.65	3.04	3.17	2.14	3.40	3.35	3.29
K ₂ O	1.26	1.32	1.26	1.64	1.44	0.79	1.99	1.19	1.69	2.60	2.79	2.29
P ₂ O ₅	0.52	0.52	0.51	0.85	0.80		0.64	0.56	0.69	0.87	0.87	0.83
CIPW norm												
Ap	1.22	1.22	1.20	2.00	1.88	1.83	1.50	1.31	1.62	2.05	2.04	1.95
Il	4.52	4.27	4.17	5.66	4.95	5.93	4.53	4.48	4.97	6.15	6.08	6.10
Mt	2.45	2.44	2.28	2.63	2.84	5.41	2.28	2.55	2.84	2.99	2.60	3.10
Or	7.54	7.89	7.53	9.82	8.63	9.75	11.89	7.12	0.0	15.28	16.70	13.75
Ab	27.15	29.03	28.67	16.51	17.05	12.92	22.48	24.94	0.0	0.0	3.21	0.76
An	27.16	26.69	26.89	19.86	20.48	14.75	23.94	21.71	21.92	12.81	13.41	14.02
Ne	0.0	0.0	0.0	7.13	6.71	12.25	1.91	1.20	9.95	15.82	13.82	14.91
Lc	0.0	0.0	0.0	0.0	0.0	0.0	0.0	0.0	7.94	0.25	0.0	0.0
Ol-Fo	4.06	4.00	4.02	11.42	11.58	11.03	11.23	15.94	5.55	14.11	14.00	15.36
Ol-Fa	4.70	4.98	4.25	7.69	9.07	4.01	7.27	9.04	5.00	8.75	7.25	9.55
Ol-Ca	0.0	0.0	0.0	0.0	0.0	0.0	0.0	0.0	1.12	0.0	0.0	0.0
Ol-En	3.75	3.24	3.80	5.23	4.80	7.92	3.97	3.74	10.57	6.77	6.86	6.37
Ol-Fs	3.93	3.66	3.64	3.19	3.42	2.61	2.33	1.92	8.64	3.81	3.22	3.59
Ol-Wo	7.80	6.98	7.60	8.86	8.57	11.47	6.65	6.02	19.84	11.19	10.78	10.53
Hy-En	2.79	2.61	3.03	0.0	0.0	0.0	0.0	0.0	0.0	0.0	0.0	0.0
Hy-Fs	2.92	2.95	2.91	0.0	0.0	0.0	0.0	0.0	0.0	0.0	0.0	0.0

Comment: KRB data from Fujii & Scarfe (1982), others from Armstrong (1985, pers. comm.). WKR1B, WKR2B and WKR3B are lower layers of the West Kettle River eruption sequence. They are nepheline-norm free subalkaline basalts that lack nodules. Others are alkali basalts that contain nodules.

Method: Armstrong's data are derived from XRF analyses of pressed powder pellets using an automated Phillips X-ray spectrometer in the Oceanography Department of U.B.C. Results are oxidized, anhydrous, and normalized to 100 per cent totals. Trace element analyses of the same pellets using the same equipment are reported in table 2-3. Major and trace element concentrations are based on comparison with USGS and other widely analysed igneous rock standards. Mass absorption coefficients are calculated from major element compositions.

Table 2-3 Concentrations of trace elements in host basalts (ppm)
(from Armstrong, 1985, pers. comm.)

	WKR1B	WKR2B	WKR3B	WKR4B	KR35B	LL1B	LL14B	JL14B	BM11B	BM26B	BM55B
Ba	316	328	293	470	397	416	415	569	932	873	891
Cr	81	103	137	231	383	324	376	445	433	454	441
Nb	34	32	31	66	56	48	48	59	95	90	94
Ni	49	49	48	164	270	273	378	386	335	397	355
Rb	17	17	17	29	26	29	21	13	57	52	54
Sr	844	676	628	914	803	806	714	1444	1231	1203	1218
V	215	217	204	216	220	149	163	122	219	241	268
Y	23	22	21	25	24	24	23	28	26	24	27
Zr	210	200	193	319	281	244	237	367	401	391	395

an angle of 15° to 30°, due to intra-crystalline glide. KR1 exhibits protogranular to porphyroclastic texture. KR35 exhibits equigranular texture and shows incipient melting of clinopyroxene.

The clinopyroxene is diopside and orthopyroxene is enstatite. Olivine has the composition of Fo = 90.3-90.6. (Table 3-1, Figure 2-5).

(4). Lassie Lake (2 on Fig. 2-3) (49°35.8'N, 118°55.3'W)

Lassie Lake is near the West Kettle River locality. The nodules are exposed on a group of hills by Lassie Lake. No basalt stratigraphy was observed during field work. Three K-Ar dates from nearby basalt flows are 4.7±0.2 Ma (Christopher, 1978), 5.0±0.2 Ma (Christopher, 1977, 1978) and 5.9±0.6 Ma (Boyle, 1980, Stevens et al., 1982). The lava is inferred to have approximately the same age as the West Kettle River lavas. The lava adhering to nodule LL1 is potassic series alkali olivine basalt and that to LL14 is sodic series picritic basalt (Armstrong, 1985, pers. comm.). The nodules, weathered and smaller than those from West Kettle River, range in size from 2 to 15 cm.

The two lherzolite nodules (LL1 and LL14) (Figure 2-4, Table 2-1) selected for this study exhibit protogranular texture. LL1 shows considerable melt, LL14 has more than average brownish alteration (iddingsite?) on grain boundaries.

The clinopyroxene is diopside and orthopyroxene is enstatite. Olivine of LL1 has the composition of Fo = 89.7 (table 3-1, Figure 2-5).

II-2. Josephine Peridotite of Southern Oregon

The Josephine Peridotite is situated in Klamath Mountains of southwestern Oregon and Northern California (Figure 2-6). In these mountains six major north - south elongated lithic belts have been described by Irwin (1960, 1972). Josephine Peridotite lies along the western margin of Irwin's western Jurassic Belt. This belt, some 8 to 32 km wide and over 320 km long, is composed of shale, greywacke, and metavolcanic rocks of the Galice and Rogue Formations, a variety of intrusive rocks, and the Illinois River Gabbro.

The Josephine Peridotite is in fault contact on the west with the Dothan and Franciscan terranes of the Oregon and California Coast Ranges. These included tectonically disrupted melange of greywacke, shale, metavolcanic rocks, chert, limestone and serpentinite.

There is general agreement that rocks in the arcuate belts of the Klamath Mountains represent fragments of island

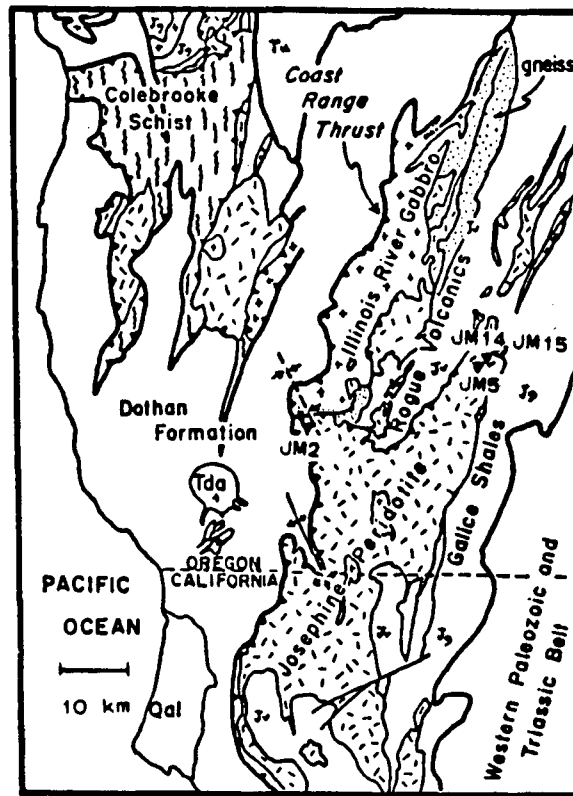


Fig. 2-6 Generalized tectonic sketch map of the Josephine Peridotite and its vicinity (from Dick, 1975).
 ▼ - sample localities.

arcs and ocean basins that collided with the continental margin (e.g., Hamilton, 1969; Irwin, 1972, Schweickert and Cowan, 1974).

The Josephine Peridotite, covering nearly 650 km² and extending continuously for almost 150 km along the western edge of the Klamath Structural Arc, is one of the largest bodies of ultramafic rock in the world.

The peridotite is commonly 10 to 30% serpentinized. The fresh peridotite consists largely of harzburgite; there is only a minor amount of irregularly distributed dunite and volumetrically insignificant orthopyroxenite and lherzolite.

An extensively petrologic study was carried out by Dick

(1975) in the area sampled. He suggested that the peridotite is the residue of at least two episodes of partial melting in the mantle and that it is the relict of the earliest stages of the construction of a circum - oceanic volcanic sequence.

Four samples from Josephine Peridotite were selected for this study. They are all harzburgite (Figure 2-4, Table 2-1).

JM2 from Vulcan Peak ($42^{\circ}11.0'N$, $123^{\circ}59.0'W$) exhibits protogranular texture. There is moderate (~15%) serpentinization along mineral boundaries and mineral cracks. Original minerals are mainly olivine and orthopyroxene.

JM14 from Eight Dollar Mountain ($42^{\circ}15.4'N$, $123^{\circ}41.0'W$) exhibits porphyroclast texture. Elongated olivine has preferred orientation and obvious kink bands. Orthopyroxene clasts are products of fragmentation. Serpentinization is minor (2-3%).

JM5 and JM15, also from Eight Dollar Mountain, exhibit original protogranular texture overprinted by later fragmentation. Serpentinization is minor (~5%)

Diopside occurs as small anhedral grains in low abundance in all samples.

III. CHEMICAL MINERALOGY

Three polished thin sections, KR1, KR2 and LL1, were prepared for wavelength dispersive microprobe analysis at the University of British Columbia. In each polished thin section, two grains of olivine, spinel, clinopyroxene and orthopyroxene were analysed, using an Applied Research Laboratories Scanning Electron Microprobe Quantameter operated at 15 kv 40 nA (on Al). The work was guided by J. Knight and J. Rice. The standards used were prepared by J. Ross and J. Knight. In each grain, the analyses were repeated at 5 to 6 scattered points. The data are in Appendix 1 and mineral formulae in Table 3-1. Fe^{2+} and Fe^{3+} contents of spinel were calculated assuming a $\text{M}^{2+}\text{M}^{3+}\text{O}_4$ formula (Appendix 2). No significant chemical zonation or variation was found within mineral grains and, in each thin section, the two mineral grains analysed gave the same chemical composition. The average value for each mineral was used for the following plots and calculations.

Clinopyroxene and orthopyroxene analyses for several other nodules in this study were provided by J.V.Ross.

Clinopyroxene and orthopyroxene data from Dick (1975) (Appendix 3) were calculated to mineral compositions in the same manner as the British Columbia nodule mineral analyses (Table 3-2). Although the data are from samples other than those involved in this Sr isotope study, they are still pertinent to our discussion because the Josephine Peridotite

Table 3-1 Nodule mineral compositions (from data in Appendix 1 and J.V. Ross, pers. comm. 1985)

Sp	Mg/(Mg+Fe)															
	Si	Al	Ti	Mn	Mg	Ca	Ni	0	Cr	0	Mg/(Mg+Fe)x100	Cr/(Cr+Al)x100	0	Wo	En	Fs
Opx	Si	Al	Ti	Fe	Mn	Mg	Ca	Na	Cr	K	0	Wo	En	Fs		
JL14	1.88	0.31	0.016	0.089	0.002	0.78	0.77	0.138	0.022	0.001	6	47.0	47.5	5.4		
BM16	1.88	0.32	0.010	0.087	0.003	0.77	0.79	0.127	0.020	0.0	6	48.1	46.7	5.3		
BM55	1.87	0.32	0.012	0.090	0.003	0.81	0.76	0.125	0.017	0.0	6	45.7	48.8	5.4		
KR 1	1.95	0.17	0.005	0.064	0.002	0.84	0.83	0.099	0.038	0.0	6	47.9	48.4	3.7		
KR 2	1.94	0.21	0.002	0.070	0.003	0.82	0.83	0.086	0.027	0.0	6	47.3	48.6	4.1		
KR35	1.89	0.30	0.015	0.081	0.003	0.76	0.79	0.128	0.021	0.0	6	47.9	47.2	4.9		
LL 1	1.90	0.28	0.008	0.087	0.003	0.80	0.78	0.111	0.028	0.0003	6	46.9	47.9	5.2		
LL14	1.94	0.14	0.001	0.075	0.003	0.90	0.85	0.050	0.035	0.0	6	46.6	49.3	4.1		
Opx	Si	Al	Ti	Fe	Mn	Mg	Ca	Na	Cr	K	0	Wo	En	Fs		
JL14	1.87	0.21	0.003	0.200	0.005	1.67	0.034	0.008	0.009	0.0006	6	1.8	87.7	10.5		
JL15	1.89	0.20	0.003	0.193	0.004	1.66	0.029	0.010	0.011	0.0	6	1.5	88.2	10.2		
JL18	1.89	0.18	0.003	0.234	0.006	1.66	0.024	0.010	0.011	0.001	6	1.2	86.6	12.2		
BM11	1.92	0.14	0.002	0.201	0.004	1.68	0.035	0.007	0.024	0.0	6	1.8	87.7	10.5		
BM16	1.88	0.23	0.003	0.194	0.005	1.63	0.041	0.007	0.011	0.0	6	2.2	87.4	10.4		
KR 1	1.93	0.12	0.001	0.168	0.004	1.76	0.022	0.005	0.014	0.0	6	1.1	90.2	8.6		
KR 2	1.91	0.15	0.004	0.171	0.004	1.74	0.021	0.005	0.011	0.0	6	1.1	90.1	8.8		
KR35	1.88	0.22	0.004	0.194	0.004	1.63	0.036	0.009	0.012	0.0	6	1.9	87.7	10.4		
LL 1	1.91	0.18	0.002	0.180	0.004	1.66	0.028	0.006	0.012	0.0	6	1.5	88.9	9.6		
LL14	1.93	0.11	0.0004	0.168	0.004	1.74	0.031	0.003	0.016	0.0	6	1.6	89.7	8.7		
O1	Si	Fe	Mn	Mg	Ca	Ni	0		Mg/(Mg+Fe)							
KR 1	0.996	0.19	0.003	1.808	0.001	0.008		4	90.6							
KR 2	1.008	0.19	0.003	1.781	0.002	0.008		4	90.3							
LL 1	0.999	0.21	0.003	1.785	0.002	0.008		4	89.7							
Sp	Si	Al	Ti	Mn	Mg	Fe++	Fe+++	Cr	0	Mg/(Mg+Fe)x100	Cr/(Cr+Al)x100					
KR 1	0.0008	1.32	0.002	0.004	0.74	0.265	0.035	0.647	4	73.7	32.9					
KR 2	0.001	1.67	0.001	0.002	0.79	0.213	0.011	0.321	4	78.7	16.1					
LL 1	0.002	1.73	0.003	0.002	0.79	0.219	0.005	0.266	4	78.2	13.3					

has limited variation in mineral composition.

All the analyses reported sum to 98.1-101.0 weight percent total oxide.

Olivine

The composition of olivine in British Columbia nodules and Josephine Peridotite is strikingly uniform. Olivines from KR1, KR2 and LL1 have forsterite contents $FO_{90.6}$, $FO_{90.3}$ and $FO_{89.7}$, respectively (Table 3-1). Josephine olivines have a range of forsterite content from $FO_{89.5}$ to $FO_{91.7}$, with an average $FO_{90.3}$ (Dick, 1975).

Clinopyroxene and orthopyroxene

Clinopyroxene and orthopyroxene both in nodules and in Josephine Peridotite are Cr-diopsides and enstatite, respectively.

Clinopyroxene in nodules varies from $Wo=45.7$ to 48.1 , $En=46.7$ to 49.3 , $Fs=3.7$ to 5.4 . Clinopyroxene in Josephine Peridotite varies from $Wo=45.9$ to 46.9 , $En=48.7$ to 50.4 , $Fs=3.5$ to 4.6 (Tables 3-1 and 3-2).

Orthopyroxene in nodules varies from $Wo=1.1$ to 2.2 , $En=86.6$ to 90.2 and $Fs=8.6$ to 12.2 . Orthopyroxene in Josephine Peridotite varies from $Wo=1.2$ to 3.5 , $En=87.7$ to 90.6 and $Fs=8.0$ to 9.0 (Table 3-1 and 3-2). Numbers of Cr and Ti per diopside and enstatite formula unit have been plotted in Figure 3-1 (after Ross, 1983).

Table 3-2
Josephine Peridotite pyroxene compositions (data from Dick, 1975)

Cpx	Si	Al	Ti	Fe	Mg	Ca	Cr	O	Wo	En	Fs
J28f	1.89	0.168	0.0011	0.0854	0.93	0.89	0.043	6	46.9	48.7	4.5
J871	1.92	0.099	0.0008	0.0730	1.00	0.91	0.029	6	45.9	50.4	3.7
J120	1.89	0.209	0.0041	0.0848	0.90	0.85	0.032	6	46.4	49.0	4.6
J120	1.93	0.090	0.0014	0.0699	0.99	0.92	0.020	6	46.5	49.9	3.5
Opx	Si	Al	Ti	Fe	Mg	Ca	Cr	O	Wo	En	Fs
J28f	1.90	0.146	0.0005	0.1756	1.71	0.063	0.025	6	3.2	87.7	9.0
J46h	1.92	0.134	0.0010	0.1662	1.69	0.067	0.024	6	3.5	87.8	8.6
J46h	1.90	0.131	0.0010	0.1685	1.74	0.052	0.023	6	2.6	88.8	8.6
J871	1.94	0.094	0.0003	0.1653	1.75	0.041	0.015	6	2.1	89.5	8.4
J114	1.90	0.085	0.0003	0.1775	1.82	0.041	0.014	6	2.0	89.3	8.7
J120	1.91	0.093	0.0005	0.1793	1.82	0.022	0.012	6	1.1	90.0	8.9
J46g	1.93	0.039	0.0008	0.1636	1.86	0.030	0.015	6	1.4	90.6	8.0

Table 3-3
Comparison of pyroxenes of depleted and undepleted nodules and Josephine Peridotite

	Mg/(Mg+Fe)x100	Cr/(Cr+Al)x100	Cr/Ti	Al	Ti	Cr	Na
Depleted nodules							
Diopside	92.2-92.9	11.4-19.7	7.6-13.5	0.14-0.21	0.001-0.005	0.027-0.038	0.050-0.099
Enstatite	91.1-91.3 *	6.8-15	12-40	0.11-0.15	0.0004-0.002	0.011-0.024	0.003-0.007
Undepleted nodules							
Diopside	89.8-90.5	5.0-9.1	1.4-3.5	0.28-0.32	0.008-0.016	0.017-0.028	0.111-0.138
Enstatite	87.7-90.2	4.1-6.1	3-3.7	0.18-0.23	0.002-0.004	0.009-0.012	0.006-0.010
Josephine peridotite							
Diopside	91.4-93.4	13.1-22.6	7.7-39.4	0.09-0.21	0.001-0.004	0.020-0.043	
Enstatite	90.7-91.9	11.3-27.7	23.6-50.4	0.04-0.15	0.0003-0.001	0.012-0.025	

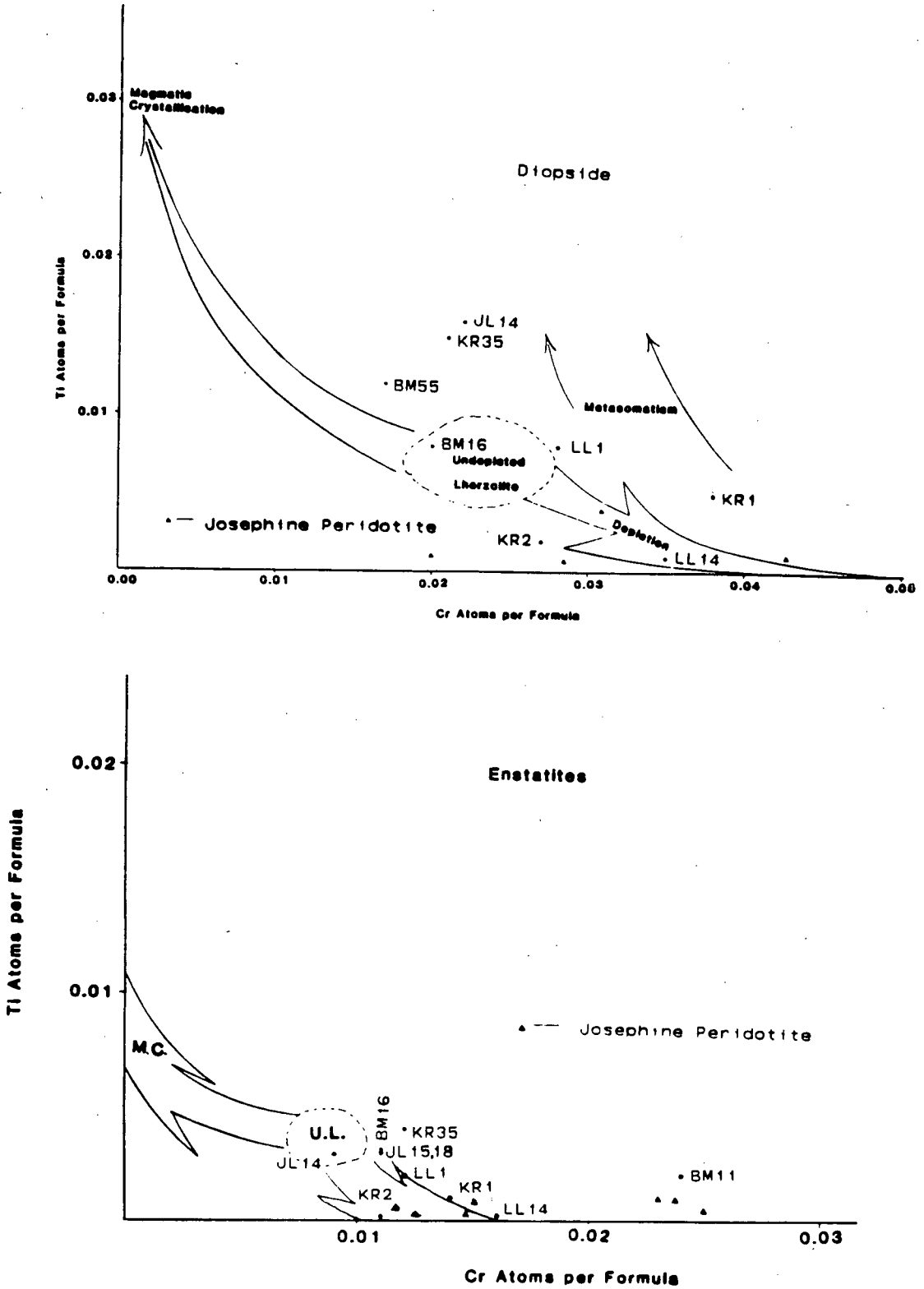


Fig. 3-1 Ti-Cr plots of diopsides and enstatites.

From Figure 3-1, we derive the following conclusions:

- a. Most of diopside underwent more intensive Ti metasomatism than enstatite.
- b. LL14 and KR2 are depleted nodules without Ti metasomatism. KR1 and BM11 are depleted nodules with Ti metasomatism.
- c. BM16 is undepleted without Ti metasomatism, KR35, JL14 and BM55 are undepleted nodules with Ti metasomatism. JL15 and JL18 are undepleted nodules with unspecified Ti metasomatism, the uncertainty due to lack of diopside data.
- d. LL1 diopside falls on the boundary of depleted and undepleted. Enstatite indicates somewhat depleted character. Because enstatite contains less Cr and Ti than diopside, the contrast in assignment is probably not significant.
- e. All pyroxenes from Josephine Peridotite are of strongly depleted character without Ti metasomatism. The degree of depletion is larger than that of the nodules.

In graphs of $\text{Cr}/(\text{Cr}+\text{Al})\times 100$ vs. Al (Figure 3-2) and $\text{Mg}/(\text{Mg}+\text{Fe})\times 100$ vs. $\text{Cr}/(\text{Cr}+\text{Al})\times 100$ (Figure 3-3), depleted and undepleted groups are sharply separated.

In the enstatite $\text{Mg}/(\text{Mg}+\text{Fe})\times 100$ vs. Cr/Ti diagram (Figure 3-4(a)), the depletion trend is well defined. In the diopside $\text{Mg}/(\text{Mg}+\text{Fe})\times 100$ vs. Cr/Ti diagram depleted nodules are somewhat more scattered (Figure 3-4(b)), presumably due

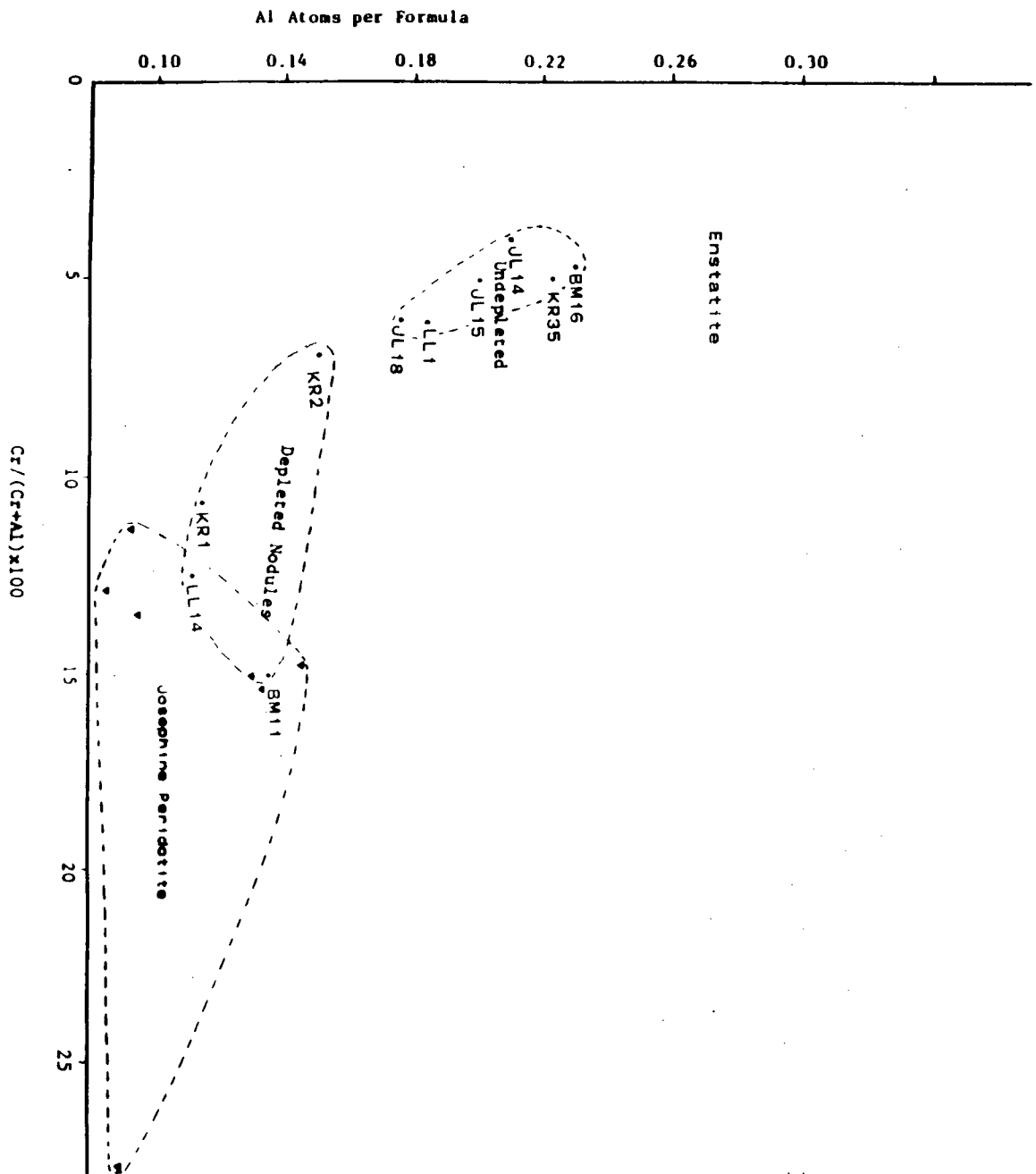


Fig. 3-2(a) Cr/(Cr+Al) x 100 vs. Al plot of enstatite

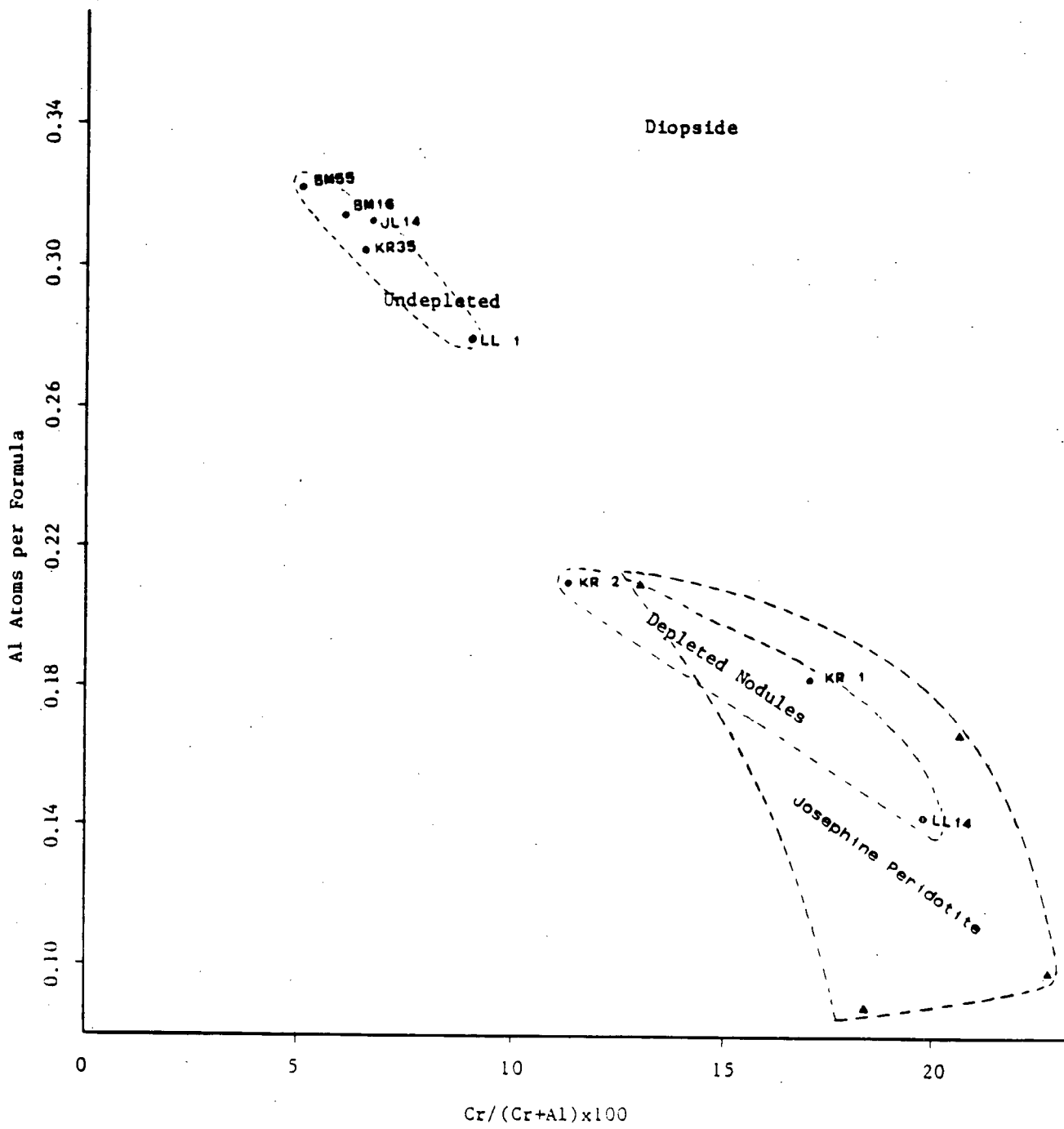


Fig. 3-2(b) Cr/(Cr+Al)x100 vs. Al plot of diopsides

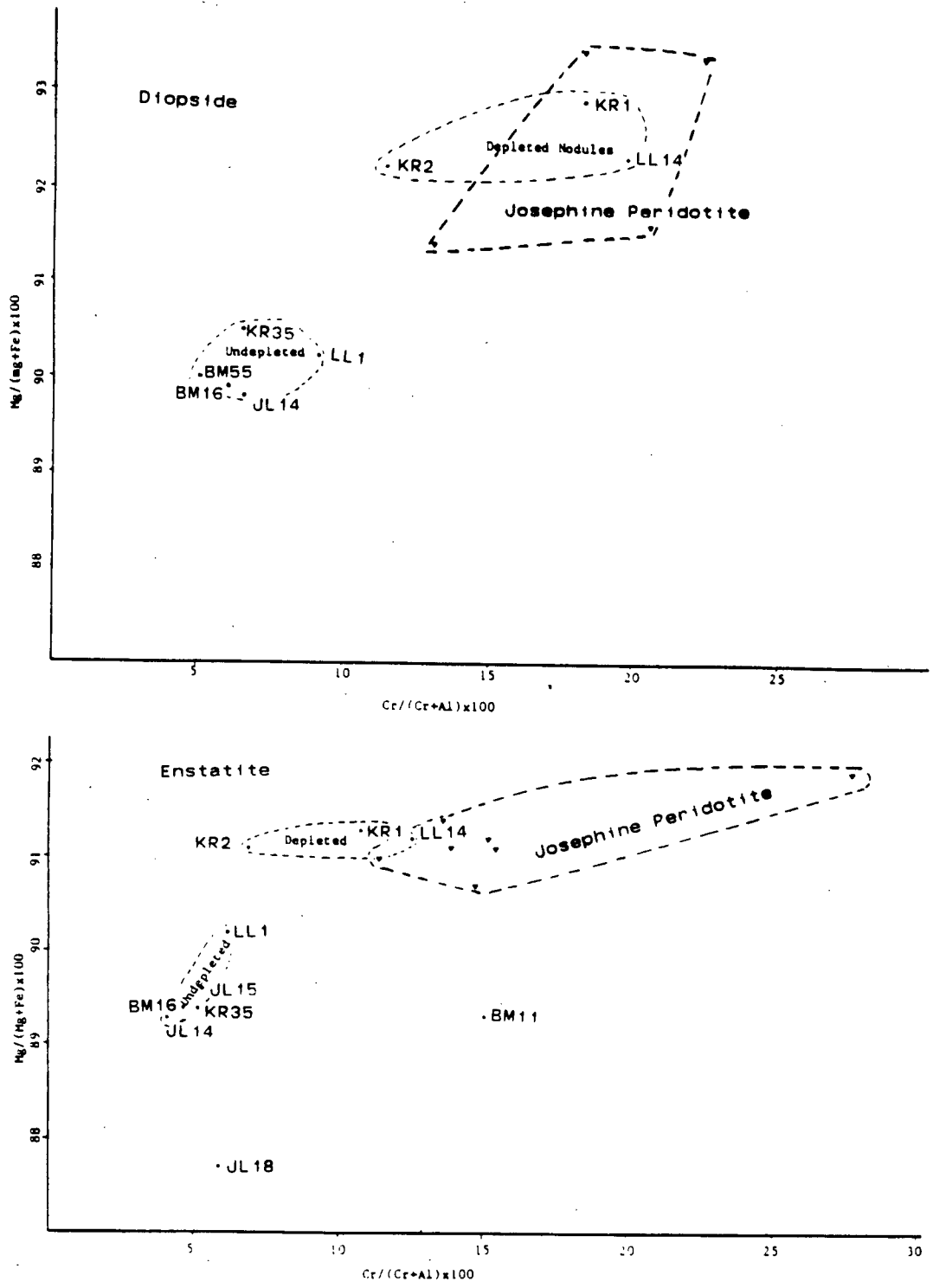


Fig. 3-3 Cr/(Cr+Al)x100 vs. Mg/(Mg+Fe)x100 plot of diopsides and enstatites

to variable Ti metasomatism.

The composition ranges of pyroxenes in depleted and undepleted nodules and Josephine Peridotite are given in Table 3-3. In every case the assignment of individual specimens can be made without contradiction.

Spinel

Only three nodules were analysed for spinel composition. There was no significant variation between two spinel grains analysed in each nodule (Appendix 1 and 2), nor was chemical variation among spinels from three nodules.

(Table 3-1): Al=1.319 to 1.729, Mg=0.742 to 0.789, Fe²⁺=0.213 to 0.265, Cr=0.266 to 0.647.

In the Cr/(Cr+Al)x100 vs. Mg/(Mg+Fe²⁺)x100 plot (Figure 3-5), the nodule spinels lie on the lower (less depleted) end of the Josephine Peridotite trend.

Pressure and temperature estimates

Pyroxene geothermometry and geobarometry techniques for ultramafic parageneses (Wood and Banno, 1973; Wood, 1975; Mercier and Carter, 1975; Mercier, 1976) are based on theoretical derivations for sets of equilibrium reactions involving enstatite, diopside and an aluminous phase, either spinel or garnet.

Based on wollastonite solid-solution in diopside and Al-concentration in co-existing enstatite, Mercier (1976) generalized the pyroxene techniques to derive both

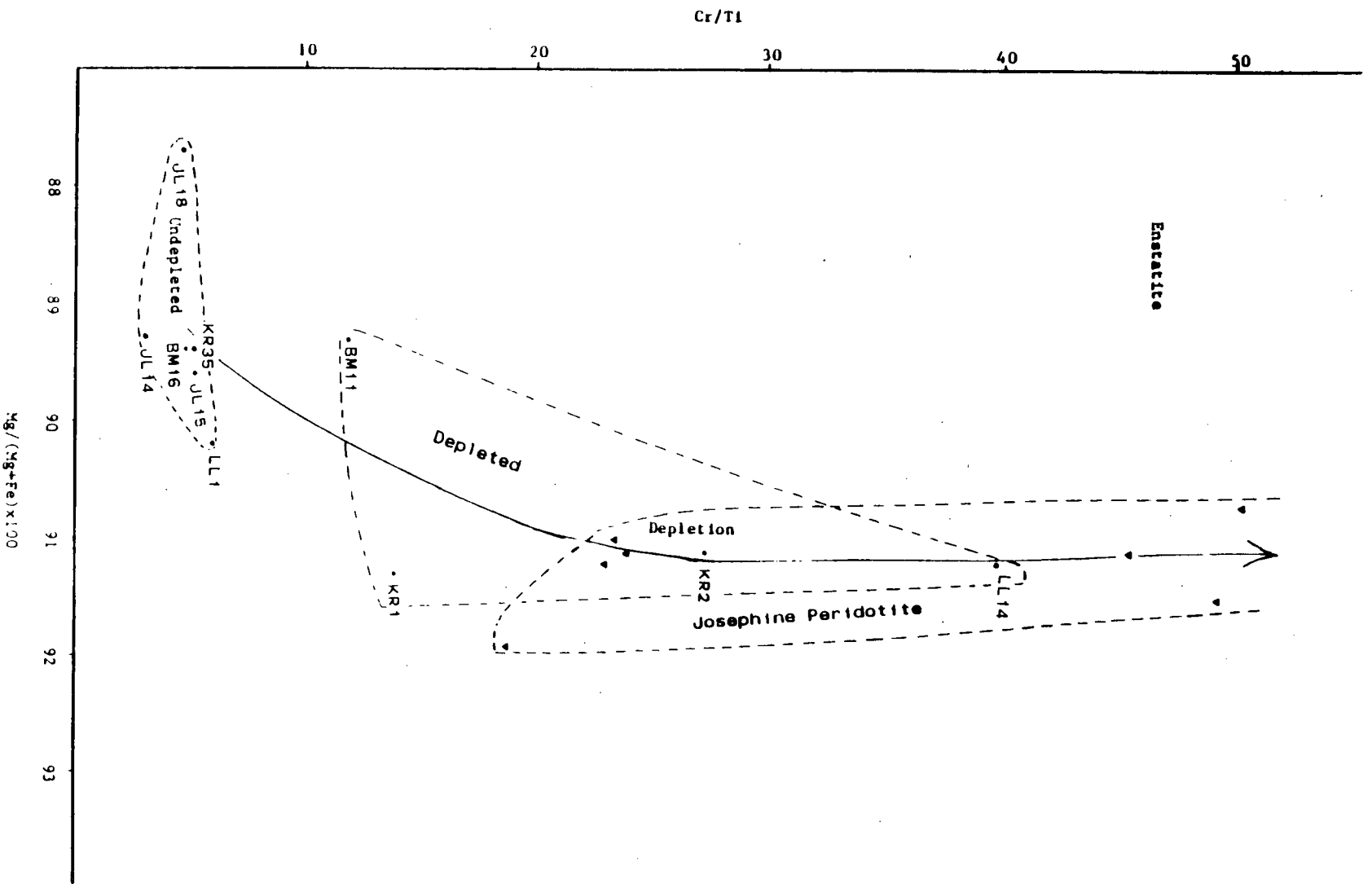


Fig. 3-4(a) $Mg/(Mg+Fe) \times 100$ vs. Cr/Ti plot of enstatites

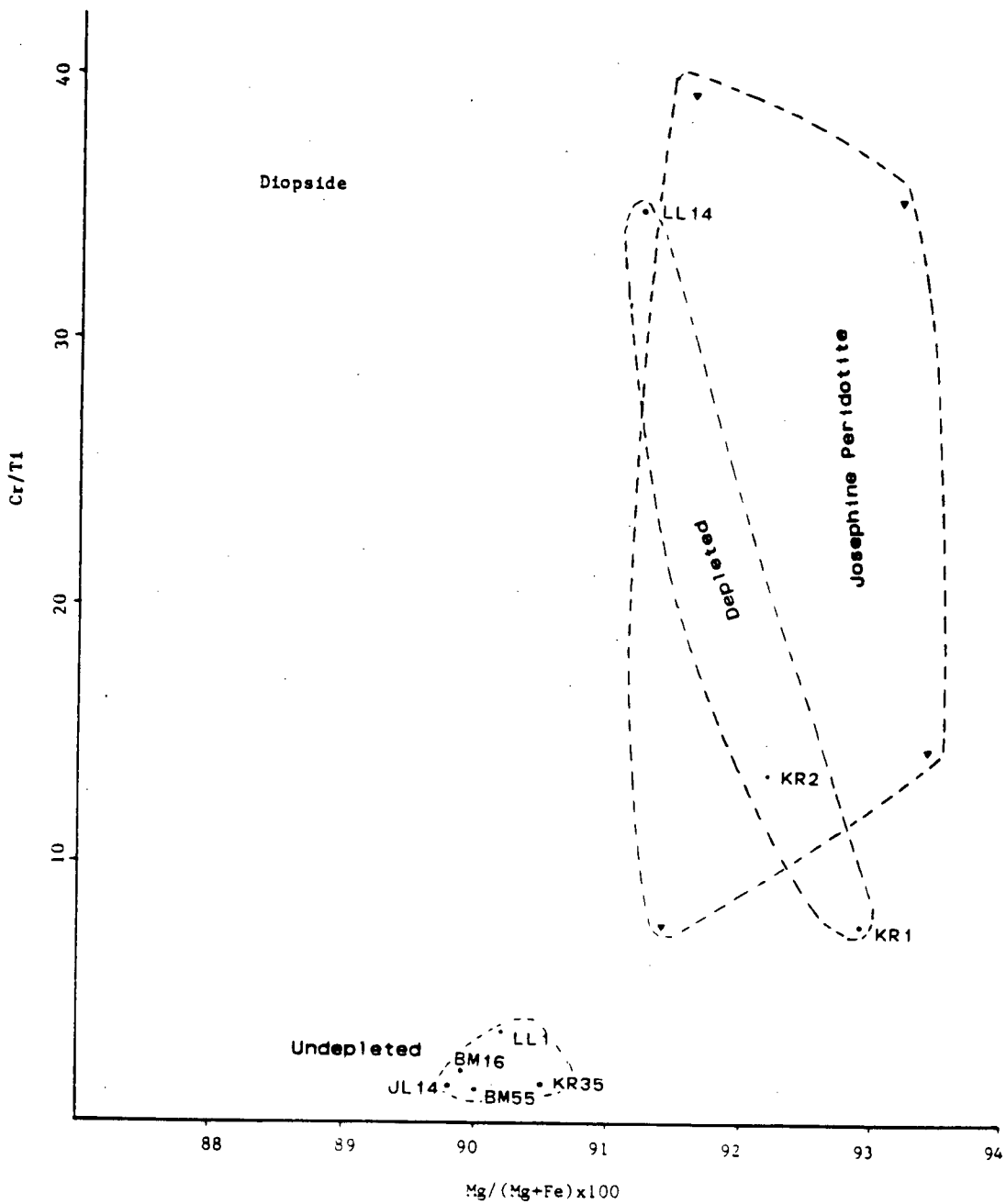


Fig. 3-4(b) Mg/(Mg+Fe)x100 vs. Cr/Ti plot of diopsides

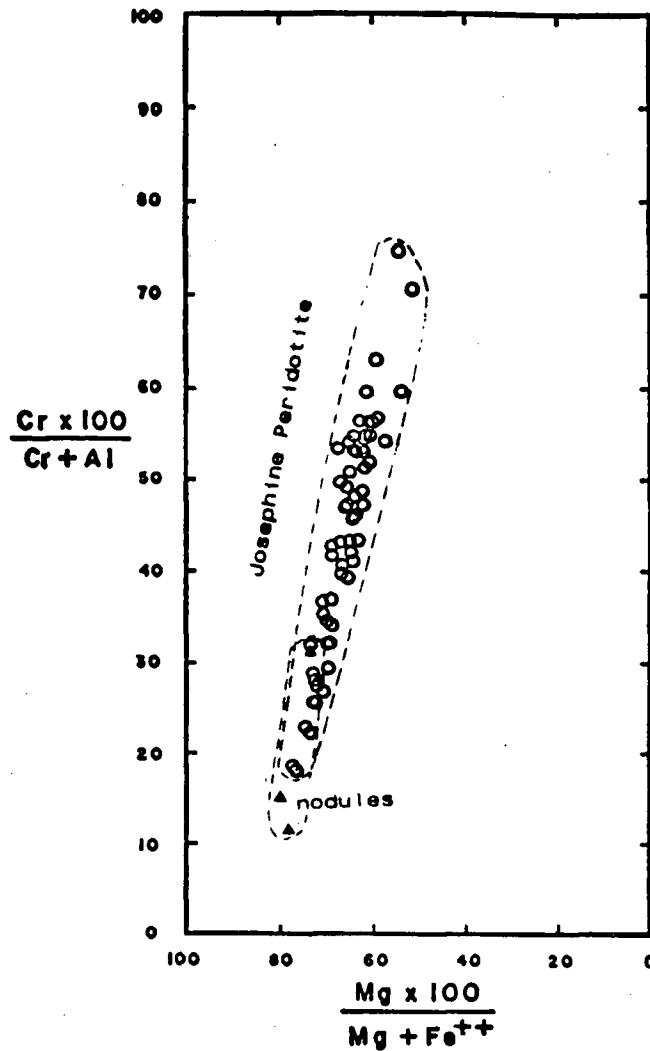


Fig. 3-5 Mg/(Mg+Fe++)x100 vs. Cr/(Cr+Al)x100 plot of spinel (Josephine Peridotite data from Dick, 1975)

temperature and pressure on the basis of a single-pyroxene analysis, the composition of the co-existing phases being inferred from this analysis and from empirically determined partition coefficients. This method can be applied to partially altered or reequilibrated facies and to xenocrysts, assuming original equilibrium between two pyroxenes and spinel or garnet. The method has been revised by Mercier (1980).

Temperature and pressure estimates are independently obtained through the use of the general equations (Mercier, 1976):

$$T = [\Delta H_a (v'_w + v''_w \ln K'_w) - \Delta H_w (v'_a + v''_a \ln K'_a)] / D$$

$$P = [\Delta H_a (R \ln K'_w + \Delta S_w) - \Delta H_w (R \ln K'_a + \Delta S_a)] / D$$

in which,

$$D = (R \ln K'_a + \Delta S_a) (v'_w + v''_w \ln K'_w) - (R \ln K'_w + \Delta S_w) (v'_a + v''_a \ln K'_a)$$

pertinent thermodynamic parameters and the partition coefficients K'_w and K'_a are given by Mercier (1980)

Mercier's refined pyroxene thermobarometry (1980) has been used to calculate equilibrium temperature and pressure of British Columbia nodules and Josephine Peridotite through the program "PGEOTH" provided by J.V. Ross.

Data in Table 3-1 were used for the calculation. Calculated T, P, and depth are listed in Table 3-4.

The T, P and depth calculated separately for diopside and enstatite do not agree: enstatite calculation gives systematically higher values than diopside.

Temperature, pressure and depth values from J.V. Ross (Appendix 4) were derived from data for individual analytical points. There is likewise a degree of inconsistency between diopside and enstatite.

The inconsistency may be due to disequilibrium between diopside and enstatite or due to significant deviation of partition coefficients from those of Mercier (1980).

Considering the well defined mineral isochrons (see Chapter V), the inconsistency seems unlikely to be due to

Table 3-4 Calculated T(°C), P(kb) and Depth(km)

	Mercier (1980)						Modified					
	CPX			OPX			CPX			OPX		
	T	P	D	T	P	D	T	P	D	T	P	D
KR#1	940	11.77	39.9	1006	16.75	55.0	936	11.49	39.1	936	12.02	40.7
KR#2	929	11.49	39.1	1002	16.82	55.2	975	14.43	48.0	974	14.88	49.3
LL#1	1004	13.72	45.8	1057	18.10	59.1	999	13.42	44.9	998	14.03	46.8
JL14	995	13.74	45.9	1089	20.18	65.4	995	13.76	45.9	995	13.64	45.6
JL15				1062	18.16	59.3						
JL18				1025	17.18	56.3						
BM11				1093	13.37	44.8						
BM16	940	9.81	34.0	1131	20.97	67.8	937	9.56	33.2	939	7.92	28.2
BM55	1053	16.95	55.6									
KR35	949	10.90	37.3	1105	19.21	62.5	947	10.77	36.9	950	8.70	30.6
LL14	1012	16.52	54.3	1068	19.11	62.1	1009	16.34	53.8	1008	15.18	50.3
Josephine peridotite												
J28f	1000	11.34	38.6	1215	20.79	67.2	1005	11.62	39.5	1002	7.62	27.3
J871	1040	19.67	63.9	1123	23.97	76.9	1042	19.80	64.2	1041	18.38	60.0
J120	1010	20.46	66.3	998	18.79	61.2	1013	20.72	67.0	1011	19.72	64.0
J114				1114	24.50	78.5						
J46h				1235	22.67	72.9						
J46h				1169	19.27	62.6						

disequilibrium between diopside and enstatite.

In Mercier's thermobarometer, the partition coefficient K'_w for En and Di solid-solutions



is given by $K'_w = (X_{\text{Mg}}^{\text{M}_2})_{\text{di}} / (X_{\text{Mg}}^{\text{M}_2})_{\text{en}} = (1-2W_{\text{di}}) / (1-2W_{\text{en}})$

where, $W = \text{Ca} / (\text{Ca} + \text{Mg} + \text{Mn} + \text{Fe}^{++})$ and the factor 2 arises from the consideration of Fe solid solution.

By plotting mineral data in W_{en} vs. $0.5 - W_{\text{di}}$, Mercier got a value of $W_{\text{en}} / (0.5 - W_{\text{di}}) = 0.333$ for spinel-facies. Thus for enstatite, $K'_w = 6.000W(1-2W)$
for diopside, $K'_w = (1-2W) / (0.667 + 0.667W)$.

If there is a large deviation from $W_{\text{en}} / (0.5 - W_{\text{di}}) = 0.333$, the difference between K'_w calculated from diopside and from enstatite will be significant. For example, for nodule LL14, the diopside calculation gives $K'_w = 0.0715$, but the enstatite calculation gives

$K'_w = 0.0989$. This difference is the main source of the inconsistency.

When coexisting enstatite and diopside data are available, calculated $K'_w = (1 - 2W_{di}) / (1 - 2W_{en})$ will be more reliable. For example, for nodule LL14, $K'_w = 0.072$.

Thus Mercier's single pyroxene thermobarometer has been modified for this study. When coexisting pyroxenes data are available, we take $K'_w = (1 - 2W_{di}) / (1 - 2W_{en})$. Otherwise, we calculate, following Mercier, $K'_w = 6.000W(1 - 2W)$ for enstatite and $K'_w = (1 - 2W) / (0.667 + 0.667W)$ for diopside. The results derived by this modification are also listed in Table 3-4.

IV. Rb-Sr ISOTOPE ANALYTICAL METHOD

IV-1. Sample preparation

(1). Nodules

Only relatively fresh nodules were selected for this study. Small basalt fragments adhering to the nodules were removed by hand picking after initial crushing using a hammer. Next the same sample was reduced in a steel mortar to less than 16 mesh, and 5 gram samples were set aside for whole rock analysis. The 40-16 mesh fraction of the remainder was used for mineral separation. The whole rock split was further crushed in the steel mortar to pass 40 mesh and then ground in a motor driven agate mortar to less than about 150 mesh.

The interstitial material in ultramafic rocks contains much higher Rb and Sr than the pristine minerals. This material must be completely removed from the surfaces of the minerals in order to get true chemical values for the minerals. The procedure for doing this is:

After washing with Quartz¹ H₂O, 20 grams of dry 40-16 mesh size fraction was allowed to stand for 6 hours in 6N Quartz HCl while heated to 80°C in a pyrex beaker. After the residue was washed with Quartz H₂O three times it was dried on a hot plate. The HCl and H₂O used in this cleaning process were dried. The resulting chlorides were used for

¹"Quartz-" is defined in section IV 2-(2).

"acid-leach material" analyses. The acid-leach material weights of JL14, JL15, JL18, BM11, BM16, BM55, KR35, and LL14 were taken as the weight difference between the sample before and after the leaching. The acid-leach material weights of KR1, KR2 and LL1 were directly weighed from dried chlorides.

From the dried leached sample 2 to 4 grams of olivine, orthopyroxene and clinopyroxene were hand picked under a binocular microscope. Only those grains with clear surfaces and free from inclusions and exsolution lamellae were chosen for analysis. Each mineral separate was then ground in a clean agate mortar to 100-40 mesh and reexamined to ensure that no fine inclusions (e.g. magnetite and spinel) remained. The pure mineral separates (>99.5%) were leached with 6N Quartz HCl in an ultrasonic bath for 15 minutes and then placed on a hot plate (80°C) in small pyrex beakers for half an hour to remove any contamination from handling during hand picking. The residues were washed with Quartz H₂O three times and dried. The residues were then ground in the agate mortar to less than 150 mesh in a laminar air flow hood. The agate mortar was washed with ultrapure acetone between samples.

(2). Josephine Peridotite

Approximately 50 grams of each sample were processed through a jaw crusher and rotary pulverizer to give less than 40 mesh starting material. The 80-40 mesh size fraction

was passed through a Carpco magnetic roll separator to remove magnetite and iron (from the crushers). Different density fractions were separated from a water-washed 80-40 mesh fraction using methylene iodide diluted by acetone. Four fractions of successively lower density were collected. Examination under a binocular microscope indicated that the second fraction was free of serpentine, spinel and other accessory minerals. It was used for further separation with a Franz magnetic separator. The "non-magnetic" fraction consisted mainly of clinopyroxene; the "magnetic" fraction, of olivine; and the "weak magnetic" fraction, orthopyroxene. Unwanted minerals in the nearly pure mineral separates were removed by hand picking. The pure (>99%) mineral concentrates then went through the same leaching and grinding procedure as described for mineral separates from nodules.

Evaporation and final grinding procedures were carried out in a laminar flow hood to avoid contamination.

IV-2. Chemical Procedures

(1). Laminar flow hood

The laminar flow hood was used for all acid evaporations and filament loading to avoid contamination from the dust in the air. The blank improvement can be seen in Tables 4-1 and 4-3 and Figures 4-3(a) and 4-3(b).

(2). Reagents

Because of low Rb and Sr concentrations in ultramafic rocks, contamination from reagents used for sample dissolution and column elution has to be minimized. In order to reduce this contamination, only G. F. Smith Vycor - double distilled HClO_4 and "Quartz"- and "2B"- reagents were used. "Quartz"- refers to reagents distilled in a quartz glass still. "2B"- refers to reagents distilled at subboiling temperature in two-bottle teflon stills.

Quartz H_2O : prepared by redistilling distilled H_2O in a quartz glass still. Rb blank is 0.013 ± 0.003 ng/g, Sr blank is 0.072 ± 0.002 ng/g.

6.2 N Quartz HCl: prepared by diluting 'Baker analysed' reagent HCl with an appropriate quantity of distilled H_2O , then distilled in a quartz glass still. Rb blank is 0.020 ± 0.015 ng/g, Sr blank is 0.64 ± 0.32 ng/g.

2.5 N Quartz HCl: prepared by diluting 6.2 N Quartz HCl with an appropriate quantity of Quartz H_2O . The normality was confirmed by 1N NaOH titration. Rb blank is 0.014 ± 0.010 ng/g, Sr blank is 0.17 ± 0.02 ng/g.

1.5 N Quartz HCl: prepared by diluting 6.2 N Quartz HCl with appropriate quantity of Quartz H_2O . The 1.5 N value was confirmed by 1 N NaOH titration.

6.0 N Quartz HCl: prepared by diluting 6.2 N Quartz HCl with appropriate quantity of Quartz H_2O . The 6.0 N value was confirmed by 1 N NaOH titration.

2B HF: prepared by distilling Mallinckrodt Analytical Reagent HF at subboiling temperature in two-bottle teflon still. Rb blank is 0.051 ± 0.032 ng/g, Sr blank is 0.27 ± 0.21 ng/g.

HClO₄: G. F. Smith Vycor - double distilled HClO₄ was used. Rb blank is 0.020 ± 0.011 ng/g, Sr blank is 0.39 ± 0.20 ng/g.

All reagent blanks were determined by isotope dilution. Rb and Sr spikes were mixed with the reagent and dried. 2.5 N HCl was used to take up the precipitated materials and loaded into a large cation resin column for chemical separation. So all the Rb and Sr blanks reported here include large-column blanks.

Table 4-1 shows all the reagent blank measurements. From Table 4-1 we reach the following conclusions:

(a). Two-bottle distillation of HF reduces the Rb blank from an average value of 0.17 to 0.051 ng/g and Sr blank from an average value of 26 to 0.26 ng/g.

(b). Quartz distillation of distilled H₂O reduces Rb blank from an average value of 0.056 to of 0.013 ng/g and Sr blank from an average value of 2.5 to of 0.072 ng/g.

(c). Using HClO₄ directly from teflon source bottle (average Rb blank is 0.020 ng/g and average Sr blank is 0.39 ng/g) significantly improved the blanks for HClO₄. From the glass dropper bottle the average Rb blank is 0.22 ng/g and average Sr blank is 3.5 ng/g. This indicated that HClO₄ in the dropper bottle had been significantly contaminated.

Table 4-1 Reagent Blanks

Reagent	Date(Yr/Mo/Da)	Rb blank(ng/g)	Sr blank(ng/g)	comment
Distilled H2O	84/6/13	0.045 ± 0.003	(6.15 ± 0.40)	Sr abnormal
	84/6/13	0.083 ± 0.001	0.61 ± 0.07	
	84/6/19	0.040 ± 0.002	0.63 ± 0.04	
	average	0.056 ± 0.024	0.62 ± 0.05	
Q-H2O	84/5/14	3.47 ± 0.05	16.4 ± 11.6	*
	84/7/13	0.015 ± 0.000	0.07 ± 0.02	
	84/7/13	0.011 ± 0.000	0.07 ± 0.01	
	avg. of 7/13	0.013 ± 0.003	0.07 ± 0.00	
6.5 N Q-HCl	84/7/13	0.030 ± 0.001	0.95 ± 0.02	
	84/7/13	0.009 ± 0.000	0.31 ± 0.03	
	average	0.020 ± 0.015	0.63 ± 0.45	
2.5 N Q-HCl	84/5/14	8.52 ± 0.09	2.65 ± 0.75	*
	84/7/13	0.023 ± 0.000	0.15 ± 0.00	
	84/7/13	0.006 ± 0.000	0.18 ± 0.01	
	avg. of 7/13	0.014 ± 0.011	0.17 ± 0.02	
Reagent HF	84/5/14	76 ± 1	140 ± 10	*
	84/6/13	0.095 ± 0.005	39 ± 4	
	84/6/19	0.24 ± 0.01	1.3 ± 0.1	
	avg. 6/13-19	0.17 ± 0.10	26 ± 18	
2B-HF	84/5/14	3.72 ± 0.06	4.8 ± 2.5	*
	84/6/13	0.080 ± 0.001		
	84/6/19	0.057 ± 0.010	0.41 ± 0.03	
	84/7/27	0.017 ± 0.000	0.12 ± 0.01	
	avg. 6/13-7/27	0.051 ± 0.032	0.27 ± 0.21	
HC104	84/5/14	9.5 ± 0.1	220 ± 140	*
	84/6/13	0.103 ± 0.003	7.2 ± 0.6	
	84/6/19	0.42 ± 0.04	1.48 ± 0.04	
	84/7/27	0.123 ± 0.001	1.70 ± 0.02	
	avg. 6/13-7/27	0.22 ± 0.18	3.5 ± 3.2	
	84/8/2	0.011 ± 0.000	0.20 ± 0.01	**
	84/8/2	0.032 ± 0.000	0.59 ± 0.03	**
	84/8/2	0.018 ± 0.000	0.39 ± 0.02	**
	average of 8/2	0.020 ± 0.011	0.39 ± 0.20	

coment: * - acid evaporation in laminar flow hood, planchette evaporation and filament loading in open air, otherwise all evaporation and filament loading in laminar flow hood.

** - applied to HC104, from teflon source bottle, otherwise from glass dropper bottle.

all the blanks went through large ion exchange columns, so "reagent blank" includes large column blank.

(d). There is a significant reduction in the blank values for all the reagents when the laminar flow hood was used for all evaporations and filament loading.

(3). Rb and Sr spikes

Diluted ^{87}Rb was used for Rb isotope dilution analysis. The measured $^{85}\text{Rb}/^{87}\text{Rb}$ was 0.00809 ± 0.00004 , giving ^{87}Rb abundance of $99.20 \pm 0.01\%$ and ^{85}Rb of $0.803 \pm 0.004\%$.

In order to determine the concentration of ^{87}Rb spike, the spike was mixed with a weighed amount of standard RbCl solution (N.B.S. standard 984). A N.B.S.-type mass spectrometer was used to determine the isotope composition of the mixture. The Rb spike concentration was calculated to be 0.01069 ± 0.00007 $\mu\text{moles Rb/gm}$.

Diluted ^{84}Sr (N.B.S. SRM 988) was used for Sr isotope dilution analysis. The measured Sr spike isotopic ratios are given in Table 4-2. The isotope ratios used ($^{86}\text{Sr}/^{84}\text{Sr} = 0.00202 \pm 0.00001$; $^{88}\text{Sr}/^{84}\text{Sr} = 0.01244 \pm 0.00012$ and $^{87}\text{Sr}/^{84}\text{Sr} = 0.00111 \pm 0.00005$) were derived from N.B.S. certificate; 1984 and 1985 measurements and consideration of common Sr contamination.

The concentration of the ^{84}Sr spike was 0.01130 ± 0.00001 $\mu\text{moles Sr/gm}$ determined gravimetricly when it was first prepared in February of 1974. By replicated calibrations using a standard Sr solution (N.B.S. standard 987), a concentration of 0.01130 $\mu\text{moles Sr/gm}$ was determined (Maxwell, 1976). During the course of this work replicate

Table 4-2 Isotopic composition of N.B.S. Sr spike SRM-988

Date of measurement	86Sr/84Sr	88Sr/84Sr	87Sr/84Sr
N.B.S. certificate of analysis	0.000589	0.000386	0.000098
1976 (R.Maxwell)	0.00093	0.0029	0.00032
1978 (R.L.A.)	0.00162	0.0086	0.00061
1984 (RLA & MS)	0.00217	0.01374	0.00124
1985 (RLA & P.Michael)	0.00202	0.01244	0.00107
	±0.00001	±0.00088	±0.00010

calibrations of the ^{84}Sr spike were done using the same standard as was used in the initial calibrations. The procedure for Sr spike calibration was essentially the same as for Rb. Concentrations of 0.011475 and 0.011533 $\mu\text{moles Sr/gm}$ were given by the new calibrations. A value of $0.01150 \pm 0.00003 \mu\text{moles Sr/gm}$ for ^{84}Sr spike concentration was used for the isotope dilution calculations during this work. Agreement with the original calibrations is good. The concentration difference largely lies in the gradual increase in common Sr that has occurred over ten years in the storage flask.

(4). Sample dissolution

(a). sample digestion was carried out in a Savilex teflon dissolution vessel with teflon screw cap. 200-300 mg of clinopyroxene or whole rock, and 400-500 mg orthopyroxene or olivine were weighed directly into the vessel on a Mettler H_2O balance. The balance has a maximum sensitivity of 10 μg . ^{87}Rb and ^{84}Sr spikes were first added to the vessel via capillary tubes mounted in the caps of teflon spike bottles, then the sample. The weights of sample and

spikes were calculated by difference. By observing the spike evaporation during weighing, the precision of all weighing in this work was estimated to be ± 0.0001 gms (1σ). Normally a group of 10 samples plus blanks were processed at one time.

(b). After approximately 5 ml of 2B HF and 1 ml of HClO_4 were added to the sample, the teflon beakers were capped tightly and placed on a hot plate at boiling temperature for at least 4 days.

(c). After digestion, the samples were evaporated to dryness in a laminar flow hood and then allowed to cool.

(d). The samples were redissolved in 5 ml 2.5N Quartz HCl and centrifuged in pyrex centrifuge tubes for 4 minutes. The sample solution was immediately loaded onto ion exchange columns.

(5). Chemical separation

Elements were initially separated by using a large cation resin column (20cm long, 1cm diameter, filled with 200-400 mesh AG 50W-X8 resin). 2.5 N HCl was used for elution. The Rb and Sr were collected for mass spectrometer measurements or further purification, respectively.

The calibration of each column was carried out in three ways:

(a). 2 drops of radioactive ^{89}Sr tracer was loaded into the column. By using a Geiger counter ^{89}Sr concentration was determined in successive 5 ml eluant aliquots, and the Sr

peak position thus determined.

(b). 5 ml 2.5N HCl solution containing 0.2 mg RbCl, 0.4 mg SrCO₃, and 0.8 mg CaCO₃ was loaded into the column. By using an atomic absorption spectrometer, Rb, Sr and Ca concentrations were determined in each 5 ml eluant aliquot. In this way the Rb, Sr and Ca elution peaks were determined. The position of the Sr peak determined by this means agreed with that determined by ⁸⁹Sr tracer.

(c). 5 ml 2.5N HCl solutions of UBC lab standard P-1 (granodiorite) and of ultramafic nodule were mixed with 0.1 mg RbCl, 0.2 mg SrCO₃, and 0.05 mg Sm₂O₃, and then loaded into the column respectively. 100 ml 2.5N HCl and then 50ml 6.0N HCl were used for elution. An atomic absorption spectrometer was used to determine Rb, Sr, Mg and Sm concentration in each 5 ml eluant aliquot. The result gave Rb, Sr, Mg and Sm elution peaks.

No significant difference was found in Rb, Sr, Mg and Sm elution between P-1 and the ultramafic sample. But the Rb peak was 2 ml and the Sr peak 3 ml earlier compared to the position determined by loading with pure elements. The elution curves are shown in Figure 4-1.

The sample Rb and Sr, during this work, were collected according to the "rock matrix" elution results for each column.

Despite the effective chemical separation of Rb and Sr by going through the large column, Rb interference was still a serious problem. Significant spike ⁸⁷Rb would be added to

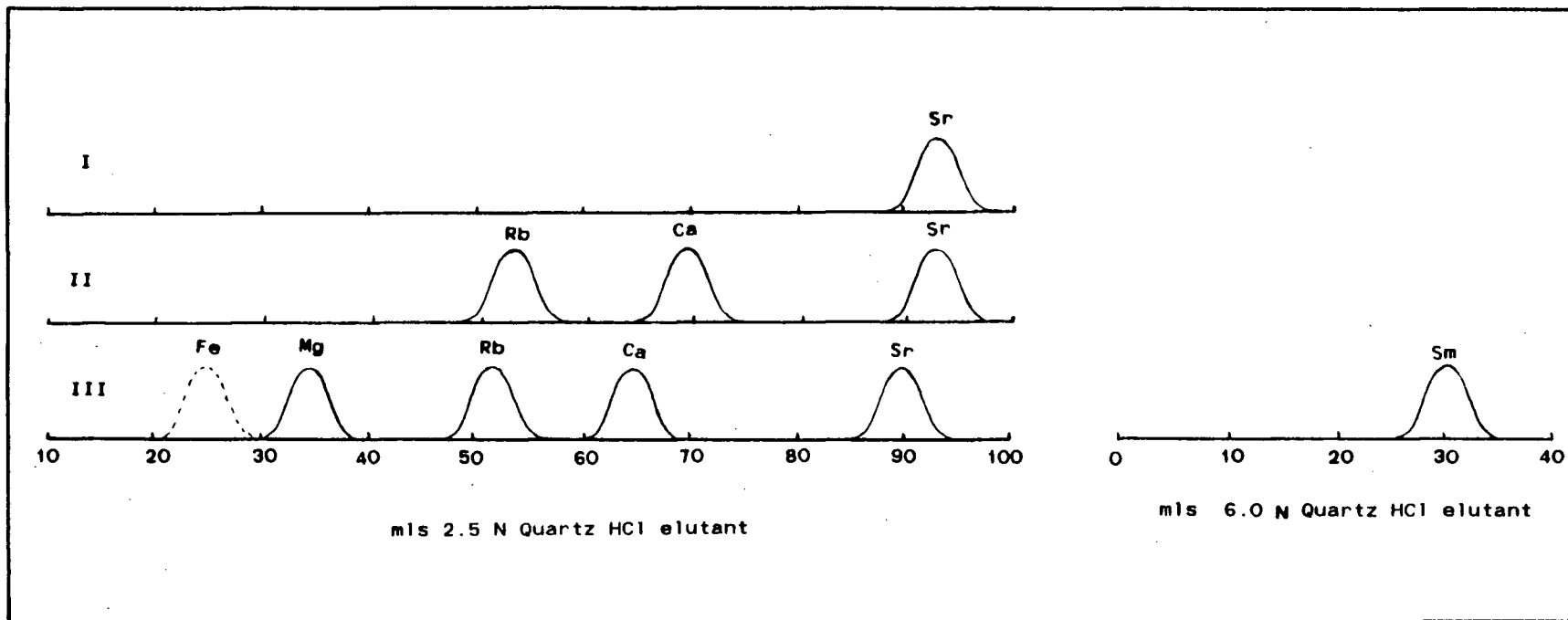


Fig. 4-1 Elution curves for Mg, Rb, Ca, Sr and Sm on large column 1. Peaks were determined during initial column calibration by collecting the eluant in 5 ml aliquots. I indicates calibration by ^{89}Sr tracer loading; II indicates calibration by loading pure reagents; III indicates loading of elements in a rock solution matrix. Relative elemental concentrations in the aliquots were measured by atomic absorption spectrometry and Geiger counter. Fe curve is from Maxwell (1976).

^{87}Sr during Sr isotope mass spectrometer measurement so as to give an incorrect $^{87}\text{Sr}/^{86}\text{Sr}$ value. During mass spectrometer Sr measurement using program "UBCSSR", the ^{87}Rb correction was done by measuring ^{85}Rb and assuming a natural Rb isotope ratio, i.e. $^{85}\text{Rb}/^{87}\text{Rb}=2.59265$. But for ^{87}Rb spiked samples this Rb correction would be incorrect. In order to solve this problem, 10 small columns were prepared for a second Sr separation to eliminate spike Rb interference.

The small columns (8 cm long, 0.5 cm diameter, filled with 200-400 mesh AG 50W-X8 resin) were calibrated by loading a solution of RbCl, SrCO₃, and CaCO₃, and eluting with 2.5 N, 2.0 N and 1.5 N Quartz HCl respectively. An atomic absorption spectrometer was used for Rb, Sr and Ca determination in each 2 ml eluant aliquot. The elution curves are shown in Figure 4-2. 1.5 N Quartz HCl was used for second Sr column elution during this work and Sr is collected from 12.5 to 20.0 ml. ^{87}Rb interference on ^{87}Sr was thus reduced to less than 0.0009 and the Rb was of nearly normal composition so $^{87}\text{Sr}/^{86}\text{Sr}$ ratios are reliable to 4th decimal place.

(6). Mass spectrometry

Rb isotope measurement was done on a N.B.S.-type mass spectrometer with programmable magnetic field control and digital data acquisition linked to a Hewlett-Packard HP85 computer.

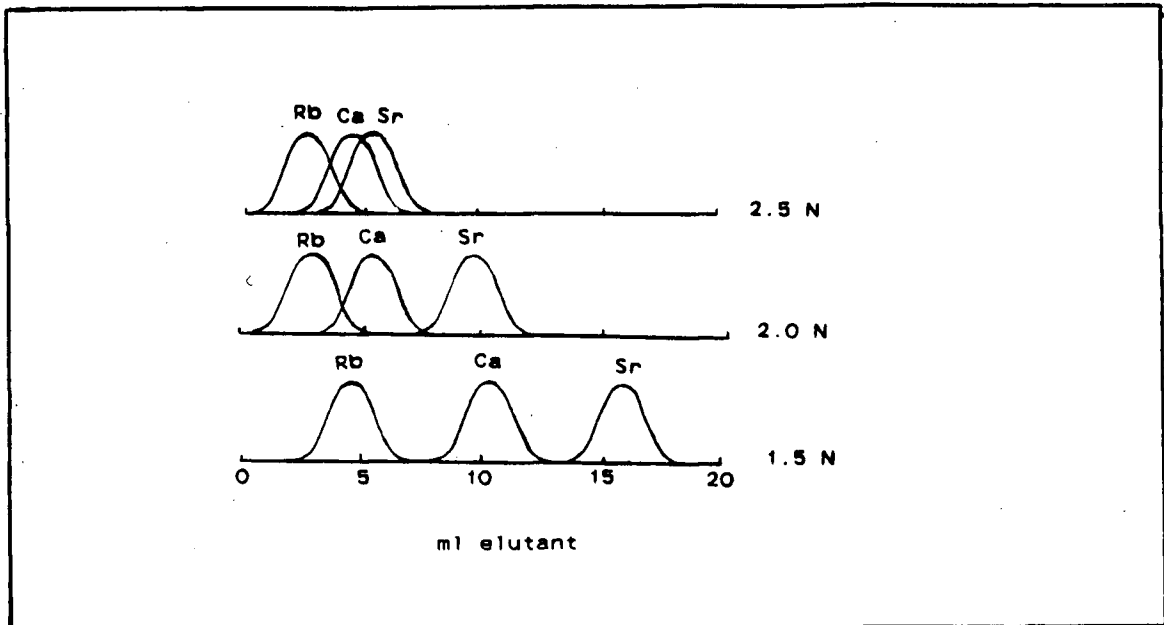


Fig. 4-2 Elution curves for Rb, Ca and Sr on small columns. Peaks were determined during initial calibration by collecting the eluant in 2.5 ml aliquots. Relative element concentration in the aliquots were measured by atomic absorption spectrometry. 1.5 N O-HCl is selected for second Sr column elution and Sr is collected from 12.5 to 20 ml.

- (a). Single tantalum filaments mounted on N.B.S. filament blocks were baked out for 15 minutes under $\leq 3.0 \times 10^{-5}$ torr vacuum and at 3.2 amps current.
- (b). One drop of sample, taken up in Quartz H_2O , was loaded on the filament ribbon at 1.5 amps current.
- (c). The loaded filament was then heated to a dull red glow for 10 seconds.
- (d). the filament was then loaded into the mass spectrometer. The sample analysis was only started when the vacuum in the mass spectrometer was less than 10^{-7} torr. This took about 2 hours by using rotary, vacsorb, and then ion pumps.
- (e). The filament current was increased until the more intense Rb peak (usually ^{87}Rb) was first detected on 30 mV

scale. The signal was focused to maximum intensity. Data were collected on 100 mV or 300 mV scale as individual blocks. Using the program "NBSRB2", within each block 3 backgrounds followed by 4 pairs of ^{85}Rb and ^{87}Rb peaks were measured, then calculations and statistics were done and $^{85}\text{Rb}/^{87}\text{Rb}$ ratio with 1 σ error was printed. Blocks were repeated to achieve acceptable overall precision.

Sr isotope measurement was done on a VG ISOMASS 54R mass spectrometer with a programmable magnetic field control and digital data acquisition linked to a Hewlett-Packard HP85 computer.

(a). Single tantalum filaments mounted on Cathodion filament beads were baked out in the same way as Rb filaments.

(b). A tiny bit of milky Ta_2O_5 suspension was placed on the baked filament.

(c). Two drops of a sample, dissolved in Quartz H_2O , were dried on the filament at 1.5 amps for 5 minutes, the second drop only being added after the first drop had dried.

(d). The filament was heated to a red glow for 10 seconds.

(e). 6 filaments were mounted on the carousel in the mass spectrometer. The source region was pumped down by rotary and then Ti sublimation and ion pumps. Analysis was started only after the mass spectrometer source had been pumped to below 10^{-6} mbar.

(f). Analysis was completed as follows:

The filament current was increased to about 2 amps, after the ^{85}Rb peak was found and focused, the filament current was increased to 3.0 to 3.2 amps until the ^{88}Sr was detected on x1000 scale. The ^{88}Sr signal was then focused to a maximum intensity. At this stage, data was collected on X100 scale by using "short block" mode. Each "short block" contains background, ^{85}Rb , 4 pairs of ^{87}Sr and ^{86}Sr , background, ^{85}Rb , 4 pairs of ^{88}Sr and ^{86}Sr , followed by 4 pairs of ^{84}Sr and ^{86}Sr measurements. The computer then reports the $^{87}\text{Sr}/^{86}\text{Sr}$ and $^{84}\text{Sr}/^{86}\text{Sr}$ ratios, normalized to $^{88}\text{Sr}/^{86}\text{Sr} = 8.3752$ and corrected for natural Rb. After 4 to 6 blocks, a summary was made and the filament current increased to run on X10 scale using "long block" mode. In each "long block", background, ^{85}Rb , 5 pairs of ^{87}Sr and ^{86}Sr , background, and ^{85}Rb bracket 5 pairs of ^{88}Sr and ^{86}Sr measurements. This is followed by printout of ratios and statistics and then, optionally, further measurement of 5 pairs of ^{84}Sr and ^{86}Sr and printout of the normalized $^{84}\text{Sr}/^{86}\text{Sr}$ ratios. After 10 to 15 "long block" measurements, a summary for $^{87}\text{Sr}/^{86}\text{Sr}$ was done. Any block with ^{87}Rb correction to $^{87}\text{Sr} > 0.0009$ or with σ for $^{87}\text{Sr}/^{86}\text{Sr} > 0.0010$ was rejected.

(7). Blanks

Low blanks were essential for the determination of the extremely low concentrations of Rb and Sr in minerals of

ultramafic rocks. During the course of this work, 24 total Rb blanks and 30 total Sr blanks were measured. The results are given in Table 4-3 and Figures 4-3 and 4-4.

Comparisons of total Rb and Sr blanks with previous work in this lab and other labs are given in Table 4-4.

After May of 1984, using laminar flow hood for all evaporations and filament loading, using 2B HF, and taking HClO₄ directly from its teflon source bottle for sample digestion, the Rb and Sr blanks were reduced by a factor of 10.

Average total Rb blank was 0.26 ± 0.13 ng. Average total Sr blank was 3.3 ± 2.2 ng. Those values are above the levels achieved in the lunar-sample-oriented clean laboratories of C.I.T., U.C.S.D. and A.N.U. Nevertheless the UBC blank levels are comparable to the level of other good earth-sample-oriented labs, i.e. of Brueckner (1974, 1975), Basu (1978), Menzies & Murthy (1978) and Mengel et al. (1984). The average total Rb and Sr blanks and blank $^{87}\text{Sr}/^{86}\text{Sr}$ ratio (0.714 ± 0.016) were used for Rb and Sr blank corrections.

The lowest concentrations of Rb and Sr for Josephine Peridotite samples are 0.02 ppm Rb in clinopyroxene and 0.12 ppm Sr in olivine. The minimum quantity of Rb from 300 mg of clinopyroxene is 6 ng and Sr from 500 mg of olivine is 60 ng. Thus the largest blank corrections for Rb and Sr are about 5%. For the nodules, Rb and Sr blank corrections are less than 1%.

Table 4-3 Total Blanks

Date yr/mo/da	Rb blanks		Sr blanks		87Sr/86Sr comment	
	ng	nanomoles	ng	nanomoles		
84/4	3.3	0.04	11	0.127	0.718	**
	17	0.19	24	0.25	0.725	*
	32	0.37	39	0.41	0.717	*
	8.3	0.097	8	0.9	0.700	*
84/5/14	0.94	0.011	7.0	0.079	0.726	**
			6.8	0.078	0.777	*
84/6/13	0.12	0.0015	1.30	0.015	0.700	*
	0.27	0.0032	2.8	0.032	0.700	*
			9.1	0.10	0.708	**
84/6/19	0.40	0.0047	2.13	0.024	(0.68)	*
	0.36	0.0042	1.09	0.012	(0.692)	*
	0.27	0.0031	7.1	0.081	(0.691)	*
	0.20	0.0023	6.3	0.072	0.711	**
	0.27	0.0031	2.2	0.025	0.701	*
			5.8	0.067	0.718	**
		3.3	0.038	0.731	small column	
84/7/5	0.22	0.0026	1.56	0.018	0.752	*
	0.39	0.0046	(106)			* Sr abnormal
84/7/18			0.78	0.009	(0.65)	small column
			3.64	0.042	(0.808)	small column
84/7/27	(1.68)		3.98	0.045	0.709	* Rb abnormal
	0.36	0.0042	3.2	0.037	0.705	*
84/8/2	0.18	0.0021	1.19	0.018	0.712	*
84/8/17	0.44	0.0052	7.2	0.083	0.708	**
	0.45	0.0052	3.87	0.044	0.706	**
	0.24	0.0029	3.1	0.035	0.705	**
84/10/9	0.33	0.0038	1.6	0.012	0.716	**
	0.49	0.0057	1.1	0.018	0.714	**
84/12/19	0.11	0.0013	2.1	0.024	0.738	**
85/2/1	0.11	0.0013	2.2	0.025	0.747	**
85/5/24	0.12	0.0014	2.25	0.026	0.699	**
	0.09	0.0010	6.16	0.070	0.703	**
	0.12	0.0014	1.55	0.018	(0.683)	**
average	0.26	0.0031	3.3	0.038	0.714	abnormal blanks
after 84/5/14	±0.13	±0.0015	±2.2	±0.025	±0.016	excluded

comment: * - single column for Rb and Sr.

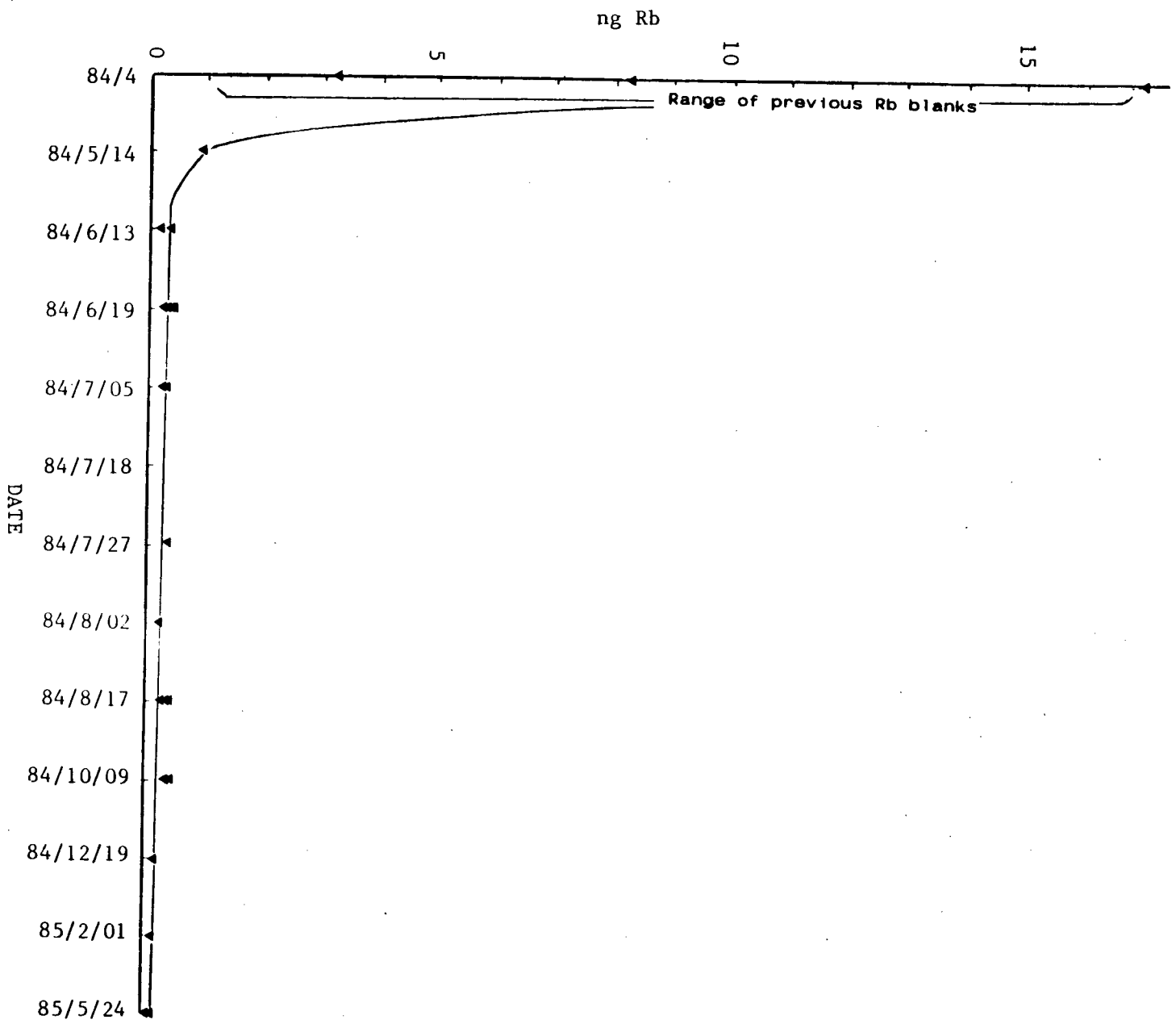
** - single column for Rb, double column for Sr.

Blanks in 84/4: using ordinary HF and HClO₄ from dropper bottler, evaporation in open air.

Blanks on 84/5/14: using 2B-HF and HClO₄ from dropperbottle, evaporation in laminar flow hood. planchette evaporation and filament loading in open air.

Blanks after 84/5/14: using 2B-HF and HClO₄ from source bottle, operation in laminar flow hood.

Fig. 4-3(a) Total Rb blanks



ng Sr

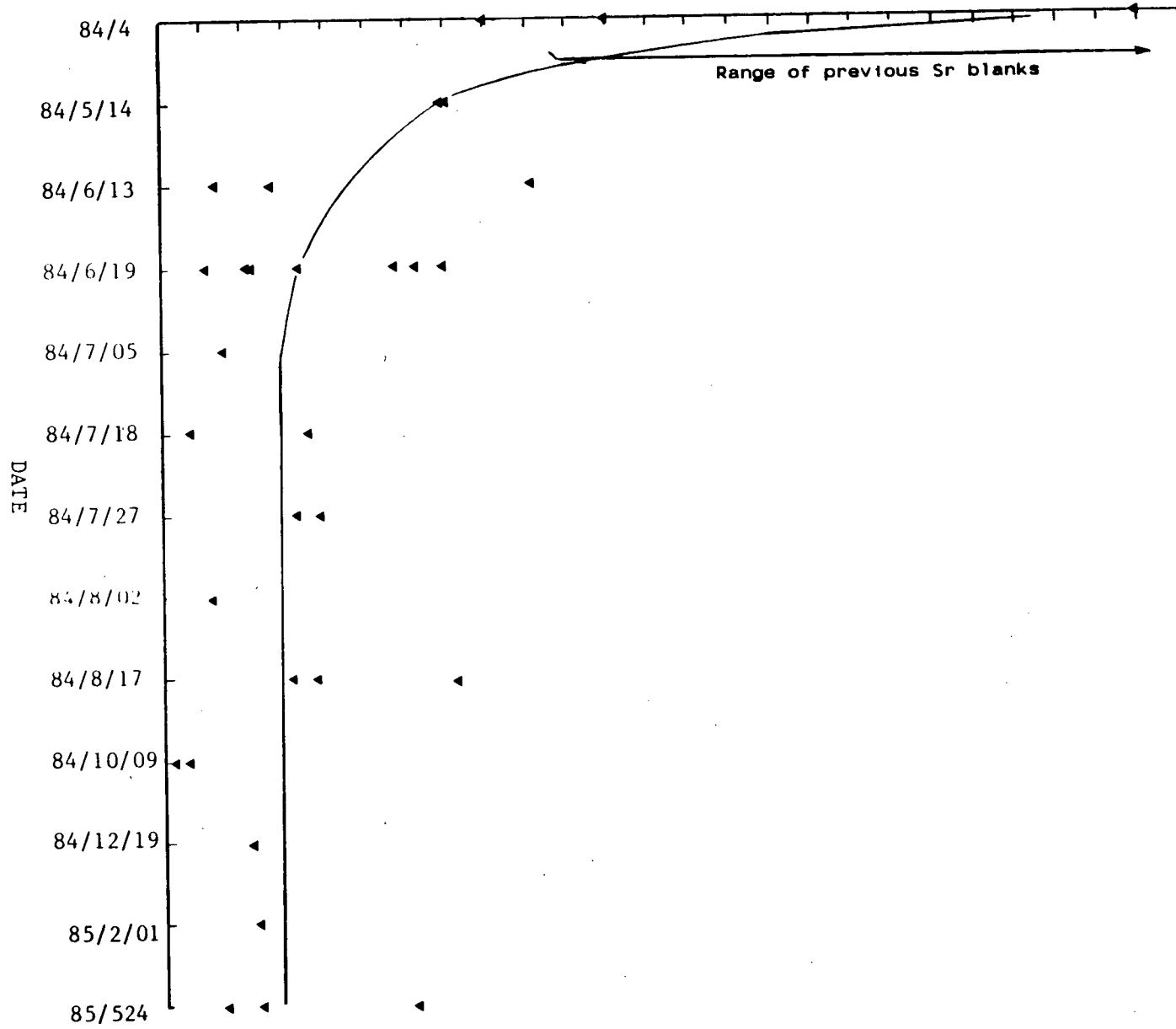


Fig. 4-3(b) Total Sr blanks

Table 4-4 Comparison of total blank with other labs

Lab	year	Rb blank(ng)	Sr blank(ng)	Data source
UBC	1984	0.3	3.4	This work
UBC	1976	1.7 - 8.9	14 - 34	Maxwell (1976)
Miami U.	1974	4 - 10	10 - 70	Steuber et al.(1974)
UCLA	1973	2	2	Mark et al. (1973)
C.I.T.	1973	0.02	0.2	Papanastassiou et.al. (1973)
ANU	1971	0.45 - 0.14	0.90 - 0.19	Compston et al.(1971)
WAIT	1970	10	100	DeLaeter et al.(1970)
Lamont	1974	0.3 - 0.07	1 - 10	Brueckner (1974)
Lamont	1975	0.3 - 0.07	1	Brueckner (1975)
UCSD	1980		0.2 - 0.5	Carlson (1980)
Minnesota	1978	0.1	1	Menzies et al.(1978)
G.I.G. Oxford	1984	0.1	2	Basu (1978) Mengel et al.(1984)
Polytec.	1975	0.8 - 1.0	0.7 - 1.4	Burwell (1975)
C.I.T.	1984		0.1	Jacobsen et al.(1984)
U. Paris	1978	0.015 - 0.059	0.045 - 0.117	Allègre et al. (1982)

Synthetic total blanks, calculated from 5 ml 2B-HF, 1ml HClO₄ and 10 ml 2.5N HCl, are 0.42 ng Rb and 3.4 ng Sr. The difference between calculated and lowest total blanks must be what is added in column step for reagent blanks. Since calculated blanks are greater than observed blanks by a small amount there must be a small column blank included in the reagent blanks. This means the "total blanks" are mainly from reagents, the column blank is less than 0.2 ng Rb and 1.0 ng Sr.

(8). Data reduction

Rb and Sr data reduction was done by a FORTRAN program "RBSR" revised from BASIC programs "RBSPK3" and "SRSPK3" (Appendix 5).

The total error (1σ), based on all uncertainties carried through the calculation is given by

$$\Delta F = \sqrt{\sum \left(\frac{\partial F}{\partial X_i} \Delta X_i \right)^2}, \text{ (Nunes, 1980)}$$

where ΔF is the final error, ΔX_i is the error in the i th variable, and $F = F(X_1, X_2, \dots, X_n)$

The computer performs the partial differentiation for each variable:

$$\frac{\partial F}{\partial X_i} = F(X_1, \dots, X_i + \Delta X_i, \dots, X_n) - F(X_1, \dots, X_i, \dots, X_n).$$

All errors listed in tables, text, or diagrams in this thesis are 1σ or standard error of the mean for averaged numbers.

(a). Rb data reduction

$$\text{Rb } \mu\text{moles} = C_{\text{sp}} \cdot W_{\text{sp}} \cdot (R_m \cdot P_t^{87} - P_t^{85}) / (P_s^{85} - R_m \cdot P_s^{87})$$

$$\text{Rb}(\mu\text{moles/gm})_{\text{sample}} = [\text{Rb}(\mu\text{moles}) - \text{Rb blank}(\mu\text{moles})] / (\text{sample weight})$$

$\text{Rb}(\text{ppm})_{\text{sample}} = \text{Rb}(\mu\text{moles/gm})_{\text{sample}} \cdot \text{atomic weight of Rb}$, where

R_m = measured $^{85}\text{Rb}/^{87}\text{Rb}$ ratio.

P_t^{87} = % abundance of ^{87}Rb in spike.

P_t^{85} = % abundance of ^{85}Rb in spike.

P_s^{87} = % natural abundance of ^{87}Rb .

P_s^{85} = % natural abundance of ^{85}Rb .

C_{sp} = spike concentration ($\mu\text{moles/gm}$).

W_{sp} = spike weight (grams).

(b). Sr data reduction

$^{88}\text{Sr}/^{86}\text{Sr}$ ratio was normalized to the natural $^{88}\text{Sr}/^{86}\text{Sr}$ ratio of 8.3752 during data collection. However ^{84}Sr spike contains ^{88}Sr and ^{86}Sr in a proportion significantly different from the natural $^{88}\text{Sr}/^{86}\text{Sr}$ ratio. To obtain true $^{84}\text{Sr}/^{86}\text{Sr}$ and $^{87}\text{Sr}/^{86}\text{Sr}$ ratios of the sample-spike mixture,

the $^{88}\text{Sr}/^{86}\text{Sr}$ ratio was renormalized iteratively by a factor derived from $(^{88}\text{Sr}/^{86}\text{Sr})_{\text{calc}} / (^{88}\text{Sr}/^{86}\text{Sr})_{\text{meas}}$ ratio. The iteration was stopped when

$$\left[(^{88}\text{Sr}/^{86}\text{Sr})_{\text{calc}} / (^{88}\text{Sr}/^{86}\text{Sr})_{\text{meas}} \right]_i - \left[(^{88}\text{Sr}/^{86}\text{Sr})_{\text{calc}} / (^{88}\text{Sr}/^{86}\text{Sr})_{\text{meas}} \right]_{i-1} < 0.000001.$$

Sr concentration was then calculated using formulae similar to those used for Rb. The total error for Sr was evaluated in the same manner as for Rb. A common Sr atomic weight of 87.62 was used for Sr ppm calculation.

(9). N.B.S. standard SRM987 measurements

The value for the N.B.S. standard SRM987 $^{87}\text{Sr}/^{86}\text{Sr}$ is taken to be 0.71020, an average of the values reported by several labs. Actual measurements during this work gave an average value of $^{87}\text{Sr}/^{86}\text{Sr} = 0.71017 \pm 0.00004$ (Table 4-5). Accordingly, all the $^{87}\text{Sr}/^{86}\text{Sr}$ ratios reported in this work have been adjusted by adding a factor of 0.00003.

(10). Isochron calculation and plot

A revised YORK REGRESSION program was used for Rb-Sr isochron slope, intercept and the date calculation (Appendix 6-a). $^{87}\text{Rb}/^{86}\text{Sr}$ and $^{87}\text{Sr}/^{86}\text{Sr}$ and their one sigma errors were read from the output of data reduction program "RBSR". Sample data points with one sigma error bars were plotted by using a FORTRAN program "PLRBSR" (Appendix 6-b).

Table 4-5 $^{87}\text{Sr}/^{86}\text{Sr}$ ratios of N.B.S. SRM-987
(K.Scott, pers. comm., 1985)

Date(yr/mo/da)	No. of Blocks	$^{87}\text{Sr}/^{86}\text{Sr}$	+/-
1984/8/8	6	0.71002	0.00012
	15	0.71016	0.00010
	15	0.70967	0.00018
	9	0.71007	0.00009
	13	0.71032	0.00005
	18	0.71026	0.00009
1984/9/11	16	0.71028	0.00009
	18	0.71017	0.00007
	16	0.71030	0.00008
	17	0.71017	0.00009
	16	0.70999	0.00013
	15	0.71017	0.00013
1984/10/10	34	0.71022	0.00006
1984/11/12	40	0.71018	0.00012
1985/1/3	18	0.71017	0.00007
	18	0.71007	0.00005
	19	0.71007	0.00005
	19	0.71021	0.00005
	16	0.71014	0.00004
	18	0.71023	0.00005
1985/3/29	9	0.71013	0.00004
	10	0.71020	0.00007
1985/4/15	18	0.71022	0.00006
	16	0.71017	0.00003
	18	0.71018	0.00002
	19	0.71020	0.00002
1985/5/22	17	0.71019	0.00005
	19	0.71022	0.00006
	19	0.71015	0.00005
	18	0.71014	0.00004
	17	0.71023	0.00003
	18	0.71021	0.00003

Average value = 0.71017 +/- 0.00004 weighted by number of analyses and individual errors.

V. Rb-Sr ISOTOPE RESULTS

V-1. Nodules and host basalts

Olivine, orthopyroxene and clinopyroxene mineral separates, whole rock, and acid leach material from 12 nodules have been analysed for Rb and Sr concentration and Sr isotope composition. Of these, 4 nodules are from Jacques Lake, 3 from Big Timothy Mountain, 3 from West Kettle River, and 2 from Lassie Lake.

Eleven host basalts were also analysed (Table 5-1).

Some samples have been repeatedly analysed during this work. The reproducibility for Rb is 1-2%, for Sr about 5%, for $^{87}\text{Sr}/^{86}\text{Sr}$ 0.0005, and for $^{87}\text{Rb}/^{86}\text{Sr}$ <6% (Appendix 7). For these samples, weighted mean values are used for further discussion, the mean value uncertainty was calculated by Nunes' equation (see IV-2-(8)).

A number of mineral isochrons are defined.

(1). Jacques Lake

Jacques Lake nodule (JL1, JL14, JL15 and JL18) mineral isochrons are shown on Figures 5-1, 5-2, 5-3 and 5-4. The data are listed in Table 5-2.

(2). Big Timothy Mountain

Big Timothy Mountain nodule (BM11, BM16 and BM55) mineral isochrons are shown on Figures 5-5, 5-6, and 5-7. The data are listed in Table 5-3.

(3). West Kettle River

West Kettle River nodule (KR1, KR2, and KR35) mineral isochrons are shown on Figures 5-8, 5-9, and 5-10. The data are listed in Table 5-4.

(4). Lassie Lake

Lassie Lake nodule (LL1 and LL14) mineral isochrons are shown on Figures 5-11, and 5-12. The data are listed in Table 5-5.

V-2. Josephine Peridotite

Mineral separates from 4 samples (JM5, JM14, JM15 and JM2) have been analysed. The data are listed in Table 5-6. Mineral isochrons are shown on Figure 5-13, 5-14, and 5-15.

For comparison, the mineral isochrons are summarized in Table 5-7.

Table 5-1 Rb-Sr data of host and associated basalts

Samples	Rb ppm	+/-	Sr ppm	+/-	87Sr/86Sr	+/-	87Rb/86Sr	+/-
JL14 BAST	12.7	0.1	1297	16	0.70254	0.00014	0.028	0.001
BM11 BAST	54.9	1.8	1514	51	0.70264	0.00010	0.105	0.005
BM55 BAST	45.5	2.8	1276	33	0.70272	0.00006	0.103	0.007
BM26 BAST	62.1	0.1	1303	6	0.70269	0.00004	0.138	0.001
KR B-1	17.1	0.5	859	19	0.70318	0.00009	0.058	0.001
KR B-2	17.2	0.5	712	4	0.70360	0.00014	0.070	0.001
KR B-3	17.5	0.2	642	19	0.70291	0.00005	0.079	0.002
KR B-4	30.4	0.6	951	9	0.70289	0.00014	0.092	0.001
KR35 BAST	21.5	1.6	842	23	0.70262	0.00012	0.074	0.006
LL1 BAST	31.8	0.4	840	8	0.70330	0.00011	0.110	0.001
LL14 BAST	18.5	0.8	702	34	0.70238	0.00005	0.076	0.005

Table 5-2 Rb-Sr isotope data of Jacques Lake nodules

Samples	Rb ppm	+/-	Sr ppm	+/-	87Sr/86Sr	+/-	87Rb/86Sr	+/-
JL18								
Acid leach	1.22	0.02	78.9	0.8	0.7029	0.0003	0.0447	0.0007
Whole rock	0.252	0.001	38.5	0.3	0.7024	0.0002	0.0191	0.0002
Syn. wr	0.208	0.001	40.6	0.1	0.7026	0.0001	0.0148	0.0001
Diopside	0.348	0.003	238.7	0.9	0.7026	0.0001	0.00421	0.00004
Enstatite	0.259	0.002	4.20	0.02	0.7034	0.0004	0.178	0.002
Olivine	0.153	0.001	2.32	0.01	0.7036	0.0006	0.191	0.002
JL15								
Acid leach	0.546	0.005	7.65	0.02	0.7030	0.0004	0.206	0.002
Whole rock	0.0958	0.0007	8.95	0.03	0.7029	0.0001	0.0310	0.0003
Syn. wr	0.161	0.001	9.58	0.05	0.7029	0.0001	0.0485	0.0004
Diopside	0.281	0.003	54.3	0.3	0.7026	0.0001	0.0150	0.0002
Enstatite	0.260	0.002	2.76	0.01	0.7051	0.0009	0.273	0.003
Olivine	0.0842	0.0009	0.325	0.007	0.7086	0.0004	0.749	0.017
JL14								
Acid leach	1.76	0.03	31.7	0.1	0.7031	0.0004	0.161	0.003
Whole rock	0.179	0.001	8.44	0.04	0.7030	0.0003	0.0613	0.0005
Syn. wr	0.146	0.001	6.82	0.02	0.7028	0.0001	0.0619	0.0001
Diopside	0.154	0.001	32.1	0.1	0.7025	0.0001	0.0139	0.0001
Enstatite	0.191	0.002	1.26	0.01	0.7051	0.0005	0.438	0.005
Olivine	0.104	0.001	0.624	0.005	0.7056	0.00045	0.483	0.005
JL1								
Syn. wr	0.0912	0.0002	13.2	0.1	0.7030	0.0002	0.0200	0.0002
Diopside	0.125	0.002	76.5	0.4	0.7029	0.0002	0.00475	0.00008
Enstatite	0.0191	0.0006	2.81	0.02	0.7029	0.0002	0.0197	0.0006
Olivine	0.116	0.001	0.344	0.007	0.7106	0.0006	0.977	0.021

Table 5-3 Rb-Sr isotope data of Big Timothy Mountain nodules

Samples	Rb ppm	+/-	Sr ppm	+/-	$^{87}\text{Sr}/^{86}\text{Sr}$	+/-	$^{87}\text{Rb}/^{86}\text{Sr}$	+/-
BM11								
Acid leach	2.79	0.0634	11.25	0.03	0.7033	0.0001	0.718	0.016
Whole rock	1.13	0.01	25.6	0.2	0.7028	0.0001	0.128	0.002
Syn. wr	0.410	0.002	9.06	0.02	0.7033	0.0001	0.131	0.001
Diopside	0.609	0.005	54.7	0.2	0.7029	0.0001	0.0322	0.0003
Enstatite	0.936	0.007	10.40	0.03	0.7036	0.0004	0.260	0.002
Olivine	0.232	0.002	3.52	0.02	0.7036	0.0002	0.191	0.002
BM16								
Acid leach	0.716	0.009	3.66	0.01	0.7044	0.0002	0.565	0.007
Whole rock	0.280	0.006	4.61	0.02	0.7035	0.0001	0.176	0.004
Syn. wr	0.113	0.001	3.49	0.01	0.7039	0.0005	0.0932	0.0006
Diopside	0.160	0.001	10.25	0.03	0.7027	0.0005	0.0451	0.0004
Enstatite	0.0730	0.0006	0.408	0.008	0.7157	0.0009	0.519	0.011
Olivine	0.102	0.001	0.457	0.007	0.7153	0.0004	0.641	0.011
BM55								
Acid leach	2.84	0.06	10.25	0.03	0.7033	0.0002	0.802	0.016
Whole rock	0.326	0.010	11.7	0.3	0.7027	0.0001	0.0818	0.0015
Syn. wr	0.159	0.001	10.73	0.02	0.7035	0.0002	0.0429	0.0002
Diopside	0.140	0.001	33.45	0.07	0.7033	0.0002	0.0119	0.0001
Enstatite	0.252	0.001	0.749	0.005	0.7086	0.0003	0.975	0.008
Olivine	0.0701	0.0004	0.260	0.005	0.7084	0.0005	0.826	0.020

Table 5-4 Rb-Sr isotope data of West Kettle River nodules

Samples	Rb ppm	+/-	Sr ppm	+/-	$^{87}\text{Sr}/^{86}\text{Sr}$	+/-	$^{87}\text{Rb}/^{86}\text{Sr}$	+/-
KR35								
Acid leach	0.253	0.003	4.28	0.01	0.7053	0.0001	0.171	0.002
Whole rock	0.125	0.001	10.53	0.09	0.7022	0.0001	0.0343	0.0004
Syn. wr	0.158	0.001	9.39	0.04	0.7029	0.0002	0.0486	0.0003
Diopside	0.278	0.002	55.6	0.2	0.7022	0.0003	0.0144	0.0001
Enstatite	0.192	0.002	0.931	0.054	0.7140	0.0003	0.597	0.035
Olivine	0.100	0.001	0.369	0.008	0.7197	0.0004	0.795	0.018
KR 1								
Acid leach	0.293	0.002	1.475	0.007	0.7067	0.0006	0.574	0.005
Whole rock	0.385	0.0051	4.33	0.03	0.7040	0.0002	0.261	0.004
Syn. wr	0.111	0.001	2.85	0.02	0.7037	0.0002	0.113	0.001
Diopside	0.149	0.003	24.5	0.1	0.7031	0.0002	0.0176	0.0004
Enstatite	0.139	0.001	0.288	0.009	0.7147	0.0002	1.40	0.04
Olivine	0.0994	0.0008	0.145	0.008	0.7162	0.0003	1.99	0.11
KR 2								
Acid leach	0.164	0.001	6.16	0.03	0.7055	0.0006	0.0768	0.0008
Whole rock	0.272	0.002	9.41	0.03	0.7037	0.0001	0.0837	0.0007
Syn. wr	0.0982	0.0005	0.761	0.006	0.7058	0.0003	0.373	0.004
Diopside	0.162	0.003	9.31	0.03	0.7032	0.0003	0.0502	0.0008
Enstatite	0.122	0.001	0.416	0.009	0.7123	0.0006	0.848	0.020
Olivine	0.0797	0.0007	0.112	0.008	0.7142	0.0001	2.06	0.15

Table 5-5 Rb-Sr isotope data of Lassie Lake nodules

Samples	Rb ppm	+/-	Sr ppm	+/-	$^{87}\text{Sr}/^{86}\text{Sr}$	+/-	$^{87}\text{Rb}/^{86}\text{Sr}$	+/-
LL 1								
Acid leach	2.87	0.02	56.3	0.2	0.7045	0.0003	0.147	0.001
Whole rock	6.05	0.13	51.1	1.3	0.7036	0.0002	0.342	0.011
Syn. wr	0.957	0.006	16.9	0.1	0.7031	0.0002	0.164	0.001
Diopside	3.47	0.03	98.5	0.4	0.7030	0.0002	0.102	0.001
Enstatite	1.05	0.01	2.93	0.02	0.7043	0.0001	1.02	0.01
Olivine	0.274	0.002	0.798	0.008	0.7047	0.0004	0.995	0.013
LL14								
Acid leach	3.24	0.13	41.0	0.6	0.7047	0.0002	0.235	0.004
Whole rock	0.769	0.007	8.77	0.04	0.7037	0.0001	0.254	0.003
Syn. wr	0.197	0.001	10.79	0.03	0.7042	0.0002	0.0528	0.0004
Diopside	0.233	0.002	16.9	0.05	0.7041	0.0002	0.0398	0.0004
Enstatite	0.154	0.001	0.797	0.007	0.7089	0.0003	0.560	0.006
Olivine	0.0546	0.0005	0.498	0.006	0.7074	0.0020	0.317	0.005

Table 5-6 Rb-Sr isotope data of Josephine Peridotite

Samples	Rb ppm	+/-	Sr ppm	+/-	$^{87}\text{Sr}/^{86}\text{Sr}$	+/-	$^{87}\text{Rb}/^{86}\text{Sr}$	+/-
JM14								
Syn. wr	0.0918	0.0008	0.449	0.008	0.7073	0.0005	0.592	0.012
Diopside	0.0761	0.0011	0.582	0.028	0.7063	0.0015	0.379	0.014
Enstatite	0.0733	0.001	0.825	0.024	0.7053	0.0008	0.257	0.008
Olivine-1	0.116	0.001	0.283	0.006	0.7111	0.0009	1.19	0.03
Olivine-2	0.084	0.001	0.305	0.009	0.7089	0.0004	0.80	0.01
JM2								
Enstatite	0.0322	0.0003	0.130	0.008	0.7087	0.0015	0.784	0.032
JM15								
Syn. wr	0.0525	0.0006	0.143	0.010	0.7091	0.0011	1.07	0.07
Diopside	0.0233	0.0007	0.256	0.012	0.7054	0.0005	0.230	0.030
Enstatite	0.0293	0.0007	0.126	0.015	0.7064	0.0020	0.676	0.082
Olivine	0.0912	0.0013	0.153	0.015	0.7133	0.0008	1.73	0.2
JM 5								
Syn. wr	0.116	0.001	0.323	0.008	0.7095	0.0011	1.04	0.03
Diopside	0.0557	0.0015	0.456	0.015	0.7056	0.0005	0.348	0.012
Enstatite	0.1518	0.0012	0.418	0.006	0.7099	0.0006	1.05	0.02
Olivine	0.102	0.001	0.267	0.013	0.7096	0.0031	1.10	0.05

Table 5-7 Summary of mineral isochrons

Sample (87Sr/86Sr) +/-	Date(Ma) +/-		Petrology		Texture	Chemistry	Depth(km)
JL1	0.7028	0.0001	560	47	Lherzolite	Protogranular	
JL14	0.7024	0.0001	450	55	Lherzolite	Protogranular	Undepleted 46
JL15	0.7025	0.0001	576	41	Lherzolite	Protogranular	Undepleted <JL14
JL18	0.7026	0.0001	341	137	Lherzolite	Protogranular	Undepleted <JL15
BM11	0.7028	0.0001	276	82	Lherzolite	Protogranular	Depleted <BM16
BM16	0.7019	0.0016	1518	241	Oliv-Lherz	Equigranular	Undepleted 30
BM55	0.7032	0.0002	396	27	Oliv-Lherz	Protogranular	Undepleted >BM16
KR1	0.7030	0.0007	561	63	Lherzolite	Proto-porph	Depleted 40
KR2	0.7028	0.0001	792	58	Lherzolite	Porphyroclastic	Depleted 49
KR35	0.7018	0.0001	1537	74	Lherzolite	Equigranular	Undepleted 33
LL1	0.7029	0.0002	101	18	Lherzolite	Protogranular	Depleted 46
LL14	0.7037	0.0002	645	50	Lherzolite	Protogranular	Depleted 52
JM5	0.7035	0.0008	428	78	Harzburgite	Protogranular	Depleted
JM14	0.7038	0.0009	441	85	Harzburgite	Porphyroclastic	Depleted 35-63
JM15	0.7041	0.0006	366	64	Oliv-Harzb.	Protogranular	Depleted

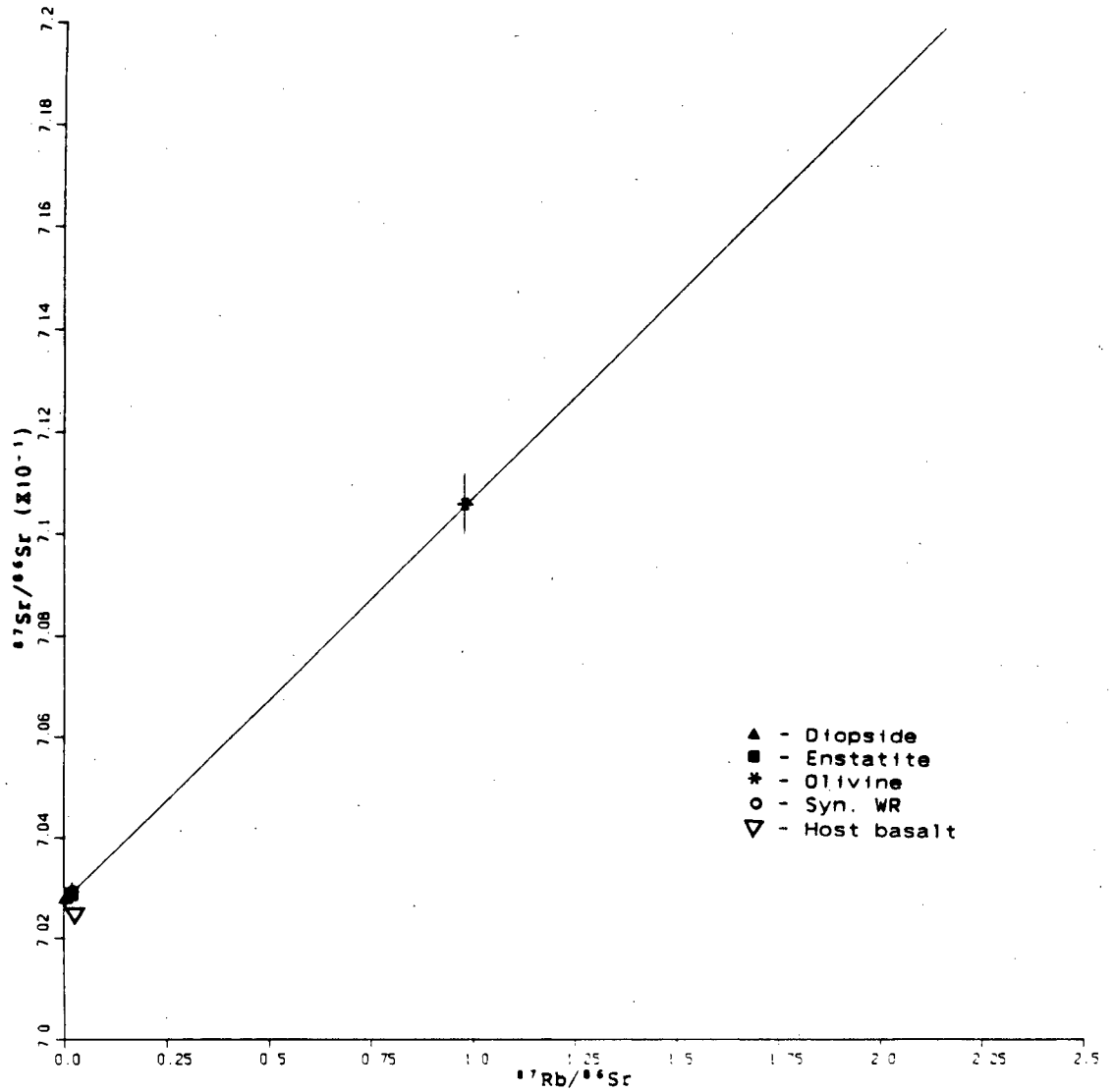


Fig. 5-1 JL1 mineral isochron defined by Di, En, Ol.
 $(^{87}\text{Sr}/^{86}\text{Sr})_0 = 0.7028 \pm 0.0001$, slope = 0.0080 ± 0.0007
 Rb-Sr date = 559 ± 47 Ma.

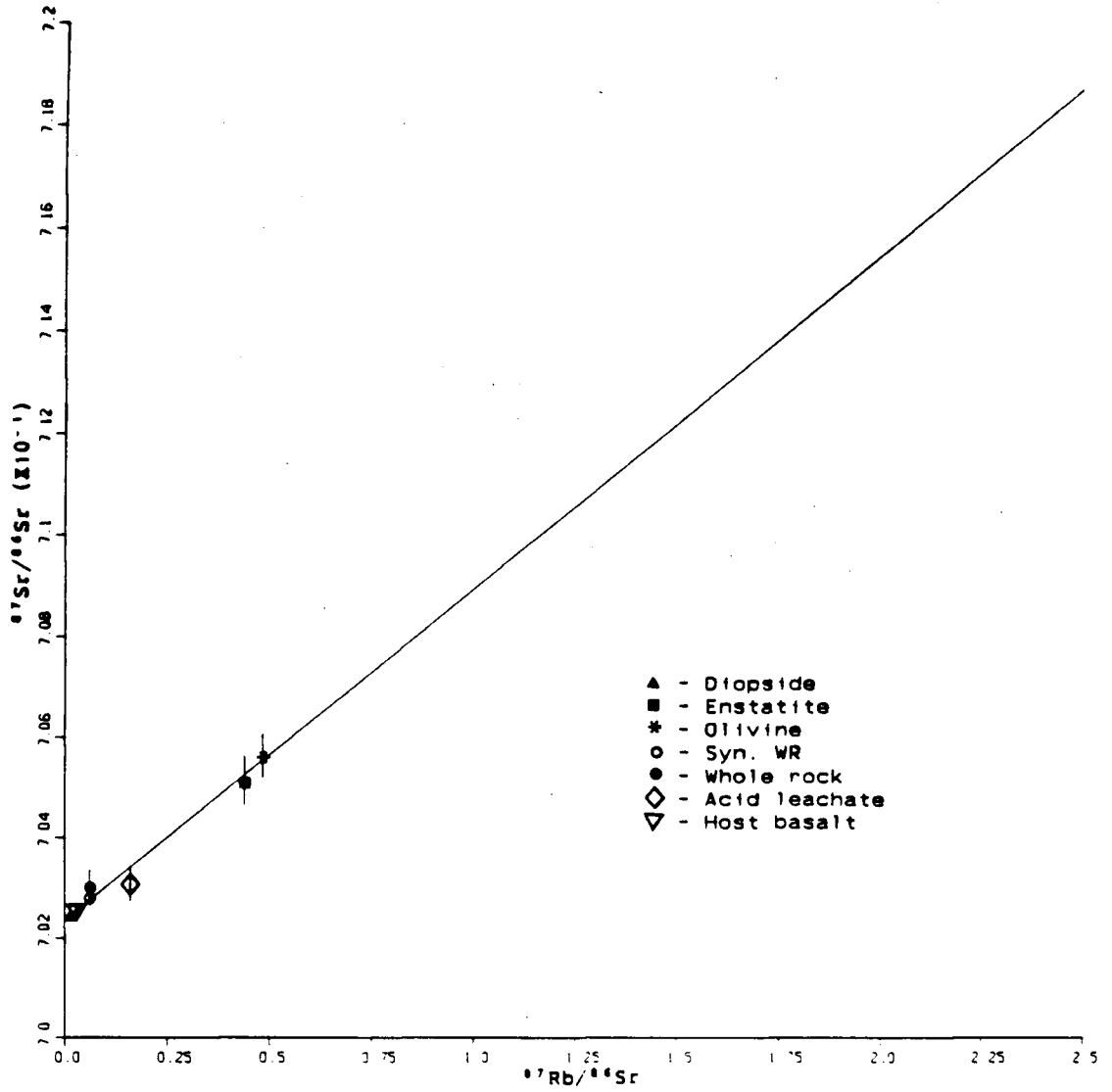


Fig. 5-2 JL14 mineral isochron defined by WR, Di, En, Ol.
 $(^{87}\text{Sr}/^{86}\text{Sr})_0 = 0.7024 \pm 0.0001$, slope = 0.0064 ± 0.0008
 Rb-Sr date = 450 ± 55 Ma.

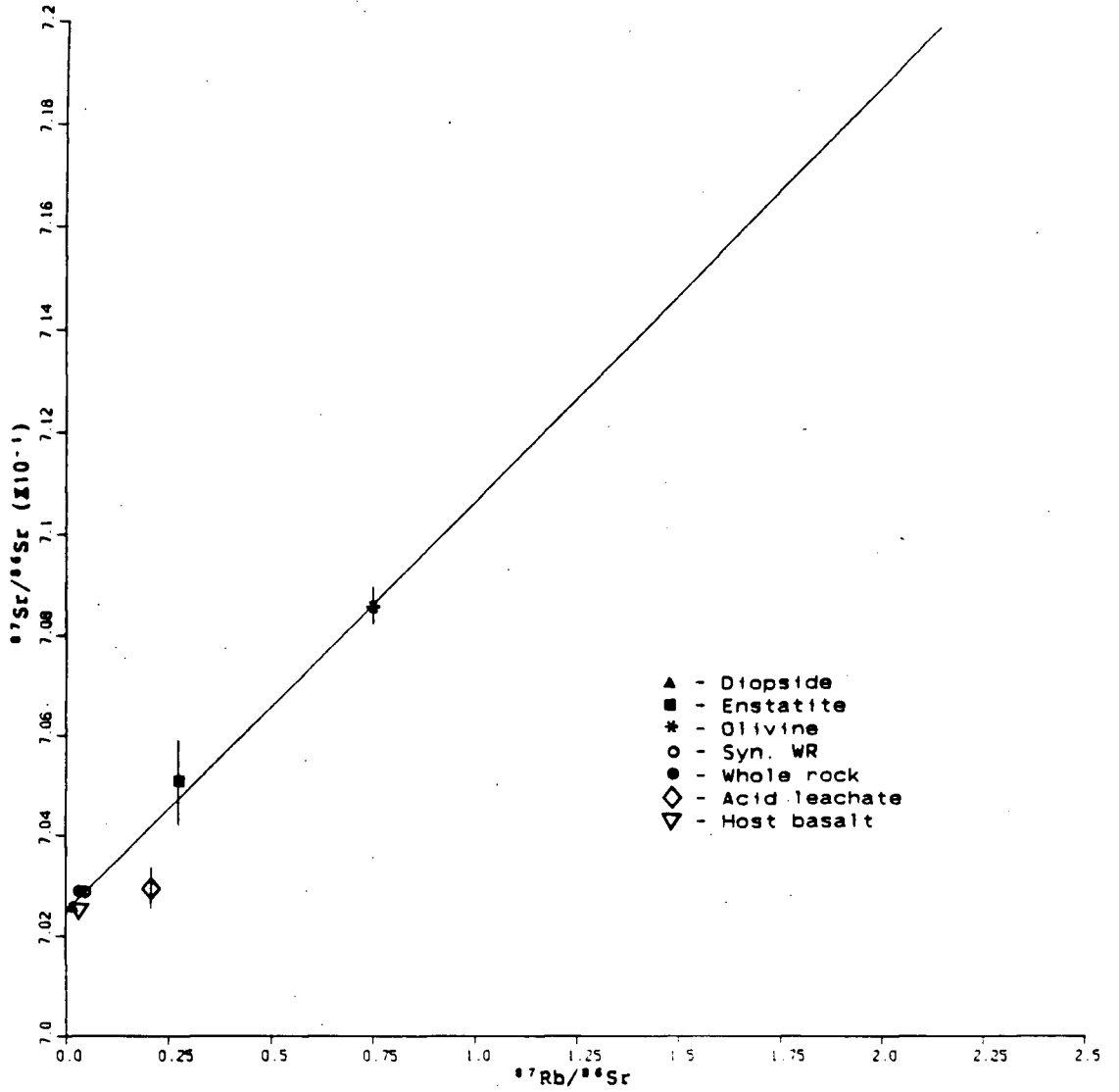


Fig. 5-3 JL15 mineral isochron defined by WR, Di, En, Ol.
 $(^{87}\text{Sr}/^{86}\text{Sr})_0 = 0.7025 \pm 0.0001$, slope = 0.0082 ± 0.0005
 Rb-Sr date = 576 ± 41 Ma.

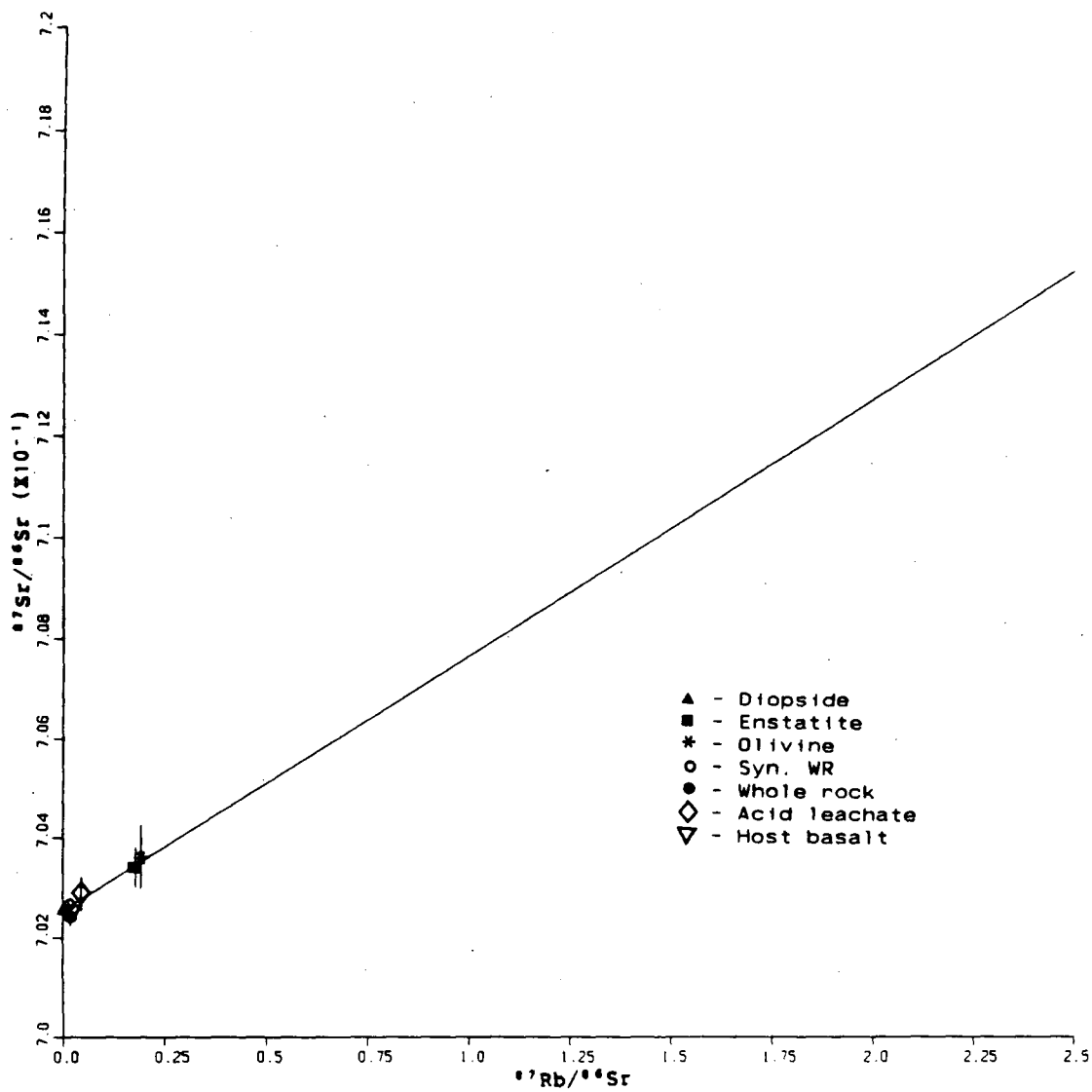


Fig. 5-4 JL18 mineral isochron defined by Di, En, Ol.
 $(^{87}\text{Sr}/^{86}\text{Sr})_0 = 0.7026 \pm 0.0001$, slope = 0.0049 ± 0.0019
 Rb-Sr date = 341 ± 137 Ma.

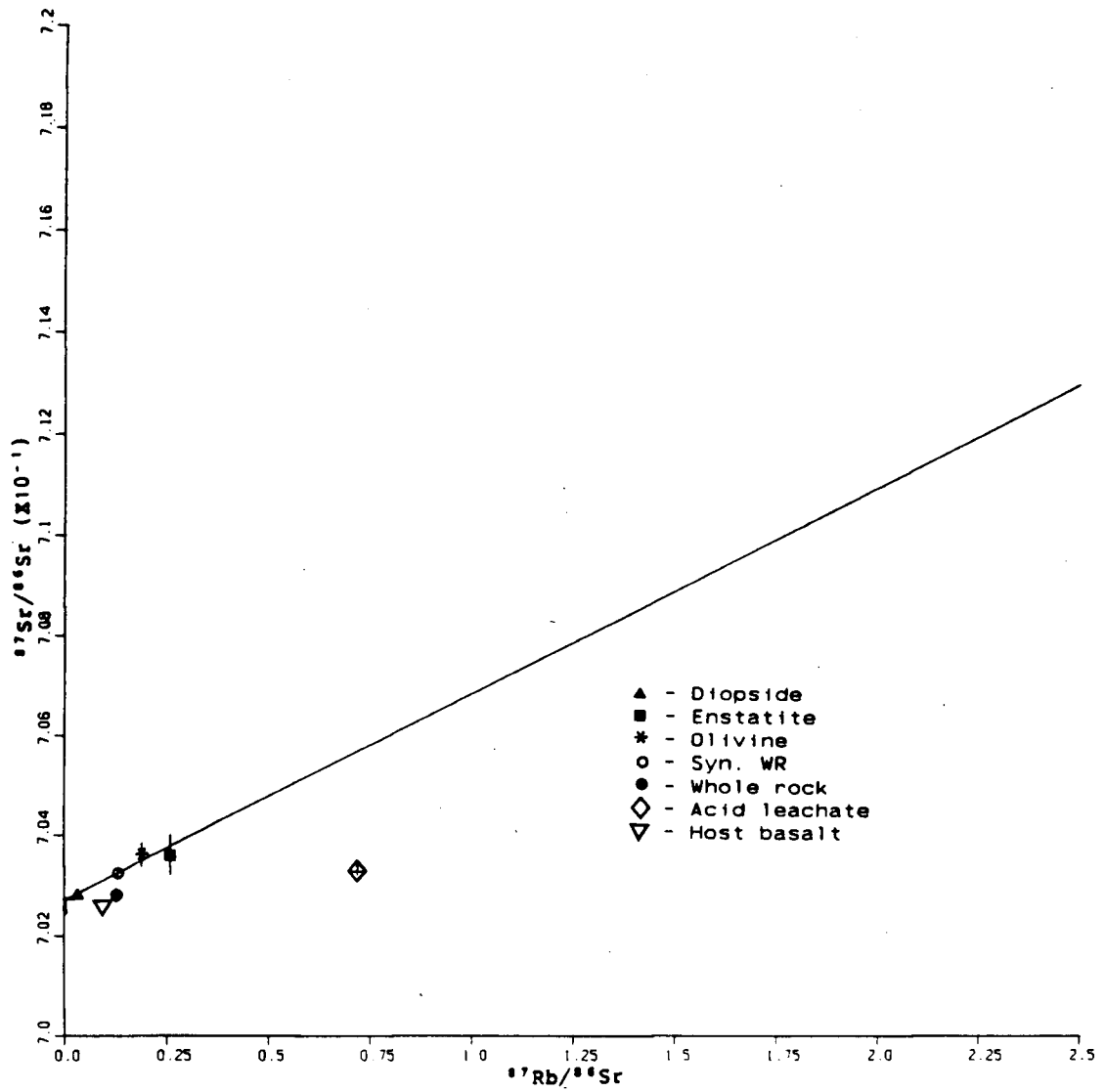


Fig. 5-5 BM11 mineral isochron defined by Di, En, Ol.
 $(^{87}\text{Sr}/^{86}\text{Sr})_0 = 0.7028 \pm 0.0001$, slope = 0.0039 ± 0.0009
 Rb-Sr date = 275 ± 82 Ma.

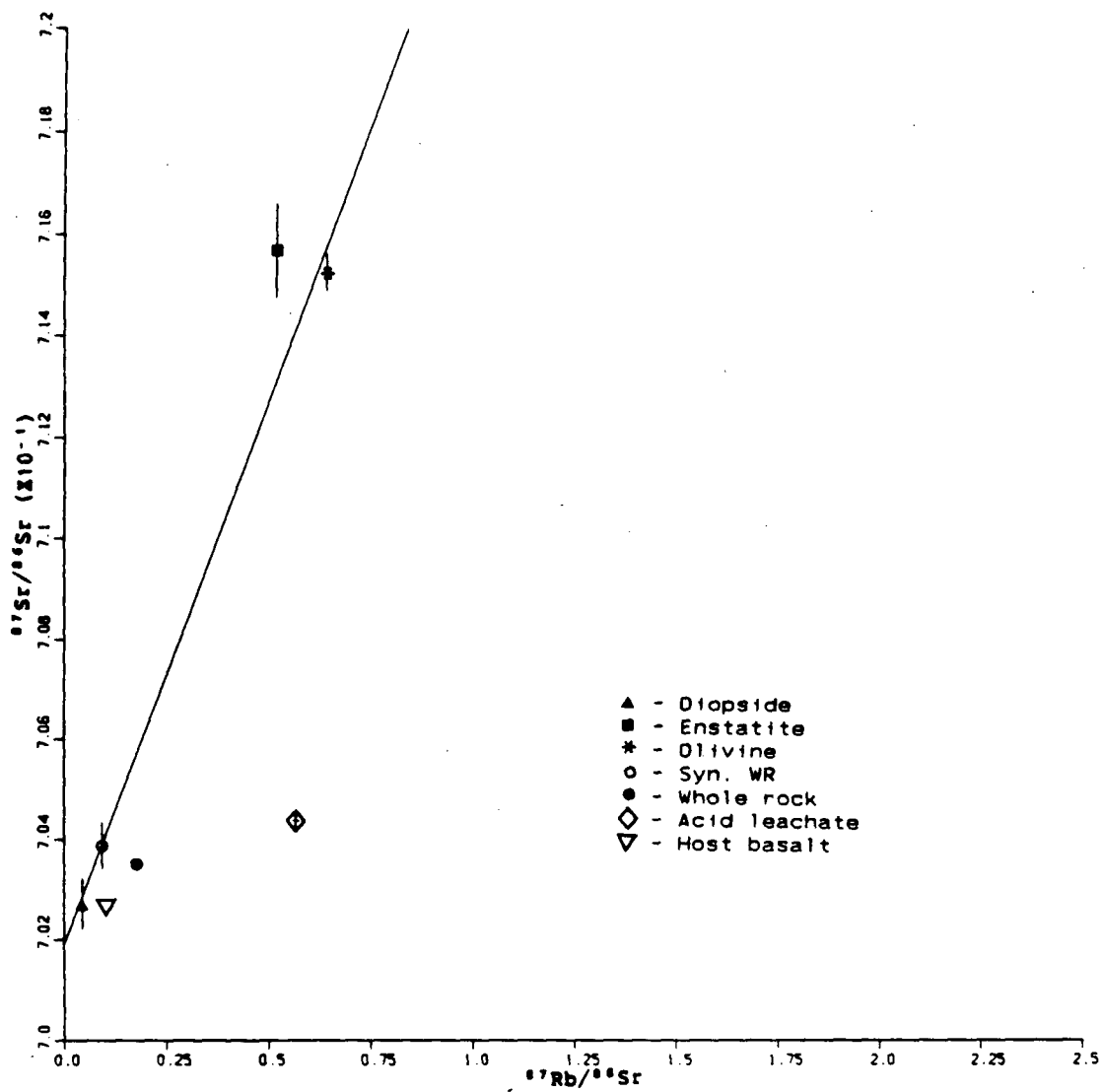


Fig. 5-6 BM16 mineral isochron defined by Di, En, Ol.
 $(^{87}\text{Sr}/^{86}\text{Sr})_0 = 0.7019 \pm 0.0012$, slope = 0.0218 ± 0.0009
 Rb-Sr date = 1518 ± 241 Ma.

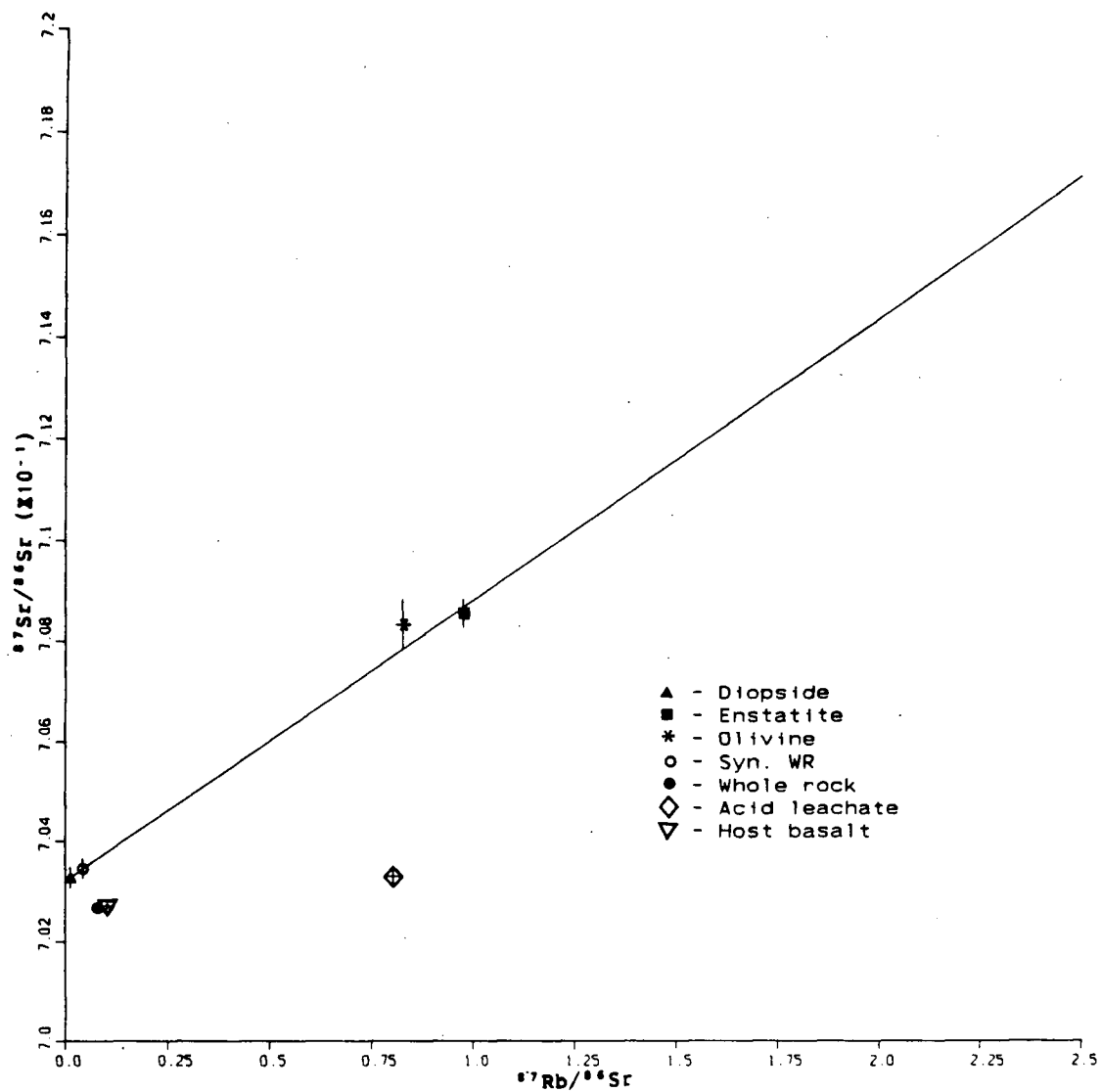


Fig. 5-7 BM55 mineral isochron defined by Di, En, O1.
 $(^{87}\text{Sr}/^{86}\text{Sr})_0 = 0.7032 \pm 0.0002$, slope = 0.0056 ± 0.0003
 Rb-Sr date = 396 ± 27 Ma.

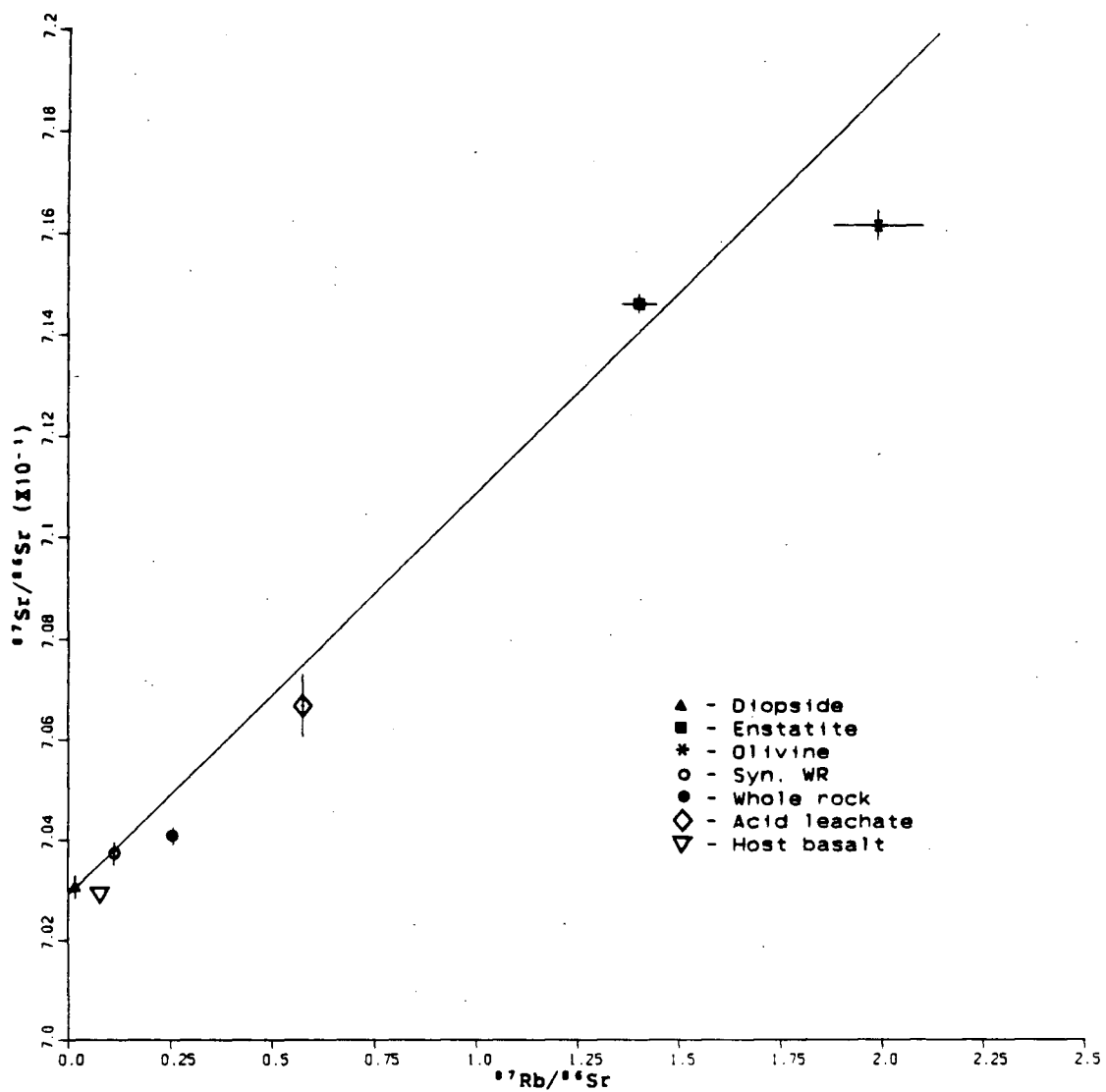


Fig. 5-8 KR1 mineral isochron defined by Di, En, Ol.
 $(^{87}\text{Sr}/^{86}\text{Sr})_0 = 0.7030 \pm 0.0007$, slope = 0.0080 ± 0.0003
 Rb-Sr date = 561 ± 63 Ma.

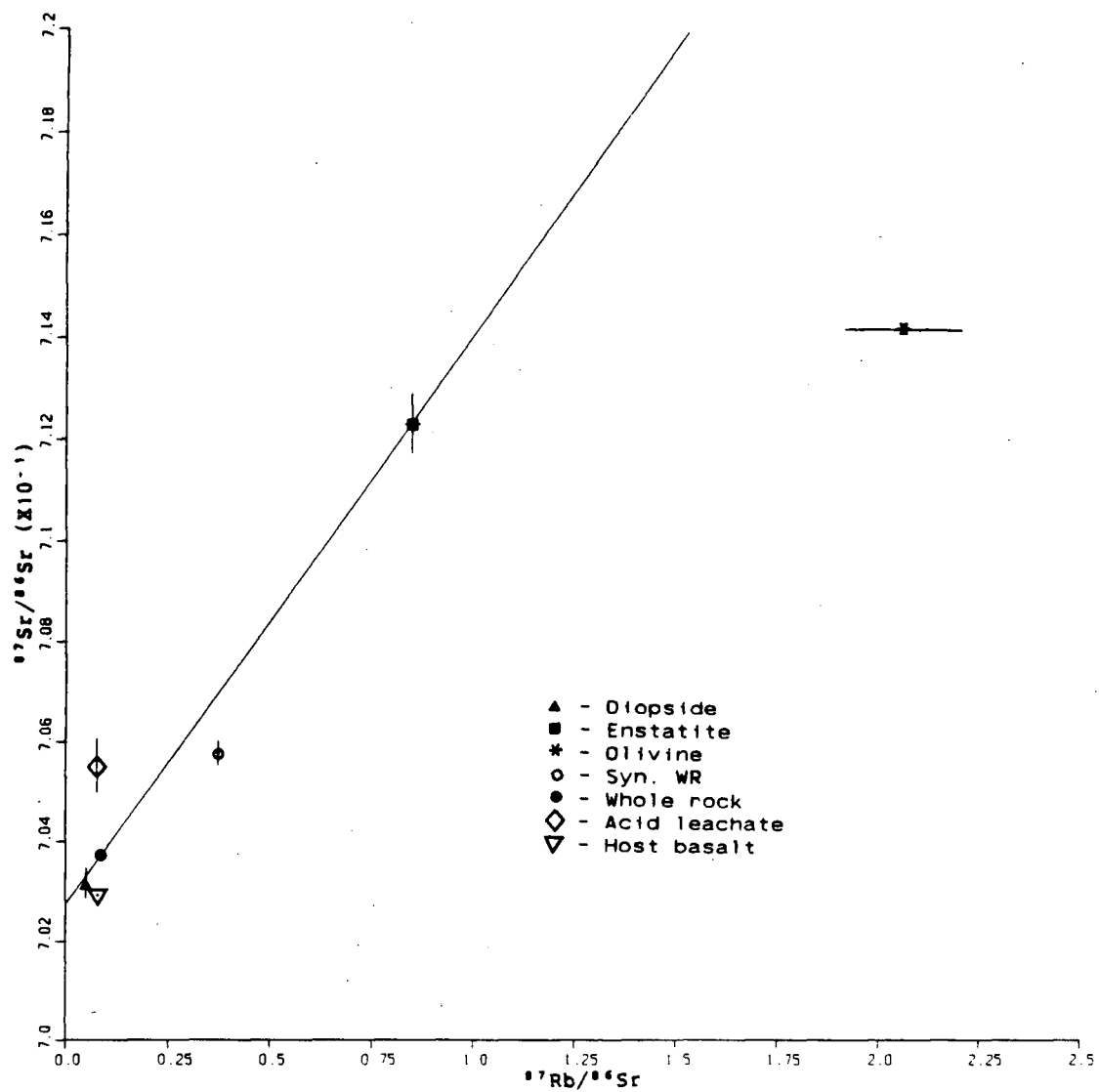


Fig. 5-9 KR2 mineral isochron defined by WR, Di, En.
 $(^{87}\text{Sr}/^{86}\text{Sr})_0 = 0.7028 \pm 0.0001$, slope = 0.0113 ± 0.0008
 Rb-Sr date = 792 ± 58 Ma.

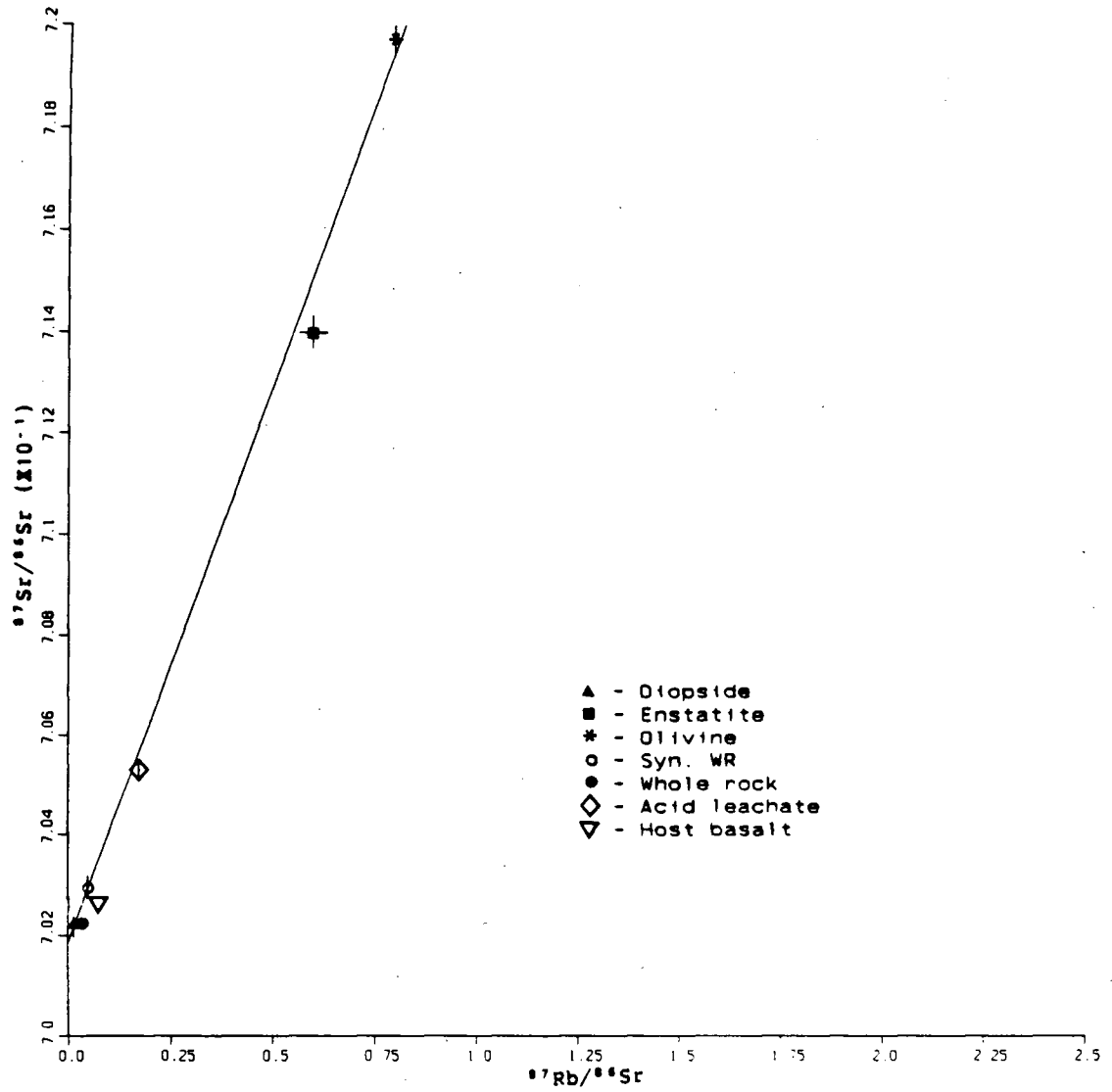


Fig. 5-10 KR35 mineral isochron defined by WR, Di, En, Ol.
 $(^{87}\text{Sr}/^{86}\text{Sr})_0 = 0.7018 \pm 0.0004$, slope = 0.0221 ± 0.0007
 Rb-Sr date = 1537 ± 74 Ma.

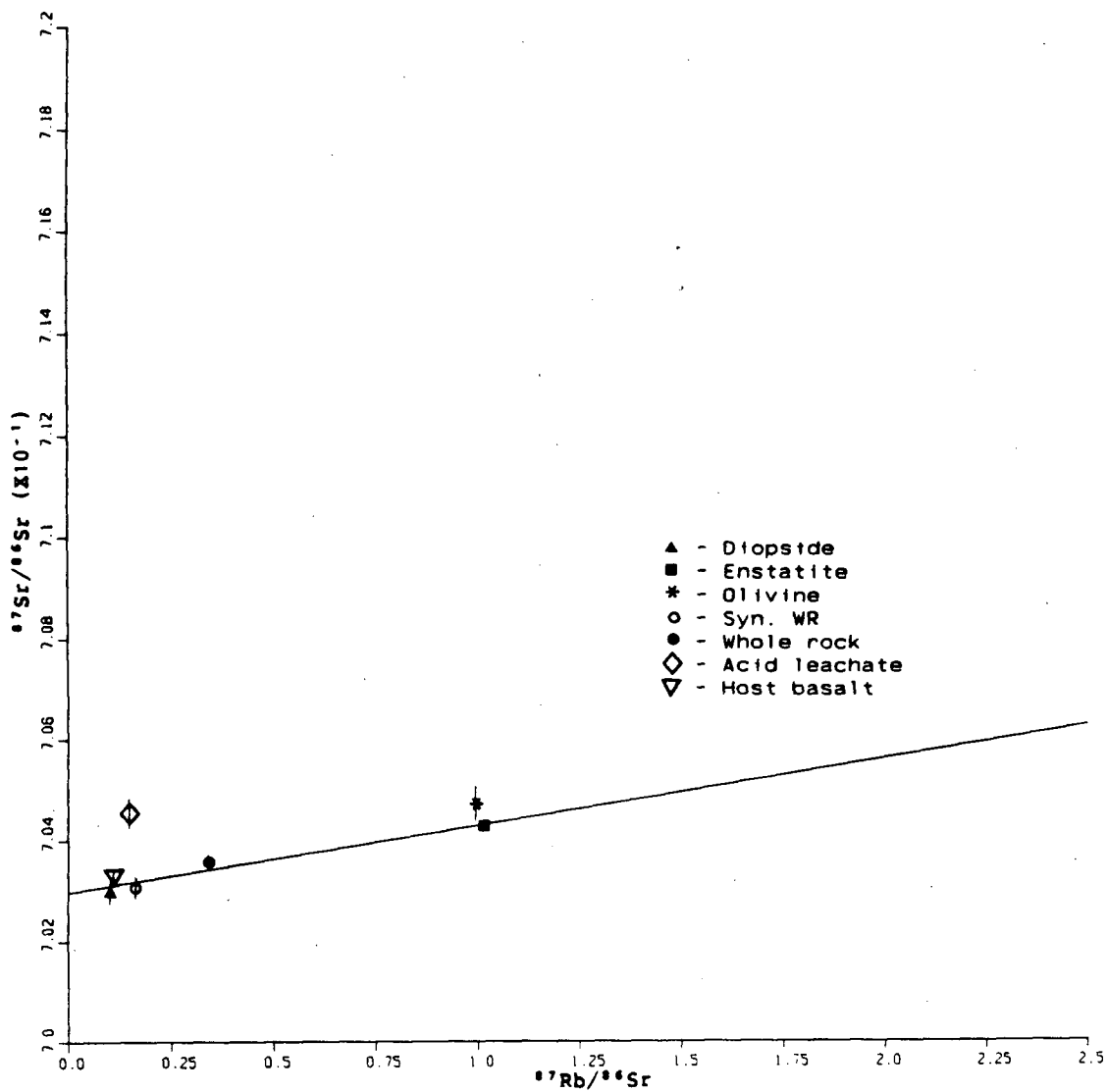


Fig. 5-11 LL1 mineral isochron defined by WR, Di, En, Ol.
 $(^{87}\text{Sr}/^{86}\text{Sr})_0 = 0.7029 \pm 0.0002$, slope = 0.0014 ± 0.0002
 Rb-Sr date = 101 ± 18 Ma. This sample is partially melted.
 The associated basalt has gained ^{87}Sr .

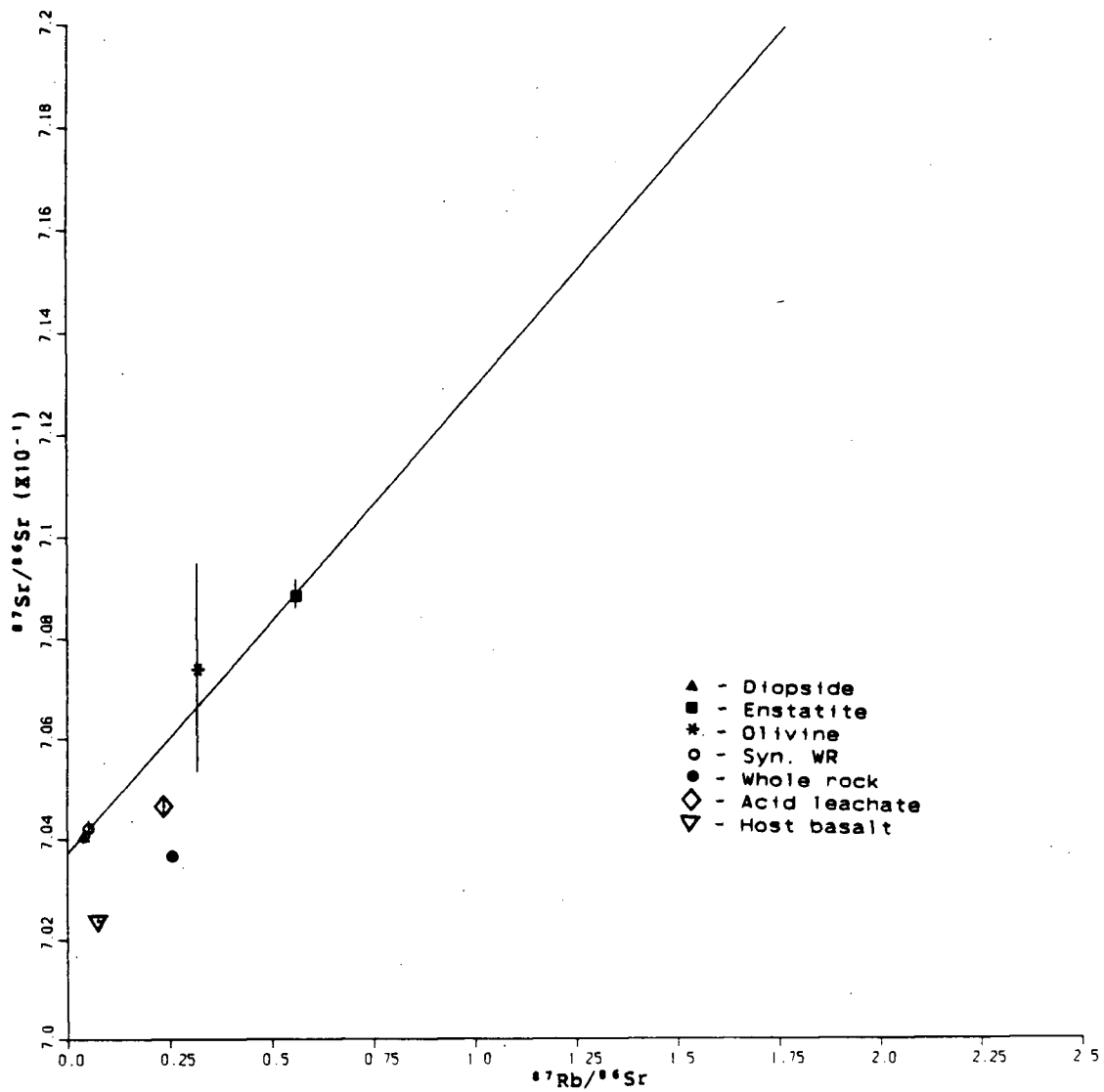


Fig. 5-12 LL14 mineral isochron defined by Di, En, Ol.
 $(^{87}\text{Sr}/^{86}\text{Sr})_0 = 0.7037 \pm 0.0001$, slope = 0.0092 ± 0.0006
 Rb-Sr date = 645 ± 49 Ma.

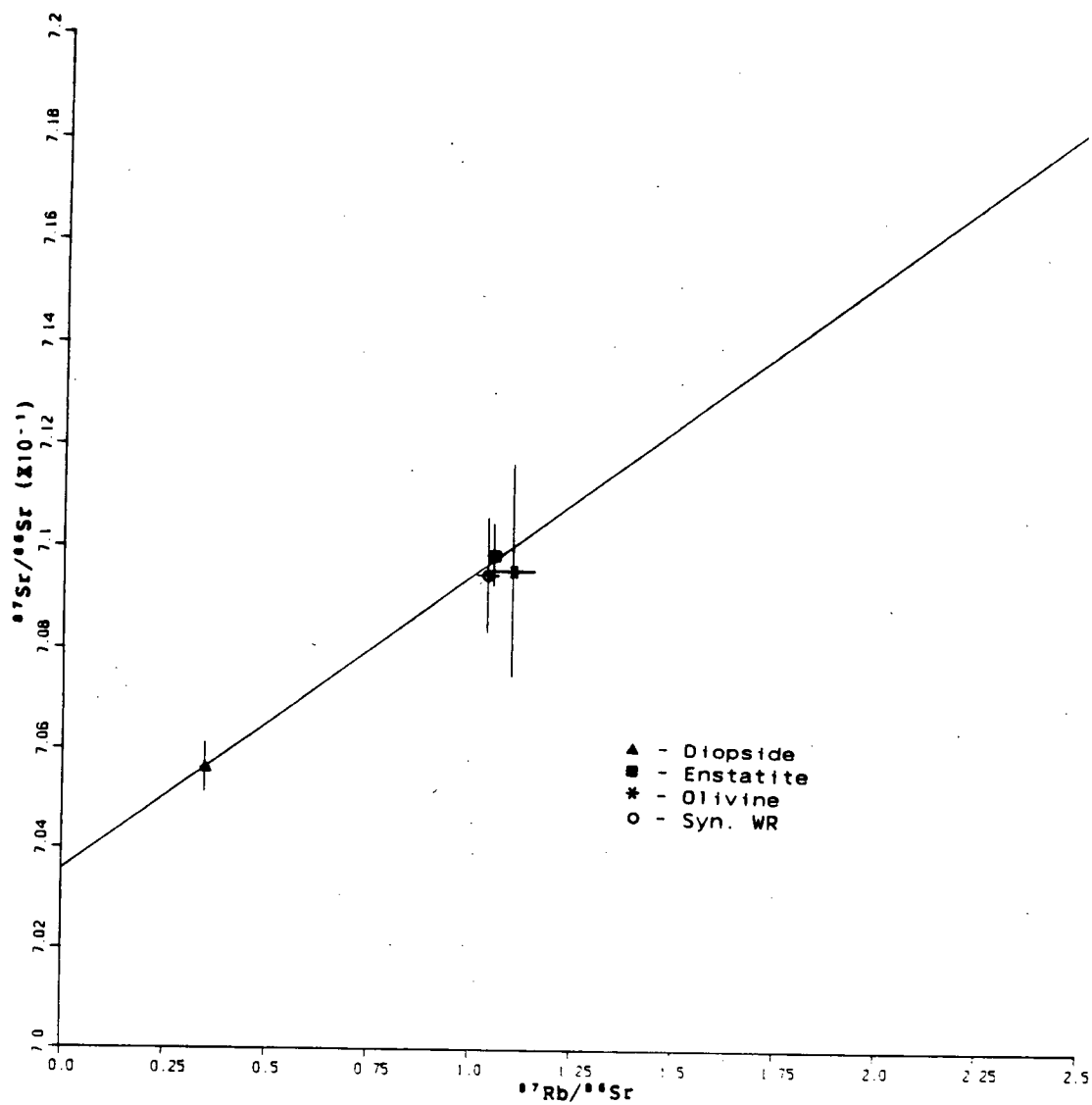


Fig. 5-13 JM5 mineral isochron defined by Di, En, Ol.
 $(^{87}\text{Sr}/^{86}\text{Sr})_0 = 0.7035 \pm 0.0008$, slope = 0.0061 ± 0.0011
 Rb-Sr date = 428 ± 78 Ma.

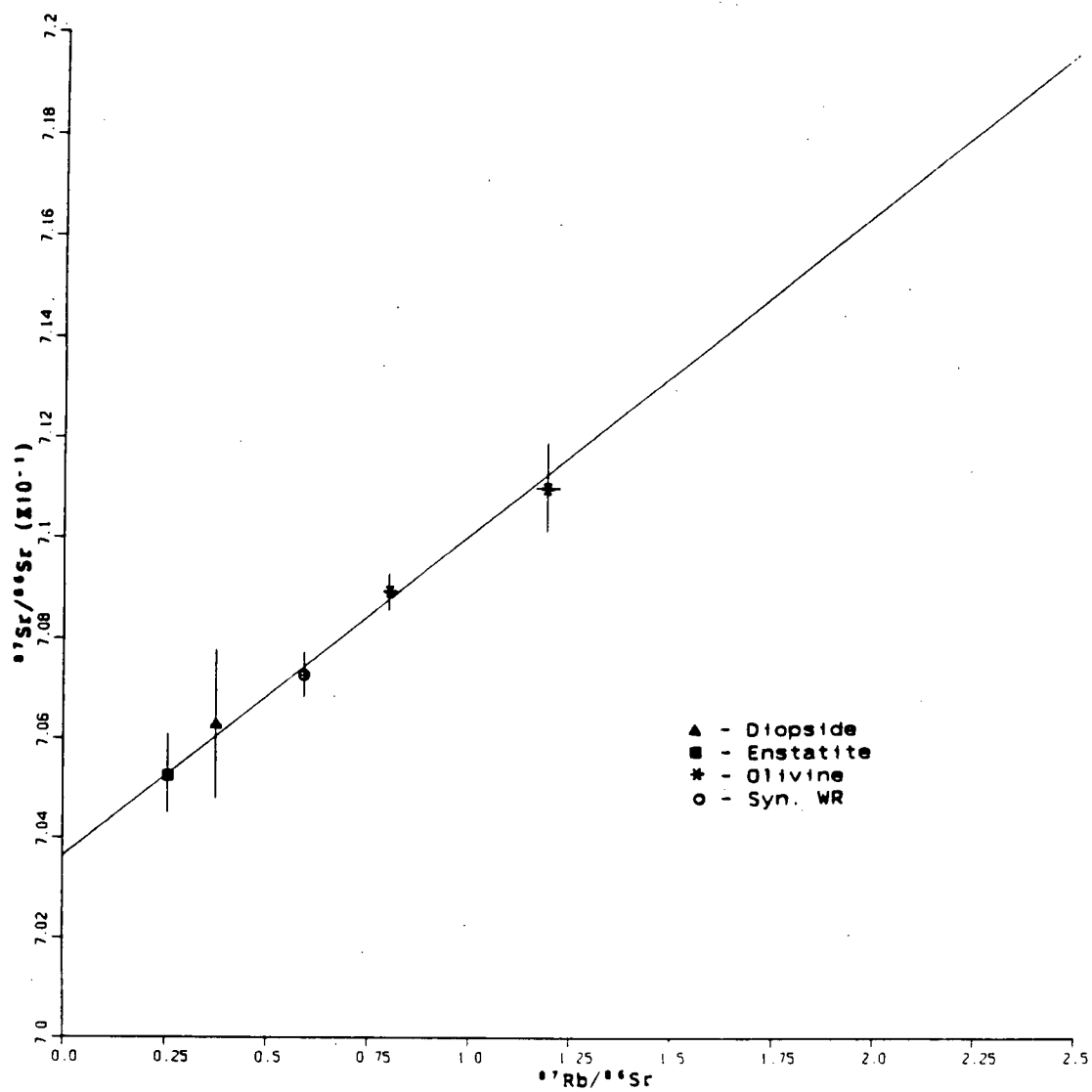


Fig. 5-14 JM14 mineral isochron defined by Di, En, Ol.
 $(^{87}\text{Sr}/^{86}\text{Sr})_0 = 0.7038 \pm 0.0009$, slope = 0.0063 ± 0.0011
 Rb-Sr date = 441 ± 85 Ma.

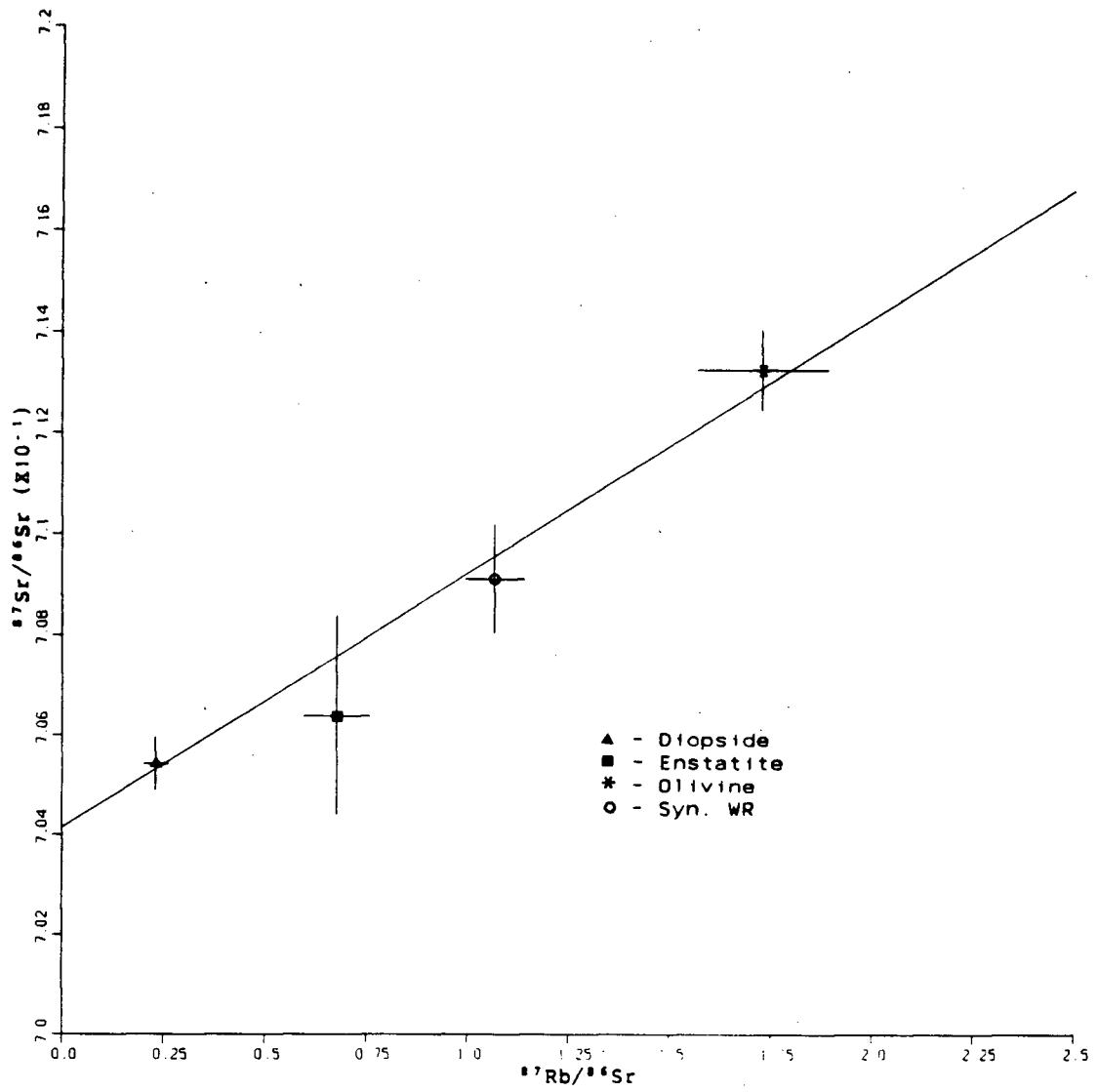


Fig. 5-15 JM15 mineral isochron defined by Di, En, Ol.
 $(^{87}\text{Sr}/^{86}\text{Sr})_0 = 0.7041 \pm 0.0006$, slope = 0.0052 ± 0.0008
 Rb-Sr date = 366 ± 64 Ma.

VI. DISCUSSION

General considerations

Mid ocean ridge basalt (MORB) has low Rb and Sr contents and low Rb/Sr and $^{87}\text{Sr}/^{86}\text{Sr}$ ratios, i.e. Rb < 10 ppm, Sr = 90-200 ppm, Rb/Sr = 0.001-0.02 (or $^{87}\text{Rb}/^{86}\text{Sr}$ = 0.0029-0.058), and $^{87}\text{Sr}/^{86}\text{Sr}$ = 0.702-0.703 (Basaltic Volcanism Study Project, 1981), and is viewed as from a typical "depleted" mantle.

If a mantle-derived sample is not so depleted in incompatible elements, it is ascribed to crustal contamination or an "undepleted" or "enriched" mantle.

Continental flood basalts have high Rb, Sr contents and $^{87}\text{Sr}/^{86}\text{Sr}$ = 0.70369-0.70503 (Basaltic Volcanism Study Project, 1981) and are most often interpreted as showing contamination from the crust (Carlson, 1984) or origin from ancient lithosphere (Church, 1985).

Ocean island alkali basalt and some continental within-plate basalts have high Rb and Sr contents and middling $^{87}\text{Sr}/^{86}\text{Sr}$ ratios, i.e. Rb > 10 ppm, Sr = 400-4000 ppm and $^{87}\text{Sr}/^{86}\text{Sr}$ = 0.703-0.707 (Basaltic Volcanism Study Project, 1981). Because there is no continental crust present, it is inferred that the basalt is from an undepleted or enriched source region in the mantle, and further enriched due to small degrees of partial melting.

Island arc basalt has Rb concentration of 2.4 - 32 ppm and Sr 135 - 540 ppm, $^{87}\text{Sr}/^{86}\text{Sr}$ = 0.70328 ± 0.00015

(Basaltic Volcanism Study Project, 1981). Island arc basalt is inferred to originate from melting and dehydration of the subducted basaltic layer of the oceanic crust, with or without a sedimentary component (Green and Ringwood, 1968; Boettcher, 1977; Stern and Wyllie, 1978); or from hydrous melting of the peridotite wedge overlying the subducted slab (e.g. Nicholls and Ringwood, 1973); or from melting of peridotite mantle modified by introduction of water or melt from the subducted oceanic crust (e.g. Nicholls and Ringwood, 1973). In any case its enrichment in LIL and ^{87}Sr is now universally attributed to contamination with subducted material.

Basalts

(1). Jacques Lake and Big Timothy Mountain

Basalts from Jacques Lake and Big Timonthy Mountain have very high Sr contents, 1276 - 1514 ppm, but rather normal range of Rb, 12.7 - 62.1 ppm. Their $^{87}\text{Sr}/^{86}\text{Sr}$ ratios are relatively low, 0.70254-0.70301.

(2) West Kettle River and Lassie Lake

Basalt layers 1 to 3 in West Kettle River locality have a uniform Rb concentration of 17 ppm. Their Sr varies from 859 ppm of layer 1 down to 642 ppm of layer 3. Accordingly, $^{87}\text{Rb}/^{86}\text{Sr}$ increases slightly upwards but $^{87}\text{Sr}/^{86}\text{Sr}$ decreases from 0.7036 to 0.7029. These basalts are quite similar to continental flood or island arc basalts.

Basalt layer 4, the top layer in the West Kettle River section, has a much higher Rb, higher Sr concentration, and higher $^{87}\text{Rb}/^{86}\text{Sr}$ ratio. Its $^{87}\text{Sr}/^{86}\text{Sr}$ ratio is the lowest of all, 0.70289, implying this layer resulted from recent more intensive metasomatism or unusually small degree of melting of a low $^{87}\text{Sr}/^{86}\text{Sr}$ mantle source. Basalt adhering to nodule KR35 has similar character, with even lower $^{87}\text{Sr}/^{86}\text{Sr}$ ratio, 0.7026.

Basalt adhering to nodule LL14 has comparable Rb and Sr concentrations, 18.5 and 701 ppm respectively, and a very low $^{87}\text{Sr}/^{86}\text{Sr}$ ratio, 0.70254.

The basalt adhering to nodule LL1 is an exception. It has a higher $^{87}\text{Sr}/^{86}\text{Sr}$ ratio, 0.7033, Rb=31.8 ppm and Sr=840 ppm. It is most like ocean island alkali basalt.

The nodule-bearing basalts (except that adhering to nodule LL1) are very similar to mid ocean ridge basalt in $^{87}\text{Sr}/^{86}\text{Sr}$ ratio, but Rb and Sr concentrations are more like ocean island - within plate continental basalts. Plateau basalts in general in British Columbia have $^{87}\text{Sr}/^{86}\text{Sr}$ above 0.703 (Armstrong, pers. comm., 1985) so these with nodules are quite exceptional. Nodules, non-nepheline, and non-radiogenic Sr are all associated.

The high Rb and Sr contents can not be explained by a "primitive mantle" or crustal contamination or the metasomatism in which the metasomatic fluid is derived from the subducted sediments or altered basalt, because any of these mechanisms will lead to distinctly higher $^{87}\text{Sr}/^{86}\text{Sr}$

ratios than MORB.

One hypothesis to explain the nodule bearing basalts is that they are generated as a result of Juan de Fuca plate subduction (see Figure 2-1). Juan de Fuca plate is typically oceanic. The oceanic sediments on the downgoing plate were first involved in the partial melting under the Garibaldi arc and the basalts generated have higher $^{87}\text{Sr}/^{86}\text{Sr}$ (0.7030 to 0.7036). The oceanic basaltic layer (0.7025) was more involved in later stages of partial melting and the degree of melting was small so that basalts with high Sr and low $^{87}\text{Sr}/^{86}\text{Sr}$ ratio were generated. Recent plume/metasomatism of a depleted mantle characterized by low $^{87}\text{Sr}/^{86}\text{Sr}$ ratio is an alternate explanation for alkali basalts but would require in this case a plume/metasomatic fluid of unusually low $^{87}\text{Sr}/^{86}\text{Sr}$ ratio. This is not previously recognized.

Ultramafic nodules

Acid-leach material from the nodules has relative high Rb (0.2-3 ppm), Sr (4-78 ppm) and high Rb/Sr ratio; $^{87}\text{Sr}/^{86}\text{Sr}$ ratio is about 0.703 in Jaques Lake and Big Timothy Mountain and 0.705-0.706 in Kettle River and Lassie Lake nodules. The acid-leach material is a mixture of interstitial material, adhering basalt, weathering products and material etched from the pyrex glass beaker during leaching. The glass has 0.36 ppm Rb, 3.6 ppm Sr, $^{87}\text{Sr}/^{86}\text{Sr} = 0.7084$ and $^{87}\text{Rb}/^{86}\text{Sr} = 0.288$. The weight loss of the glass for one sample leaching is about 1 mg. Compared to the

amounts of Rb and Sr in the acid-leach mixture of chlorides, the Rb and Sr contributed by the glass is insignificant.

(1). Jacques Lake

An early to mid Paleozoic isotopic equilibration or minimum age are recorded by four mineral isochrons (576-341 Ma), with low Sr isotope initial ratios (0.7024 to 0.7028). The synthetic whole rock has identical Rb, Sr and $^{87}\text{Sr}/^{86}\text{Sr}$ ratio with measured whole rock. Whole rock Sr isotope composition and $^{87}\text{Rb}/^{86}\text{Sr}$ ratio are like MORB today. The acid-leaching material from JL14 and JL18 plot on the corresponding mineral isochrons, implying that the interstitial materials might have been in equilibrium with the nodule minerals during the mantle events recorded by the isochrons. The acid-leach material from JL15 does not plot on the isochron due to high Rb/Sr ratio. The high Rb/Sr ratio can be interpreted as later metasomatism in the mantle or while in contact with molten basalt, but not to weathering because the $^{87}\text{Sr}/^{86}\text{Sr}$ ratio is low. In contrast to the depleted-source characteristic of the Sr, pyroxenes in the nodules display an undepleted major element chemistry and JL14 diopside indicates Ti-metasomatism. Thus the mantle (40 km, 995°C) represented by these nodules is a suitable MORB source. The basalt adhering to JL14 has similar Rb, Sr and $^{87}\text{Sr}/^{86}\text{Sr}$ ratio to the nodule diopside and whole rock and lies on the isochron. But they are not cognate because if so, the mineral isochron would be reset during partial melting and give the same age as the host basalt. The nodule

is interpreted as an accidental inclusion; the host basalt resulted from melting of a mantle similar to the nodules.

(2). Big Timothy Mountain

Mid-Proterozoic and mid-Paleozoic dates (1518 Ma and 276 - 396 Ma), are given by three mineral isochrons.

None of the synthetic whole rocks is consistent with the measured whole rocks. The measured whole rock data plot to the right-below the isochrons. This might be due to the effect of interstitial material, because the acid-leach material has a high Rb/Sr ratio. The synthetic whole rock $^{87}\text{Sr}/^{86}\text{Sr}$ ratios, 0.7033 to 0.7039, are in the range of oceanic island basalts from only slightly depleted mantle. Pyroxenes in BM16 and BM55 display an undepleted, but in BM11 a depleted, major element chemistry. Pyroxenes in BM11 and BM55 show Ti-metasomatism but BM16 does not. We can infer that either an equigranular mid-Proterozoic mantle layer or lens (30km, 940°C) may have lain between protogranular mid-Paleozoic mantle layers or the younger isochrons are reset by a mid-Paleozoic or later event.

Host basalt from Big Timothy Mountain plots right-below the nodule mineral isochrons. It could not be derived from the same mantle as that represented by the nodules. The explanation is that the host basalt came from a depleted mantle underlying a less depleted mantle from which the nodules are extracted.

(3). Kettle River

An equigranular mantle was dated as Middle Proterozoic by KR35. This mantle has the same date, Sr initial ratio, texture, depth, and equilibrium temperature as BM16. Pyroxenes are undepleted in major element chemistry and show Ti-metasomatism. The whole rock $^{87}\text{Sr}/^{86}\text{Sr}$ and $^{87}\text{Rb}/^{86}\text{Sr}$ are on the boundary between depleted and undepleted mantle types. The measured whole rock is not identical with the synthetic whole rock, but is on the isochron. The basalt adhering to KR35 is not on the isochron, implying a non-cognate relationship between the nodule and the host basalt. Acid-leaching material is on the mineral isochron, implying it could have been in equilibrium with the minerals during the event recorded by the isochron.

Under this mantle layer, the mantle represented by KR1 and KR2 is porphyroclastic, undepleted in Sr isotopes but depleted in major element chemistry of pyroxenes. KR1 gives a poorly defined mineral isochron date of 561 Ma. Data from KR2 are too scattered to give an isochron. Ignoring olivine, KR1 and KR2 give dates of 588 and 799 Ma, respectively, Late Precambrian. Ignoring orthopyroxene, they give dates of 466 and 384 Ma, middle Paleozoic, respectively. Olivines are seriously deviated from the isochrons, implying that mantle deformation or higher temperature or longer exposure to elevated temperatures has resulted in partial resetting of these mineral isochrons. Host basalts from Kettle River plot right-below the nodule mineral isochrons, they are not cognate with the nodules.

(4). Lassie Lake

A protogranular mantle (52 km, 1008°C), was dated by LL14 to be 645 Ma, late Precambrian. Pyroxenes are depleted and lack Ti-metasomatism. The whole rock has been analysed in triplicate, it plots well below the isochron. The host basalt could only affect the nodule $^{87}\text{Sr}/^{86}\text{Sr}$ ratio, the reason why the nodule whole rock has high $^{87}\text{Rb}/^{86}\text{Sr}$ ratio is not clear. The synthetic whole rock has undepleted Sr isotope character. The host basalt is not in equilibrium with the nodule, implying the basalt came from a depleted mantle underlying the undepleted mantle from which the nodule came.

In a shallower depth of the mantle (46 km, 995°C) the youngest event, 101 Ma, Mesozoic, was recorded by LL1. Considering the considerable melt visible in the thin section and that the pyroxenes are not on the magmatic crystallization trend, this date may be drastically reset by the partial melting event. The host basalt adhering to the nodule has exceptional high $^{87}\text{Sr}/^{86}\text{Sr}$ ratio compared to other nodule-bearing basalts. Although the basalt plots on the isochron, the nodule is not cognate with the basalt because the observed melting occurred about 5 Ma ago.

The Middle Proterozoic to middle Paleozoic Cordilleran miogeoclinal wedge occupies most of the core of the Rocky Mountain Belt and underlies parts of the Omineca Crystalline Belt, but it is not observed in the Intermontane Belt (Monger and Price, 1979). The Omineca western exposures of

basement and stratigraphic equivalents of this wedge locally contain evidence of Middle and Late Precambrian (e.g. Duncan, 1978; Armstrong, 1985, pers. comm.) and mid-Paleozoic (e.g. Okulitch et al., 1975) granitic intrusion, metamorphism and deformation. Considering that the isochron dates may be directly related to synchronous events in overlying crust (e.g. Burwell, 1975), the nodule mineral isochron dates may be related to mid-Proterozoic to Mid-Paleozoic regional geological history. Alternative explanations for the nodule mineral isochrons are that they record the events that only involved mantle rocks or that they are hybrid - partially and recently reset from a single Early to Middle Proterozoic time of crystallization. In any case old mantle lithosphere must extend at least to the western edge of the Omineca Belt.

Josephine Peridotite

The Josephine Peridotite has not been dated isotopically before this work. The isotopic dates on gabbro to trondhjemite of the ophiolite suite, which are traditionally related to its age of formation (Harper, 1984), are all about 150 to 160 Ma (Dick, 1973; Coleman and others, 1976; Hotz, 1971; Saleeby et al., 1982). Harper (1984) inferred the Josephine Peridotite was generated 157 Ma ago in the earliest stages of back-arc spreading.

However, Josephine Peridotite is dated to be middle Paleozoic, 366 to 441 Ma, by three mineral isochrons. The

discrepancy between the dates of Josephine Peridotite and the associated rocks indicates that the ophiolite base does not necessarily have the same age as overlying volcanic rocks and dykes. It preserves evidence of an older mantle event. Other rocks in the Klamath region also give mid-Paleozoic metamorphic or intrusive dates but it is not obvious how these can be related to the Josephine Peridotite.

Josephine Peridotite is extremely depleted in Sr, more so than Rb, compared to the nodules. Both $^{87}\text{Rb}/^{86}\text{Sr}$ and $^{87}\text{Sr}/^{86}\text{Sr}$ are much higher than the nodules, today, and when the rocks were last equilibrated. The pyroxenes display extreme depletion and lack Ti-metasomatism.

Josephine Peridotite may be interpreted as a residue of a large degree of melt extraction, and the melt had island arc basalt Rb/Sr ratio and Sr isotopic composition. Evidence for multiple episodes of partial melting was recognized by Dick (1975).

Mantle growth curve

The fifteen mineral isochron dates and Sr initial ratios have been plot on a Time - $^{87}\text{Sr}/^{86}\text{Sr}$ diagram (Figure 6-1). All nodules are depleted compared with the bulk earth. Most nodules are near the depleted-mantle evolution curve connecting BABI and MORB. Some deviate from this curve. Only LL14 is on "bulk earth" evolution curve, indicating an undepleted prehistory. The Josephine Peridotite has

undepleted character, near to bulk earth evolution curve. But its extreme Rb and Sr depletion eliminates the "primitive mantle" explanation. Considering its island arc environment in the Jurassic and perhaps also in the Paleozoic, the high $^{87}\text{Sr}/^{86}\text{Sr}$ must be due to contamination from subducted material during partial melting, and reaction with rising volcanic arc magmas.

Summary

Jacques Lake nodules represent a depleted MORB source-type mantle, other nodules represent somewhat less depleted mantle. Equigranular nodules give a mid-Proterozoic mineral isochron date. Protogranular nodules give late Precambrian, early-mid Paleozoic and Mesozoic dates. Porphyroclastic nodules do not define mineral isochrons, but must also be Paleozoic or older in age. Host basalts are not cognate with the nodules and come from a low $^{87}\text{Sr}/^{86}\text{Sr}$ mantle with small degree of melting or with recent metasomatism by fluids of low $^{87}\text{Sr}/^{86}\text{Sr}$ ratio. A Paleozoic date for the Josephine Peridotite is in conflict with the view that it was generated in the late Jurassic just before Nevadan Orogeny.

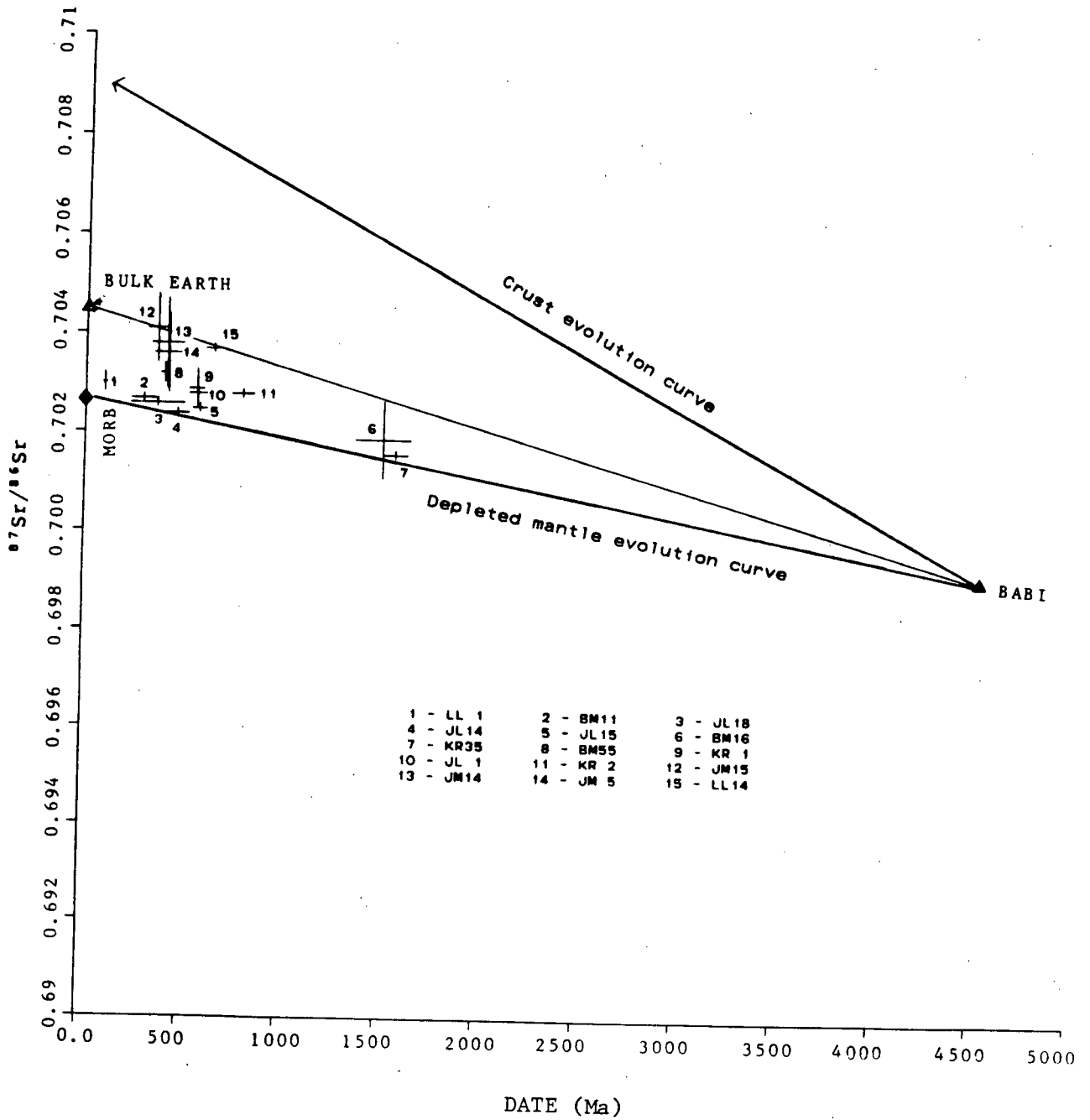


Fig. 6-1 Earth evolution curves

REFERENCES

- Allègre, C.J., Shimizu, N. and Rousseau, D. (1982) History of the continental lithosphere recorded by ultramafic xenoliths. *Nature*, 296, 732-735.
- Allègre, Staudacher, T., Sarda P. and Kurz, M. (1983) Constraints on evolution of Earth's mantle from rare gas systematics. *Nature*, 303, 762-766.
- Armstrong, R.L. (1968) A model for the evolution of strontium and lead isotopes in a dynamic Earth. *Reviews of Geophysics* 6, 175-199.
- Armstrong, R.L. (1981) Radiogenic isotopes: the case for crustal recycling on a near-steady-state no-continental-growth earth. *Phil. Trans. R. Soc. Lond*, A301, 443-472.
- Basalt Volcanism Study Project (1981) Basaltic volcanism on the terrestrial planets. Pergamon Press, Inc., New York. 1286pp.
- Basu, A.R. and Murthy, V.R. (1976) Sr-isotopes and trace elements in spinel lherzolite xenoliths in basalts, San Quintin, Baja California. *EOS*, 57, 355.
- Basu, A.R. and Murthy, V.R. (1977) Ancient lithospheric lherzolite xenolith in alkali basalt from Baja California. *Earth and Planetary Science letters*, 35, 239-246.
- Basu, A.R. (1978) Trace elements and Sr-isotopes in some mantle-derived hydrous minerals and their significance. *Geochemica et Cosmochimica Acta*, 42, 659-668.
- Berry, M.J. and Mair, J.A. (1977) The nature of the Earth's crust in Canada. *American Geophysical Union Geophysical Monograph* 20, 319-348.
- Betton, P.J. and Civetta, L. (1984) Strontium and neodymium isotopic evidence for the heterogeneous nature and development of the mantle beneath Afar (Ethiopia). *Earth and Planetary Science Letters*, 71, 59-70.

- Bevier, M.L., Armstrong, R.L. and Souther, J.G. (1979) Miocene peralkaline volcanism in west-central British Columbia--its temporal and plate tectonic setting. *Geology*, 7, 389-392.
- Bevier, M.L. (1983) Regional stratigraphy and age of Chilcotin Group basalts, south-central British Columbia. *Canadian Journal of Earth Sciences*, 20, 515-524.
- Bielski-Zyskind, M., Wasserburg, G.J. and Nixon, D.H. (1984) Sm-Nd and Rb-Sr systematics in volcanics and ultramafic xenoliths from Malaita, Solomon Island, and nature of the Ontong Java Plateau. *Journal of Geophysical Research*, 89, 2415-2424.
- Boettcher, A.L. (1977) The role of amphiboles and water in circum-Pacific volcanism. In: *High Pressure Research* (M.H. Managhnani, ed.) Academic Press, N.Y., 107-126.
- Boyd, F.R. (1973) The pyroxene geotherm. *Geochimica et Cosmochimica Acta*, 37, 2533-2546.
- Breearley, M., Scarfe, C.M. and Fujii, T. (1984) The petrology of ultramafic xenoliths from Summit Lake, near Prince George, British Columbia. *Contributions to Mineralogy and Petrology*, 88, 53-63.
- Breearley, M., and Scarfe, C.M. (1984) Amphibole in a spinel lherzolite xenolith: evidence for volatiles and partial melting in the upper mantle beneath southern British Columbia. *Canadian Journal of Earth Sciences*, 21, 1067-1072.
- Brueckner, H.K. (1974) "Mantle" Rb/Sr and Sr^{87}/Sr^{86} ratios for clinopyroxenes from Norwegian garnet peridotites and pyroxenites. *Earth and Planetary Science Letters*, 24, 26-32.

- Brueckner, H.K. (1975) Contact and fracture ultramafic assemblages from Norway: Rb-Sr evidence for crustal contamination. *Contributions to Mineralogy and Petrology*, 49, 39-48.
- Burwell, A.D.M. (1975) Rb-Sr isotope geochemistry of lherzolites and their constituent minerals from Victoria, Australia. *Earth and Planetary Science Letters*, 28, 69-78.
- Campbell, R.B. (1978) Quesnel Lake map-area. Geological Survey of Canada. Open File Map 574.
- Carlson, R.W. (1980) Crust-mantle differentiation on the earth and moon: evidence from isotopic studies for contrasting mechanisms and duration. unpublished Ph.D.thesis, University of California at San Diego, 219pp.
- Carlson, R.W. (1984) Isotopic constraints on Columbia River flood basalt genesis and the nature of the subcontinental mantle. *Geochimica et Coschimica Acta*, 48, 2357-2372.
- Challis, G.A. (1969) Discussion of the paper, "The origin of ultramafic and ultrabasic rocks"; by P.J. Wyllie, *Tectonophysics*, 7, 495-505.
- Chase, C.G. (1981) Oceanic island Pb: two-stage histories and mantle evolution. *Earth and Planetary Science Letters*, 52, 277-284.
- Church, S.E. (1985) Genetic interpretation of lead-isotopic data from the Columbia River Basalt Group, Oregon, Washington, and Idaho. *Geological Society of America Bulletin*, 96, 676-690.
- Cohen, R.S., O'Nions, R.K. and Dawson, J.B. (1984) Isotope geochemistry of xenoliths from East Africa: implications for development of mantle reservoirs and their interaction. *Earth and Planetary Science Letters*, 68, 209-220.

- Coleman, R.G. (1971) Plate tectonic emplacement of upper mantle peridotites along continental edges. *Journal of Geophysical Research*, 76, 1212-1221.
- Coleman, R.G., Garcia, M. and Anglin, C. (1976) The amphibolite of Briggs Creek: a tectonic slice of metamorphosed oceanic crust in southwestern Oregon (abstract). *Geological Society of America Abstracts with Programs*, 8, 3.
- Davies, H.L. (1968) Papuan ultramafic belt. XXIII International Geological Congress Report, 1, 209.
- Davies, H.L. (1971) Peridotite-gabbro-basalt complex in eastern Papua, an overthrust plate of oceanic mantle and crust. *Bureau of Mineral Resources, Australia Bulletin*, 128.
- Dick, H.J.B. (1973) K-Ar dating of intrusive rocks in the Josephine Peridotite and Rogue Formation west of Cave Junction, Southwestern Oregon (abstract). *Geological Society of America Abstracts with Programs*, 5, 33-34.
- Dick, H.J.B. (1975) The origin and emplacement of the Josephine peridotite of southwestern Oregon. unpublished Ph.D. thesis, Yale University, New Haven, 301pp.
- Dickey, J.S. (1970) Partial fusion products in alpine-type peridotites, Serania de la Ronda and other examples. *Min. Society of America Special Paper*, 3, 33-49.
- Duncan, I.J. (1978) Rb/Sr whole-rock evidence for three Precambrian events in the Shuswap Complex, Southeast British Columbia (abstract). *Program with Abstracts, Geological Association of Canada*, 3, 392-393.
- Farley, A.L. (1979) Atlas of British Columbia--people, environment, and resource use. University of British Columbia Press, 136pp.

- Fiesinger, D.W. and Nicholls, J. (1977) Petrography and petrology of Quaternary volcanic rocks, Quesnel Lake region, east-central British Columbia. In: Baragar, W.R.Q., Coleman, L.C. and Hull, J.M. (ed.) Volcanic regimes in Canada. Geological Association of Canada Special Paper, 16, 25-38.
- Forbes, R.B. and Kuno, H. (1965) The regional petrology of peridotite inclusions and basaltic host rocks. Upper mantle symposium, New Delhi, 1964, Copenhagen, International Union of Geological Sciences, 161-179.
- Forbes, R.B. and Kuno, H. (1967) Peridotite inclusions and basaltic host rocks, In: P.J. Wyllie (ed.) Ultramafic and related rocks, New York, Wiley, 328-337.
- Fujii, T. and Scarfe, C.M. (1982) Petrology of ultramafic nodules from West Kettle River, near Kelowna, Southern British Columbia. Contributions to Mineralogy and Petrology, 80, 297-306.
- Fuster, J.M., Pasz, A. and Sagredo, J. (1970) Significance of basic and ultramafic rock inclusions in the basalts of Canary Islands. Bulletin Volcanologique, 33, 665-693.
- Gast, P.W. (1972) The chemical composition of the earth, the moon and chondritic meteorites, In: E.C. Robertson (ed.) The Nature of the Solid Earth, McGraw Hill, New York, 19-40.
- Green, T.H. and Ringwood, A.E. (1968) Genesis of the calc-alkaline igneous rock suite. Contributions to Mineralogy and Petrology, 18, 105.
- Green, H.W. (1976) On the Origin of spinel-pyroxene symplectites. EOS, Transactions of the American Geophysical Union, 57, 1026.
- Griffin, W.L. and Murthy, V.R. (1968) Abundances of K, Rb, Sr and Ba in some ultramafic rocks and minerals. Earth and Planetary Science Letters, 4, 497-501.

- Hamilton, W.E. (1969) Mesozoic California and underflow of Pacific mantle. Geological Society of America Bulletin, 80, 2409-2430.
- Harper, G.D. (1984) Middle to late Jurassic tectonic evolution of the Klamath Mountains, California-Oregon. Tectonics, 3, 759-772.
- Harris, P.G., Reay, A. and White, I.G. (1967) Chemical composition of the upper mantle. Journal of Geophysical Research, 72, 6359-6369.
- Hess, H.H. (1938) A primary peridotite magma. American Journal of Science, 35, 321-344.
- Hess, H.H. (1955) Serpentine, orogeny and epirogeny. Geological Society of America Special Paper 62, 391-408.
- Hess, H.H. (1964) The oceanic crust, the upper mantle and the Mayaguez serpentinitized peridotite. National Academy of Sciences National Research Council Publication 118, 169-175.
- Hofmann, A.W. and White, W.M. (1982) Mantle plumes from ancient oceanic crust. Earth and Planetary Science Letters, 57, 421-436.
- Hotz, P.E. (1971) Plutonic rocks of the Klamath Mountains, California and Oregon. U.S. Geological Survey, Professional Paper 684-B, 20pp.
- Irwin, W.P. (1960) Geologic reconnaissance of the Northern Coast Ranges and Klamath Mountains, California, with a summary of the mineral resources. California Division of Mines Bulletin 179, 80pp.
- Irwin, W.P. (1972) Terranes of the Western Paleozoic and Triassic belt in the southern Klamath Mountains, California. U.S. Geological Survey Professional Paper 800C, 103-111.

- Jackson, E.D. (1968) The character of the lower crust and upper mantle beneath the Hawaiian Island. Proceedings of the 3rd International Geological Congress, 1, 135-150.
- Jackson, E.D. (1970) Xenoliths in the Honolulu volcanic areas, Hawaii. Journal of Petrology, 11, 405-430.
- Jacobson, S.B., Quick, J.E. and Wasserburg, G.J. (1984) A Nd and Sr isotopic study of the Trinity peridotite: implications for mantle evolution. Earth and Planetary Science Letters, 68, 361-378.
- Jagoutz, E., Palme, H., Baddenhausen, H., Blum, K., Cendates, M., Dreibus, G., Spettel, B., Lorenz, V. and Wänke, H. (1979) The abundance of major, minor and trace elements in the earth's mantle as derived from primitive ultramafic nodules. Proceedings of the 10th Lunar and Planetary Science Conference. 2031-2050.
- Jaoutz, E., Lorenz, V. and Wänke, H. (1979) Major trace elements of Al-augites and Cr-diopsides from ultramafic nodules in European alkali basalts. In: Boyd, F.R., Mayer, H.O.A. (eds.) The mantle sample: inclusions in kimberlites and other volcanics. American Geophysical Union, 382-390.
- Jagoutz, E., Carlson, R.W. and Lumair, G.W. (1980) Equilibrated Nd - unequilibrated Sr isotopes in mantle xenoliths. Nature, 286, 708-711.
- Kennedy, G.C. and Ito, K. (1972) Comments on: "A comparison of recent experimental data on the gabbro-garnet granulite-eclogite transition". Journal of Geology, 80, 289-292.
- Kramers, J.D. (1977) Lead and strontium isotopes in Cretaceous kimberlites and mantle-derived xenoliths from Southern Africa. Earth and Planetary Science Letters, 34, 419-431.
- Kuno, H. (1969) Mafic and ultramafic nodules in basaltic rocks of Hawaii. Geological Society of America Memoir, 115, 189-234.

- Kushiro, I. (1969) The system forsterite-diopside-silica with and without water at high pressures. *American Journal of Science*, 267-A, 269-294.
- Larimer, J. (1971) Composition of the earth: Chondritic or achondritic? *Geochimica et Cosmochimica Acta*, 31, 1239-1270.
- Littlejohn, A.L. and Greenwood, H.J. (1974) Lherzolite nodules in basalts from British Columbia, Canada. *Canadian Journal of Earth Sciences*, 11, 1288-1308.
- Lupton, J.E. (1983) Terrestrial inert gases: isotope trace studies and clues to primordial components in the mantle. *Annual Review of Earth and Planetary Science*, 11, 371-414.
- Macdonald, G.J.F. (1959) Chondrites and the chemical composition of the earth. In: Abelson, P. (ed.) *Researches in Geochemistry*. Wiley, New York, 476-494.
- MacGregor, I.D. (1974) The system $MgO-Al_2O_3-SiO_2$: solubility of Al_2O_3 in enstatite for spinel and garnet peridotite compositions. *American Mineralogist*, 59, 110-119.
- Mark, R.K., Lee-Hu C. and Wetherill, G.W. (1973) Rb-Sr Studies of lunar breccias and soils. *Proceedings of the 4th Lunar Science Conference*, 1785-1795.
- Maxwell, R.J. (1976) A study of rubidium, strontium and strontium isotopes in some mafic and sulphide minerals. unpublished M. Sc. thesis, University of British Columbia, Vancouver, 123pp.
- McTaggart, K.C. (1971) On the origin of ultramafic rocks. *Geological Society of America Bulletin*, 82, 23-42.
- Mengel, K., Kramm, U., Wedepohl, K.H. and Cohn, E. (1984) Sr isotope in peridotite xenoliths and their basaltic host rocks from the northern Hessian Depression (NW Germany). *Contributions to Mineralogy and Petrology*, 87, 369-375.

- Menzies, M and Murthy, V.R. (1978) Strontium isotope geochemistry of Alpine tectonite lherzolites: data compatible with a mantle origin. *Earth and Planetary Science Letters*, 38, 346-354.
- Menzies, M and Murthy, V.R. (1980) Nd and Sr isotope geochemistry of hydrous mantle nodules and their host alkali basalts: implications for local heterogeneities in metasomatically veined mantle. *Earth and Planetary Science Letters*, 46, 323-334.
- Mercier, J-C and Carter, N.L. (1975) Pyroxene geotherms. *Journal of Geophysical Research*, 80, 3349-3362.
- Mercier, J-C and Nicolas, A. (1975) Textures and fabrics of upper mantle peridotites as illustrated by xenoliths from basalts. *Journal of Petrology*, 16, 454-487.
- Mercier, J-C (1976) Single-pyroxene geothermometry and geobarometry. *American Mineralogist*, 61, 603-615.
- Mercier, J-C (1980) Single-pyroxene thermobarometry. *Tectonophysics*, 70, 1-37.
- Miyashiro, A. (1973) The Troodos complex was probably formed in an island arc. *Earth and Planetary Science Letters*, 19, 218-224.
- Monger, J.W.H. and Price, R.A. (1979) Geodynamic evolution of the Canadian Cordillera - progress and problems. *Canadian Journal of Earth Sciences*, 16, 770-791.
- Nicholls, I.A. and Ringwood, A.E. (1973) Effect of water on olivine stability in tholeiites and production of silica-saturated magmas in the island arc environment. *Journal of Geology*, 81, p.285.
- Nicholls, J., Stout, M.Z. and Fiesinger, D.W. (1982) Petrologic variations in Quaternary volcanic rocks, British Columbia. *Contributions to Mineralogy and Petrology*, 79, 201-218.

- Nunes, P.D. (1980) The Ontario Geological Survey Geochronology Research - An Overview. In: Pye, E.G. (ed.) Summary of geochronology studies 1977-1979, Ontario Ministry of Natural Resources, Miscellaneous Paper 92,4-6.
- O'Hara, M.J. and Mercy, E.L.P. (1963) Petrology and Petrogenesis of some garnetiferous peridotites. Transactions of the Royal Society of Edinburgh, 65, 251-314.
- O'Hara, M.J. (1965) Primary magmas and the origin of basalts. Scottish Journal of Geology, 1, 19-40.
- O'Hara, M.J. (1967) Mineral parageneses in ultramafic rocks. In: Wyllie, P.J. (ed.) Ultramafic and related rocks, 393-402.
- O'Hara, M.J. (1968) The bearing of phase equilibria studies in synthetic and natural systems on the origin and evolution of basic and ultrabasic rocks. Earth-Science Reviews, 4, 69-331.
- Okulitch, A.V., Wanless, R.K. and Loveridge, W.D. (1975) Devonian plutonism in south-central British Columbia. Canadian Journal of Earth sciences, 11, 976-997.
- O'Nions, R.K., Hamilton, P.J. and Evensen, N.M. (1977) Variations in $^{143}\text{Nd}/^{144}\text{Nd}$ and $^{87}\text{Sr}/^{86}\text{Sr}$ ratios in oceanic basalts. Earth and Planetary Science Letters, 34, 13-22.
- Osborn, E.F. (1969) The complementariness of orogenic andesite and alpine peridotite. Geochimica et Cosmochimica Acta, 33, 307-324.
- Papanastassou, D.A. and Wasserburg, G.J. (1973) Rb-Sr ages and initial $\text{Sr}^{87}/\text{Sr}^{86}$ ratios in Apollo 15 basalts. Earth and Planetary Science Letters, 17, 324-337.
- Paul, D.K. (1971) Strontium isotope studies on ultramafic inclusions from Dreiser Weiher, Eifel, Germany. Contributions to Mineralogy and Petrology, 34, 22-28.

- Polvé, M. and Allègre, C.J. (1980) Orogenic lherzolite complexes studies by ^{87}Rb - ^{87}Sr : a clue to understand the mantle convection processes? Earth and Planetary Science Letters, 51, 71-93.
- Richard, P. and Allegre, C.J. (1980) Neodymium and strontium isotope study of ophiolite and orogenic lherzolite petrogenesis. Earth and Planetary Science Letter, 47, 65-74.
- Riddihough, R.P. (1982a) Contemporary movements and tectonics on Canada's west coast: a discussion. Tectonophysics, 86, 319-341.
- Riddihough, R.P. (1982b) One hundred million years of plate tectonics in western Canada. Geoscience Canada, 9, 28-34.
- Riddihough, R.P. (1984) Recent movements of the Juan de Fuca plate system. Journal of Geophysical Research, 89, 6980-6994.
- Ringwood, A.E. (1962) Present status of the chondritic earth models. In: C.B. Moore (ed.) Researches in Meteorites Wiley, New York, 198-216.
- Ringwood, A.E. (1975) Composition and petrology of the earth's mantle. New York, McGraw-Hill, 618pp.
- Rogers, G.S. (1983) Seismotectonics of British Columbia. Unpublished Ph.D. thesis, University of British Columbia, Vancouver, 1-20.
- Ross, C.S., Foster, M.D. and Myers, A.T., (1954) Origin of dunites and of olivine-rich inclusions in basaltic rocks. American Mineralogist, 39, 693-736.
- Ross, J.V. (1983) The nature and rheology of the Cordilleran upper mantle of British Columbia: inferences from peridotite xenoliths. Tectophysics, 100, 321-357.

- Saleeby, J.B., Harper, G.D., Snoke, A.W. and Sharp, W.D. (1982) Time relations and structural-stratigraphic patterns in ophiolite accretion, west central Klamath Mountains, California. *Journal of Geophysical Research*, 87, 3831-3848.
- Schweickert, R.A. and Cowan D.S. (1974) Pre-Tithonian magmatic arcs and subduction zones of the western Sierra Nevada, California. *Geological Society of America Abstracts with Programs*, 6, 251-252.
- Soregaroli, A.E. (1968) Geology of the Boss Mountain Mine, British Columbia. unpublished Ph.D. thesis, University of British Columbia, Vancouver, 200pp.
- Souther, J.G. and Hickson, C.J. (1984) Crystal fractionation of the basalt comendite series of the mout Edziza volcanic complex, British Columbia: major and trace elements. *Journal of Volcanology and Geothermal Research*, 21, 79-106.
- Stacey, R.A. (1974) Plate tectonics, volcanism and the lithosphere in British Columbia. *Nature*, 250, 133-135.
- Steinmann, G. (1926) Die ophiolitischen zonen in dem Mediterranean Kettengebirgen. 14th International Geological Congress, Madrid, *Compte Rendu*, 2, 638-667.
- Stern, C.R. and Wyllie, P.J. (1978) Phase compositions through crystallization intervals in basalt - andesite - H₂O at 30 kb with implications for subduction zone magmas. *American Mineralogist*, 63, 641-663.
- Stosch, H.G., Carlson, R.W. and Lugmair, G.W. (1980) Episodic mantle differentiation: Nd and Sr isotopic evidence. *Earth and Planetary Science Letters*, 47, 263-271.
- Stueber, A.M. and Ikramuddin, M. (1974) Rubidium, strontium and the isotopic composition of strontium in ultramafic nodule minerals and host basalts. *Geochimica et Cosmochimica Acta*, 38, 207-216.

- Thayer, T.P. (1964) Principle features and origin of podiform chromite deposits and some observations on the Guleman Soridag District, Turkey. *Economic Geology*, 59, 1497-1524.
- Thayer, T.P. (1967) Chemical and structural relations of ultramafic and feldspathic rocks in alpine intrusive complexes. In: P.J. Wyllie (ed.) *Ultramafic and related rocks*, Wiley, New York, 222-239.
- Thayer, T.P. (1969) Gravity differentiation and magmatic reemplacement of podiform chromite deposits. In: H.D.B. Wilson (ed.) *Magmatic ore deposits*. *Economic Geology Monograph*, 4, 132-146.
- Trask, N.J. (1969) Ultramafic xenoliths in basalt, Nye County, Nevada. *U.S. Geological Survey Professional Paper*, 650-D, 43-48.
- Vollmer, R. (1983) Earth degassing, mantle metasomatism, and isotopic evolution of the mantle. *Geology*, 11, 452-454.
- Wagner, P.A. (1928) The evidence of the kimberlite pipes on the constitution of the outer part of the earth. *South African Journal of Science*, 25, 127-148.
- Wells, P.R.A. (1977) Pyroxene thermometry in simple and complex systems. *Contributions to Mineralogy and Petrology*, 62, 129-139.
- White, R.W. (1966) Ultramafic inclusions in basaltic rocks from Hawaii. *Contributions to Mineralogy and Petrology*, 12, 245-314.
- White, W.M. and Hofmann, A.W. (1982) Sr and Nd isotope geochemistry of oceanic basalts and mantle evolution. *Nature*, 296, 821-825.
- White, W.M. and Patchett, J. (1984) Hf-Nd-Sr isotopes and incompatible element abundances in island arcs: implications for magma origins and crust-mantle evolution. *Earth and Planetary Science Letters*, 67, 167-185.

- White, W.M. (1985) Sources of oceanic basalts: radiogenic isotope evidence. *Geology*, 13, 115-118.
- Wilshire, H.G. and Binns, R.A. (1961) Basic and ultrabasic xenoliths from volcanic rocks of New South Wales. *Journal of Petrology*, 2, 185-208.
- Wilshire, H.G. and Shervais, J.W. (1975) Al-augite and Cr-diopside ultramafic xenoliths in basaltic rocks from western United States. In: Ahrens, L.H. et al. (eds.), *Physics and Chemistry of the Earth*, 9, Pergamon, New York, 257-272.
- Wyllie, P.J. (1967) Mafic and ultramafic nodules introduction. In: P.J. Wyllie (ed.) *Ultramafic and related rocks*. Wiley, New York, 327-328.
- Wood, B.J. and Banno, S. (1973) Garnet - orthopyroxene and clinopyroxene - orthopyroxene relationships in simple and complex systems. *Contributions to Mineralogy and Petrology*, 42, 109-124.
- Wood, B.J. (1975) The application of thermodynamics to some subsolidus equilibria involving solid solutions. *Fortschritte Mineralogie*, 52, 21-45.
- Zindler, A., Jagoutz, E. and Goldstein, S. (1982) Nd, Sr and Pb isotopic systematics in a three-component mantle: a new perspective. *Nature*, 298, 519-523.

APPENDIX 1 PROBE ANALYTICAL DATA OF NODULE MINERALS

CPX	MgO	Al2O3	Na2O	SiO2	CaO	K2O	FeO	Cr2O3	TiO2	MnO	Total											
KR1	15.71	3.89	1.41	54.05	21.12	0	2.09	1.27	0.21	0.08	99.83											
	15.45	3.99	1.32	53.47	21.42	0	2.06	1.45	0.18	0.08	99.43											
	15.66	3.90	1.36	54.54	21.20	0	2.06	1.18	0.19	0.05	100.13											
	15.02	3.99	1.64	55.22	20.41	0	2.16	1.13	0.15	0.05	99.76											
	14.82	3.97	1.42	54.11	21.36	0	2.12	1.28	0.20	0.09	99.47											
	15.86	4.06	1.36	53.57	21.35	0.02	2.13	1.42	0.17	0.11	100.05											
KR2	15.15	4.80	1.17	54.46	21.42	0	2.35	0.84	0.08	0.09	100.36											
	15.04	5.06	1.18	53.94	21.32	0.02	2.33	0.97	0.08	0.06	100.01											
	14.93	4.86	1.26	53.76	21.59	0.01	2.35	0.98	0.05	0.08	99.87											
	15.21	4.98	1.24	53.12	21.39	0	2.33	1.02	0.04	0.11	99.46											
	15.68	4.68	1.25	53.29	21.36	0	2.31	0.86	0.09	0.10	99.63											
	15.53	4.69	1.20	54.04	21.44	0.01	2.27	0.88	0.10	0.04	100.20											
	15.37	5.00	1.21	51.57	21.47	0	2.30	1.02	0.08	0.09	98.11											
	15.19	5.05	1.29	53.62	21.26	0	2.28	1.04	0.11	0.11	99.93											
LL1	14.93	6.60	1.58	52.85	20.10	0.01	2.85	1.00	0.26	0.06	100.23											
	14.87	6.40	1.63	53.13	20.04	0	2.88	0.96	0.31	0.10	100.32											
	14.82	6.60	1.67	53.01	20.14	0.01	2.92	0.99	0.32	0.08	100.55											
	14.68	6.76	1.58	52.43	20.15	0.01	2.83	0.98	0.38	0.09	99.89											
	14.60	6.75	1.58	52.92	20.02	0	2.97	0.98	0.44	0.12	100.38											
	14.76	6.80	1.54	51.55	19.95	0	2.87	0.94	0.34	0.08	98.84											
	14.55	6.45	1.49	51.83	20.04	0.01	2.88	0.95	0.27	0.14	98.64											
	14.83	6.45	1.65	51.76	20.12	0.01	2.77	1.03	0.28	0.13	99.0											
	14.68	6.25	1.49	51.86	20.12	0.01	2.78	0.92	0.25	0.09	98.45											
OPX	MgO	Al2O3	Na2O	SiO2	CaO	FeO	Cr2O3	TiO2	MnO	Total												
											KR1	34.08	2.75	0.08	56.40	0.61	5.90	0.53	0.02	0.14	100.51	
												32.82	2.82	0.12	55.42	0.59	5.91	0.54	0.04	0.16	98.41	
												35.06	2.80	0.05	56.44	0.59	5.90	0.58	0.03	0.18	101.63	
												34.80	2.83	0.05	56.29	0.59	5.80	0.53	0.03	0.16	101.09	
												34.89	2.84	0.07	56.41	0.60	5.87	0.55	0.06	0.15	101.44	
												35.00	2.77	0.04	56.19	0.61	5.81	0.50	0.06	0.14	101.12	
												34.33	2.76	0.16	56.75	0.59	5.82	0.51	0.06	0.15	101.12	
												33.81	2.90	0.09	56.72	0.61	5.87	0.52	0.03	0.15	100.69	
												33.98	2.92	0.06	56.32	0.61	5.87	0.54	0.05	0.17	99.52	
												34.51	2.88	0.12	55.76	0.58	5.74	0.51	0.06	0.14	100.29	
												KR2	33.93	3.71	0.09	55.67	0.57	6.07	0.39	0.03	0.13	100.59
													34.03	3.82	0.05	56.10	0.55	5.94	0.39	0.00	0.19	101.07
													34.01	3.64	0.07	55.14	0.58	5.89	0.34	0.00	0.14	99.81
33.70	3.66	0.09	55.49	0.57	5.85	0.40	0.03	0.15	99.94													
34.28	3.82	0.04	55.78	0.53	5.91	0.44	0.01	0.12	100.93													
33.99	3.68	0.10	56.15	0.58	5.93	0.47	0.01	0.14	101.06													
33.51	3.79	0.08	55.75	0.61	5.88	0.38	0.01	0.20	100.21													
33.28	3.74	0.05	55.84	0.60	5.95	0.38	0.01	0.15	100.01													
34.44	3.72	0.09	53.60	0.58	5.95	0.45	0.02	0.13	98.98													
34.33	3.65	0.07	55.26	0.59	5.91	0.41	0.02	0.17	100.42													

LL1	32.72	4.55	0.10	55.66	0.78	6.37	0.43	0.07	0.14	100.82
	31.89	4.49	0.10	55.90	0.76	6.25	0.46	0.07	0.18	100.10
	31.20	4.49	0.10	54.94	0.77	6.25	0.41	0.07	0.16	98.37
	31.66	4.43	0.08	55.16	0.76	6.19	0.43	0.09	0.14	98.96
	31.97	4.46	0.09	54.49	0.74	6.23	0.44	0.06	0.14	98.62
	32.11	4.51	0.11	55.33	0.72	6.13	0.42	0.06	0.14	99.51
	32.17	4.55	0.10	55.30	0.74	6.18	0.48	0.07	0.18	99.76
	32.17	4.46	0.09	55.05	0.74	6.13	0.44	0.08	0.17	99.34
	32.58	4.53	0.09	53.44	0.80	6.12	0.42	0.02	0.16	98.16
	32.12	4.54	0.09	54.06	0.75	6.22	0.40	0.07	0.14	98.39
	33.05	4.36	0.08	54.66	0.79	6.19	0.46	0.07	0.12	99.78
	32.97	4.61	0.10	55.28	0.73	6.21	0.42	0.08	0.14	100.53

OL	MGO	S102	CaO	Fed	MnO	NiO	Total
KR1	50.25	40.36	0.06	9.24	0.11	0.37	100.38
	50.46	40.57	0.06	9.21	0.13	0.41	100.84
	50.05	41.33	0.06	9.26	0.13	0.38	101.21
	50.66	41.06	0.07	9.42	0.12	0.43	101.75
	50.44	41.42	0.06	9.19	0.11	0.36	101.58
	49.96	40.20	0.05	9.44	0.14	0.38	100.17
	50.07	41.72	0.04	9.18	0.16	0.37	101.54
	49.48	41.73	0.05	9.31	0.13	0.36	101.05
	49.97	41.48	0.05	9.50	0.15	0.40	101.55
	49.77	41.66	0.06	9.22	0.13	0.42	101.26

KR2	49.14	40.99	0.07	9.24	0.10	0.41	99.95
	48.77	40.68	0.05	9.26	0.13	0.41	99.28
	47.81	41.30	0.03	9.41	0.14	0.36	99.05
	48.31	41.71	0.08	9.34	0.11	0.41	99.96
	47.95	41.40	0.07	9.17	0.12	0.40	99.11
	47.45	41.01	0.07	9.32	0.12	0.39	98.36
	50.28	41.46	0.06	9.30	0.11	0.37	101.59
	49.00	41.56	0.06	9.29	0.13	0.42	100.46
	48.77	40.89	0.05	9.43	0.12	0.40	99.67
	50.04	40.40	0.06	9.42	0.14	0.37	100.43

LL1	48.43	40.22	0.09	9.88	0.10	0.39	99.11
	48.66	39.80	0.10	9.87	0.15	0.40	98.98
	48.17	39.85	0.07	9.73	0.13	0.41	98.36
	48.50	39.63	0.09	9.90	0.14	0.38	98.62
	48.26	40.64	0.08	9.83	0.10	0.39	99.30
	47.98	40.37	0.05	9.81	0.13	0.39	98.70
	47.75	39.90	0.00	9.93	0.04	0.40	98.02
	48.22	40.17	0.08	9.83	0.18	0.38	98.88
	47.33	40.36	0.09	9.83	0.12	0.34	98.07
	47.44	40.30	0.10	9.87	0.13	0.40	98.23
	48.30	40.05	0.09	9.91	0.16	0.36	98.85

SP	MgO	Al2O3	SiO2	FeO	Cr2O3	MnO	Ti2O3	total
KR1	17.45	38.44	0.04	13.08	29.63	0.15	0.09	98.88
	17.56	39.65	0.06	12.72	29.03	0.15	0.09	99.27
	17.69	38.58	0.00	12.82	29.55	0.19	0.07	98.91
	17.76	40.00	0.00	12.32	28.44	0.17	0.06	98.75
	17.60	40.01	0.00	12.72	29.01	0.17	0.10	99.61
	17.64	40.25	0.04	12.19	28.35	0.16	0.10	98.74
	17.54	39.84	0.05	12.72	28.38	0.17	0.05	98.75
KR2	20.15	53.24	0.04	10.06	15.05	0.13	0.00	98.67
	19.84	53.52	0.03	10.08	15.27	0.12	0.07	98.93
	19.87	53.41	0.05	10.13	15.32	0.09	0.02	98.88
	19.74	53.43	0.06	10.05	15.40	0.13	0.00	98.82
	20.03	52.80	0.00	10.06	15.37	0.07	0.00	98.34
LL1	19.93	55.77	0.06	9.45	12.80	0.12	0.07	98.21
	20.09	55.87	0.07	9.73	12.86	0.12	0.11	98.84
	20.05	55.77	0.09	9.56	12.95	0.11	0.22	98.75
	19.91	55.49	0.07	9.70	12.66	0.11	0.01	97.95
	20.05	55.87	0.00	9.85	12.74	0.09	0.20	98.79

APPENDIX 2

Fe²⁺ and Fe³⁺ in Spinel Calculation (KR1 as an example)

KR1 Sp.	Mg	Al	Si	Fe	Cr	Mn	Ti	Total
oxide	17.61	39.54	0.027	12.65	28.94	0.166	0.08	99.01
wt. %								
# of	0.742	1.319	0.0008	0.300	0.647	0.004	0.0017	3.014
ions								

Formula (Mg, Fe, Mn)(Al, Cr, Fe)₂O₄

$$\text{Mg} + \text{Mn} + \text{Fe}^{2+} = 0.742 + 0.004 + 0.254 = 1$$

$$\text{Al} + \text{Cr} + \text{Fe}^{3+} = 1.319 + 0.647 + 0.034 = 2$$

Total Fe will be partitioned into the formula as Fe²⁺ and Fe³⁺ according to the ratio Fe²⁺/Fe³⁺ = 0.254/0.034.

Therefore

$$\text{Fe}^{2+} = 0.300 \times 0.254 / (0.254 + 0.034) = 0.265$$

$$\text{Fe}^{3+} = 0.300 \times 0.034 / (0.254 + 0.034) = 0.035$$

Accordingly, mineral composition has been recalculated to:

	ion #	oxide wt.	oxide wt%
Mg	0.742	29.9	17.73
Al	1.319	67.2	39.86
Si	0.0008	0.048	0.0003
Fe ²⁺	0.265	19.04	11.3
Fe ³⁺	0.035	2.79	1.65
Cr	0.647	49.2	29.18
Mn	0.004	0.28	0.166
Ti	0.0017	0.14	0.08
Total		168.6	99.97

APPENDIX 3
 PROBE ANALYTICAL DATA FOR JOSEPHINE PERIDOTITE PYROXENES
 (from Dick, 1975)

CPX	FeO	MgO	SiO ₂	CaO	Al ₂ O ₃	Cr ₂ O ₃	TiO ₂	Total
J28f	2.86	16.98	51.24	22.73	3.84	1.46	0.04	99.15
J871	2.43	18.55	52.96	23.42	2.36	1.00	0.03	100.75
J120	2.91	17.30	54.04	22.73	5.11	1.10	0.16	103.35
J120	2.30	18.27	53.45	23.77	2.10	0.69	0.05	100.63
OPX	FeO	MgO	SiO ₂	CaO	Al ₂ O ₃	Cr ₂ O ₃	TiO ₂	Total
J28f	6.01	32.83	54.31	1.73	3.56	0.91	0.02	99.37
J46h	5.83	33.37	56.30	1.83	3.34	0.89	0.04	101.60
J46h	5.79	33.63	54.61	1.39	3.18	0.85	0.04	99.49
J871	5.84	34.78	57.28	1.11	2.37	0.55	0.01	101.94
J114	6.02	34.70	54.01	1.04	2.05	0.49	0.01	98.32
J120	6.17	35.08	55.01	0.55	2.27	0.43	0.02	99.53
J46g	5.58	35.64	55.09	0.79	0.95	0.55	0.03	98.62

APPENDIX 4

CALCULATED TEMPERATURE, PRESSURE, DEPTH FROM J.V.ROSS

	DIOPSIDE			ENSTATITE		
	T°C	P(kb)	D(km)	T°C	P(kb)	D(km)
JL15				1063	18.61	60.6
				1051	17.98	58.7
				1071	17.73	58.0
				1059	17.71	57.9
				1072	19.50	63.3
	1011	14.47	48.1	1053	18.13	59.2
	1013	14.57	48.4	1034	17.49	57.3
	995	14.84	49.2	1059	17.89	58.5
	992	12.67	42.6	1067	17.57	57.5
JL18	1003	14.74	48.9	1024	17.28	56.6
	1017	14.73	48.9	1018	16.32	53.7
				1025	17.87	58.4
				1034	17.69	57.9
				1040	17.85	58.3
BM55	1038	16.05	52.9			
	1067	17.76	58.1			
BM16	935	9.27	32.3	1187	25.70	82.1
	943	10.41	35.8	1064	16.62	54.6
				1145	21.70	70.0
				1083	17.74	58.0
				1171	23.46	75.4
BM11				1093	13.37	44.8
LL14	1024	17.49	57.3	1055	17.28	56.6
	998	15.70	51.8	1067	17.72	57.9
				1074	20.51	66.4
				1068	19.07	62.0
				1068	18.10	59.1
KR35	922	8.76	30.8	1058	16.44	54.1
	973	13.06	43.8	1051	15.55	51.4
				1039	14.10	47.0
				1127	19.91	64.6

APPENDIX 5 PROGRAM "RBSR"

```

C PROGRAM "RBSR"
C REWRITTEN FROM BASIC PROGRAMS "RBSPK3" AND "SRSPK3"
C BY MIN SUN, 1984.
C THIS PROGRAM IS FOR SPIKED RB,SR DATA REDUCTION.
C TO RUN IT,2=(DATAFILE),GETTING SAMPLE NAME,WEIGHT,RB
C SPIKE WEIGHT,
C RB85/87,+/-,SR SPIKE WEIGHT,4/6,+/-,7/6,+/-.
C BLANK VALUES HAVE BEEN PUT INTO THE PROGRAM. TO CHANGE
C THEM, JUST
C CORRECT XRB(5),YRB(5),XSR(6),YSR(6),XSR(7),YSR(7).
C RB,SR SPIKE VALUES HAVE BEEN PUT IN THE PROGRAM. TO CHANGE
C THEM, JUST
C CORRECT XRB(I),YRB(I),I=2-4,XSR(J),YSR(J),J=2-5
C WEIGHING ERRORS ARE .0001. SR88/86=8.3752+/- .00001.
C
      DIMENSION XRB(9),YRB(9),ERB(4),SRB(4,9),
1 XSR(12),YSR(12),T(11),F(11),SSR(6,12),ESR(6)
      WRITE(7,10)
      WRITE(8,11)
      WRITE(9,12)
10 FORMAT(//'RB SPIKE CONC(MICMOL/G)=.01069+/- .00007'/
1 '%87=99.2+/- .01, %85=0.803+/- .004'/'RB BLANK=.0000036+/-',
1 '.0000012 MOCROMOLES'//15X,'RBMICMOL/G',4X,'+/-',
1 6X,'RBPPM',5X,'+/-',3X,'RB87MICMOL/G',2X,'+/-',6X,'%BLANK',
1 3X,'RB87/SR86 +/-' )
11 FORMAT(//'SR SPIKE CONC(MICMOL/G)=.01150+/- .00003'/
1 'SR6/4=.00202+/- .00001,8/4=.01244+/- .00012,7/4=.00111+/- .00005'
1 'SR BLANK=.000047+/- .000032 MICROMOLES, 7/6=.7114+/- .0054'//
1 1X,'SRMICMOL/G',4X,'+/-',6X,'SRPPM',6X,'+/-',3X,'SR86MICMOL'
1 ',/G',2X,'+/-',5X,'7/6 NORM',4X,'+/-',2X,'7/6 NORM-BLK',
1 3X,'+/-',5X,'%BLANK',3X,'86/88 MIX',2X,'CONV.CYS')
12 FORMAT(//18X,'RBPPM',6X,'+/-',6X,'%BLANK',4X,'SRPPM',6X,
1 '+/-',5X,'SR87/86',6X,'+/-',5X,'%BLANK',3X,'RB87/SR86 +/-' )
      IC=0
      READ(2,20)CH1,CH2,CH3,XRB(7),XRB(6),XRB(8),YRB(8),XSR(11),
1 XSR(8),YSR(8),XSR(9),YSR(9)
      IF(IC.EQ.0)GOTO 17
20 FORMAT(//A4,1X,A4,1X,A4,F9.5,4F8.5,F10.5,F9.5,2F8.5)
C 20 FORMAT(A4,1X,A4,1X,A4,F9.5,4F8.5,F10.5,F9.5,2F8.5)
15 READ(2,21)CH1,CH2,CH3,XRB(7),XRB(6),XRB(8),YRB(8),XSR(11),
1 XSR(8),YSR(8),XSR(9),YSR(9)
21 FORMAT(A4,1X,A4,1X,A4,F9.5,4F8.5,F10.5,F9.5,2F8.5)
17 WRITE(6,20)CH1,CH2,CH3,XRB(7),XRB(6),XRB(8),YRB(8),XSR(11),
1 XSR(8),YSR(8),XSR(9),YSR(9)
      DATA BLAN/'BLAN'/
      IF(CH2.EQ.BLAN)GOTO 18
      XRB(5)=0.0000036
      YRB(5)=0.0000012
      XSR(6)=0.000047

```

```

        YSR(6)=0.000032
        GOTO 19
18     XRB(5)=0.00000001
        YRB(5)=0.000000005
        XSR(6)=0.0000001
        YSR(6)=0.000000005
19     XSR(7)=0.7114
        YSR(7)=0.0054
C *****SR DATA REDUCTION*****
        XSR(2)=0.0115
        YSR(2)=.00003
        XSR(3)=.00202
        YSR(3)=.00001
        XSR(4)=.01244
        YSR(4)=.00012
        XSR(5)=.00111
        YSR(5)=.00005
        XSR(10)=8.3752
        YSR(10)=.00001
        YSR(11)=.00001
        YSR(12)=.00001
        XSR(12)=XRB(7)
        XSR(12)=XRB(7)
        XSR(1)=0.0
        YSR(1)=0.0
C-----CALCULATION-----
        DO 150 I=1,12
          XSR(I)=XSR(I)+YSR(I)
C.....SPIKE (4+6+8)/(4+6+7+8)
        A=(XSR(3)+XSR(4)+1.0)/(XSR(3)+XSR(4)+XSR(5)+1.0)
        W=A*XSR(2)*XSR(11)
C.....SPIKE 4/(4+6+8)
        A4=1/(XSR(3)+XSR(4)+1)
C.....SPIKE 6/(4+6+8)
        A6=XSR(3)/(XSR(3)+XSR(4)+1)
C.....SPIKE 8/(4+6+8)
        A8=XSR(4)/(XSR(3)+XSR(4)+1)
        R1=XSR(8)
        F(1)=XSR(10)
C-----ITERATION FOR FRACTIONATION-----
        DO 100 J=2,11
C...COMMON SR 4/6=.056584,8/6=8.3752 SO 6/(4+6+8)=0.106024
C.....4/(4+6+8)=.005999,8/(4+6+8)=.887976
C.....SAMP+BLK (4+6+8)
        T(J)=W*(A4-R1*A6)/(R1*0.106024-0.005999)
C.....SAMP+BLK 86
        B6=T(J)*0.106024
C.....SAMP+BLK 88
        B8=T(J)*0.887973
C.....SAMP+BLK 88/86 CAL
        C=B8/B6
C.....SAMP+BLK+SP 88/86 CAL
        R3=(B8+A8*W)/(B6+A6*W)

```

```

C.....SAMP+BLK+SP (88/86)CAL/(88/86)MEAS
  F(J)=R3/XSR(10)
  F2=F(J)-0.5*(F(J)-1.0)
  R1=XSR(8)*(1/F(J))
  R2=XSR(9)*F2
  K=J-1
  IF(ABS(F(J)-F(K)).LT.0.000001) GOTO 110
100 CONTINUE
C-----CALCULATION-----
C.....SSR(L,1)=F(X2,...X12) VALUES WITHOUT ERRORS
C.....SSR(L,2)=F(X2+DX2,...X12) VALUES WITH ERRORS
110 SSR(1,I)=T(J)
C.....6/8 MIX
  IF(I.EQ.1) R4=1/R3
C.....SAMP+BLK+SP 87
  G=R2*(B6+A6*W)
C.....SAMP+BLK 87
  B7=G-XSR(2)*XSR(11)*XSR(5)/(XSR(3)+XSR(4)+XSR(5)+1.0)
C.....SR MICMOL/G
  SSR(2,I)=(T(J)+B7-XSR(6))/XSR(12)
C.....SR PPM (COMMON SR ATMWT=87.62)
  SSR(3,I)=SSR(2,I)*87.62
C.....BLANK 87
  C7=XSR(6)*XSR(7)/(XSR(7)+0.056584+1+8.3752)
C.....BLANK 86
  C6=C7/XSR(7)
C.....SR86 MICMOL/G
  SSR(4,I)=(B6-C6)/XSR(12)
C.....SR87/86
  SSR(5,I)=B7/B6
C.....SR87/86 (-BLK)
  SSR(6,I)=(B7-C7)/(B6-C6)
  XSR(I)=XSR(I)-YSR(I)
150 CONTINUE
C-----ERRORS-----
C.....DELTF=SQRT(SIGMA(DF/DXI*DXI)**2)
C.....DF/DX2*DX2=F(X2+DX2,...X12)-F(X2,...X12)
  DO 170 J=2,6
    ESR(J)=0
    DO 160 I=2,12
      ESR(J)=ESR(J)+(SSR(J,I)-SSR(J,1))**2
160 CONTINUE
    ESR(J)=SQRT(ESR(J))
170 CONTINUE
C-----RESULTS-----
  BLKSR=XSR(6)/(SSR(1,1)+B7)*100
  WRITE(8,180)CH1,CH2,CH3,SSR(2,1),ESR(2),SSR(3,1),ESR(3),
1 SSR(4,1),ESR(4),SSR(5,1),ESR(5),SSR(6,1),ESR(6),BLKSR,
1 R4,K
180 FORMAT(A4,1X,A4,1X,A4/2F10.6,2F10.5,2F10.7,6F10.5,6X,I2)
C ***** RB DATA REDUCTION *****
  XRB(2)=.01069

```

```

YRB(2)=.00007
XRB(3)=99.2
YRB(3)=.01
XRB(4)=.803
YRB(4)=.004
YRB(6)=.0001
YRB(7)=.0001
C.....FRACTIONATION FACTOR

XRB(9)=1.0
YRB(9)=.003
C-----CALCULATION-----
C.....S(J,1)=F(X2,...X9) VALUES WITHOUT ERRORS
C.....S(J,2)=F(X2+DX2,...X9) VALUES WITH ERRORS
XRB(1)=0
YRB(1)=0
DO 50 I=1,9
XRB(I)=XRB(I)+YRB(I)
XRB(8)=XRB(8)*XRB(9)
C.....MMOL RB(SAMP+BLK)
SRB(1,I)=(XRB(3)*XRB(8)-XRB(4))/(72.1654-XRB(8)*27.8346
1)*XRB(2)*XRB(6)
IF(SRB(1,I).LT.0.0) WRITE(6,40)
40 FORMAT('WARNING!! UNDERSPIKED...RB<0')
C.....MMOL/G RB(SAMP)
SRB(2,I)=(SRB(1,I)-XRB(5))/XRB(7)
C.....PPMRB
SRB(3,I)=SRB(2,I)*85.48
C.....RB87 MMOL/G
SRB(4,I)=SRB(2,I)*0.278346
XRB(I)=XRB(I)-YRB(I)
50 CONTINUE
C-----ERRORS-----
C.....DELTF=SQRT(SIGMA(DF/DXI*DXI)**2)
C.....DF/DX2*DX2=F(X2+DX2,...X9)-F(X1,...X9)
DO 70 J=2,4
ERB(J)=0.0
DO 60 I=2,9
ERB(J)=ERB(J)+(SRB(J,I)-SRB(J,1))**2
60 CONTINUE
C.....ERRORS
ERB(J)=SQRT(ERB(J))
70 CONTINUE
C-----RESULTS-----
RBBLK=XRB(5)/SRB(1,1)*100
RBTSR=SRB(4,1)/SSR(4,1)
ERBSR=SQRT(ERB(4)**2/SRB(4,1)**2+ESR(4)**2/SSR(4,1)**2)
1*RBTSR
WRITE(9,200)CH1,CH2,CH3,SRB(3,1),ERB(3),RBBLK,SSR(3,1),
1 ESR(3),SSR(6,1),ESR(6),BLKSR,RBTSR,ERBSR
200 FORMAT(A4,1X,A4,1X,A4,10F10.5)
WRITE(7,80)CH1,CH2,CH3,SRB(2,1),ERB(2),SRB(3,1),ERB(3).

```

```
1 SRB(4,1),ERB(4),RBBLK, RBTSR,ERBSR  
80 FORMAT(A4,1X,A4,1X,A4,2F10.7,2F10.6,2F10.7,3F10.6)  
IF(CH1.NE.END)GOTO 15  
STOP  
END
```

APPENDIX 6-a PROGRAM "YORK"

```

C      REVISED FOR RB-SR ISOCHRONS IN JAN., 1985 BY MIN SUN.
C      B= APPROX. SLOPE,  N = NO. OF POINTS
C      X = 87RB/86SR,  P = 1/SIGMA SQUARED OF X
C      Y = 87SR/86SR,  Q = 1/SIGMA SQUARED OF Y
C      (THUS EACH POINT IS INDIVIDUALLY WEIGHTED ACCORDING TO
C      ITS ACCURACY)
C      FOR PB,
C      WHEN R=1  ALL ERROR IS ASSUMED TO BE IN THE 204
C      MEASUREMENT
C      WHEN R=0 , RANDOM ERRORS ARE ASSUMED : THIS IS EQUIVALENT
C      TO THE OLD LEAST SQUARES CUBIC RESULTS.
C      INTERMEDIATE VALUES OF R ASSIGN ERRORS PROPORTIONALLY
C      BETWEEN THESELIMITS
C      FOR RB-SR, R=0
C.....

      DIMENSIONX(100),Y(100),U(100),V(100),P(100),Q(100),Z(100),
      1R(100),F(100),G(100),ZIP(100),DX(100),DX2(100),ZAP(100),
      2DY2(100),DAX(100),SDAX(100),DAY(100),SDAY(100),RESX(100),
      3C(100),EX(100),EY(100),SANO(100),CH1(100),CH2(100),
      4AL(100),DY(100),RESY(100),CH3(100)
100 WRITE(6,99)
99  FORMAT('INPUT # OF POINTS(I3), TITLE(A12)')
      READ(5,1)N,TITLE1,TITLE2,TITLE3
1   FORMAT(I3,1X,A4,A4,A4)
      IF(N.EQ.0) GOTO 300
      DO 110 I=1, N
      R(I)=0.0
      READ(2,7) CH1(I),CH2(I),CH3(I),Y(I),EY(I),X(I),EX(I)
7   FORMAT(A4,1X,A4,1X,A4,50X,2F10.5,10X,2F10.5)
      P(I)=1/EX(I)**2
      Q(I)=1/EY(I)**2
110 CONTINUE
      B=(Y(N)-Y(1))/(X(N)-X(1))
      EPS=0.0001
      ITMAX=10
      ITER=0
      SLOPE=B
      WRITE(7,50)TITLE1,TITLE2,TITLE3
50  FORMAT(//40X,'YORK REGRESION FOR ',3A4/)
10  B=SLOPE
      WRITE(7,55)B
55  FORMAT(10X,'TRIAL SLOPE=',F10.5)
      ITER=ITER+1
      SUMZ = 0.0
      XBAR = 0.0
      YBAR = 0.0
      BE = 0.0
      D = 0.0
      E = 0.0

```

```

ZU2 = 0.0
SUMT = 0.0
SUMS = 0.0
SUMF = 0.0
SUMG = 0.0
ZIPS = 0.0
DXS = 0.0
ZAPS = 0.0
DYS = 0.0
DBS = 0.0
SZUM = 0.0
SDAXS = 0.0
SDAYS = 0.0
ALPHA = 0.0
DUJB = 0.0
DVJB = 0.0
BETA = 0.0
SUPER=0.0
RENO=0.0
DO 2 I=1,N
AL(I) = SQRT(P(I)*Q(I))
Z(I) = P(I)*Q(I)/(B*B*Q(I)+P(I)-2.0*B*R(I)*AL(I))
2 SUMZ = SUMZ + Z(I)
DO 3 I=1,N
XBAR = XBAR + Z(I)*X(I)/SUMZ
3 YBAR = YBAR + Z(I)*Y(I)/SUMZ
DO 4 I=1,N
U(I) = X(I) - XBAR
V(I) = Y(I) - YBAR
BE = BE + (Z(I)**2)*((U(I)**2)/Q(I) - (V(I)**2)/P(I))
D = D + (Z(I)**2)*(U(I)*V(I)/P(I)-R(I)*(U(I)**2)/AL(I))
ZU2 = ZU2 + Z(I)*U(I)*U(I)
SUMT = SUMT + Z(I)*X(I)*X(I)
F(I)=(Z(I)**2)*V(I)*(U(I)/Q(I)+B*V(I)/P(I)-R(I)*V(I)/AL(I))
G(I)=(Z(I)**2)*U(I)*(U(I)/Q(I)+B*V(I)/P(I)-B*R(I)*U(I)
1/AL(I))
SUMF = SUMF + F(I)
SUMG = SUMG + G(I)
4 E = E + (Z(I)**2)*(U(I)*V(I)/Q(I)-R(I)*(V(I)**2)/AL(I))
SLOPE = (-BE + SQRT(BE**2 + 4.0*D*E))/(2.0*D)
IF(ITER.GT.ITMAX) GOTO 101
IF(ABS(SLOPE-B).GT.ABS(EPS*SLOPE)) GOTO 10
SLOPE2 = SUMF/SUMG
DO 5 I = 1,N
5 SUMS = SUMS + Z(I)*((V(I) - SLOPE*U(I))**2)
CINT = YBAR - SLOPE*XBAR
VARB = 1.0/ZU2
SIGMAB = SQRT(VARB)
VARA = VARB*SUMT/SUMZ
SIGMAA = SQRT(VARA)
DO 80 I = 1,N
ZIP(I) = Z(I)**2*(SLOPE**2*V(I)/P(I)-2.0*(SLOPE**2)*
1R(I)*U(I)/AL(I) + 2.0*SLOPE*U(I)/Q(I) - V(I)/Q(I))

```

```

ZAP(I) = Z(I)**2*(SLOPE**2*U(I)/P(I)-2.0*SLOPE*V(I)
1/P(I)-U(I)/Q(I) + 2.0*R(I)*V(I)/AL(I))
ZIPS = ZIPS + ZIP(I)
ZAPS = ZAPS + ZAP(I)
ALPHA=ALPHA+4.0*(Z(I)**3*(R(I)*AL(I)-SLOPE*Q(I))*
1(SLOPE*U(I)-V(I))
1*(U(I)/Q(I)+SLOPE*V(I)/P(I)-R(I)*(SLOPE*U(I)+V(I))/
2AL(I)))/AL(I)**2
DUJB=DUJB+2.0*Z(I)**2*U(I)*(SLOPE*Q(I)-R(I)*AL(I))/
1(SUMZ*AL(I)**2)
DVJB=DVJB+2.0*Z(I)**2*V(I)*(SLOPE*Q(I)-R(I)*AL(I))/
1(SUMZ*AL(I)**2)
80 DBS = DBS + Z(I)**2*(U(I)**2*(1.0/Q(I)-2.0*SLOPE*R(I)/
1AL(I)+V(I)*(2.0*SLOPE*U(I)-V(I))/P(I))
DO 81 I=1,N
DX(I) = ZIP(I) - Z(I)*ZIPS/SUMZ
DX2(I) = DX(I)**2/P(I)
DXS = DXS + DX2(I)
DY(I) = ZAP(I) - Z(I)*ZAPS/SUMZ
DY2(I) = DY(I)**2/Q(I)
BETA=BETA+Z(I)**2*(DUJB*(SLOPE**2*V(I)/P(I)+2.0*SLOPE*
1U(I)/Q(I)-V
1(I)/Q(I))+DVJB*(SLOPE**2*U(I)/P(I)-2.0*SLOPE*V(I)/P(I)
1-U(I)/Q(I))
2-2.0*R(I)*(SLOPE**2*U(I)*DUJB-V(I)*DVJB)/AL(I))
81 DYS = DYS+DY2(I)
DCS = ALPHA + BETA
DDS = DBS+DCS
DO 82 I = 1,N
82 SZUM = SZUM + Z(I)**2*(R(I)*AL(I)-SLOPE*Q(I))*(V(I)-
1SLOPE*U(I))/(AL(I))**2
DO 83 I = 1,N
DAX(I) = -SLOPE*Z(I)/SUMZ + (2.0*SZUM/SUMZ-XBAR)*(-
1DX(I)/DDS)
SDAX(I) = DAX(I)**2/P(I)
DAY(I) = Z(I)/SUMZ + (2.0*SZUM/SUMZ-XBAR)*(-DY(I)/DDS)
SDAY(I) = DAY(I)**2/Q(I)
SDAXS = SDAXS + SDAX(I)
SDAYS = SDAYS + SDAY(I)
SUPER=SUPER+DX(I)*DY(I)*R(I)/AL(I)
83 RENO=RENO+DAX(I)*DAY(I)*R(I)/AL(I)
ERRAA = SQRT(SDAXS + SDAYS)
ERRAB=(SQRT(DXS+DYS))/DDS
E5=ERRAB*SQRT(SUMS/(N-2))
E6=ERRAA*SQRT(SUMS/(N-2))
DO 84 I=1,N
C(I)=R(I)*AL(I)
RESX(I)=Z(I)*(CINT+SLOPE*X(I)-Y(I))*(C(I)-SLOPE*Q(I))
1/(P(I)*Q(I))
84 RESY(I)=Z(I)*(CINT+SLOPE*X(I)-Y(I))*(P(I)-SLOPE*C(I))/
1(P(I)*Q(I))
TEMP=SUMS/(N-2)
WRITE(7,52)TEMP

```

```

52 FORMAT(78X,6HMSWD= ,F15.8)
   WRITE(7,60)SLOPE2,SLOPE,SIGMAB,ERRAB,E5,CINT,SIGMAA,
   1ERRAA,E6
60 FORMAT(10X,8HSLOPE2= ,F15.8,5X,7HSLOPE= ,F15.8,10X,
   1'EST SIGMA=',F15.8/
   168X,'EXACT SIGMA=',F15.8,' OR',F15.8//10X,'INTERCEPT=',
   1,F15.8,35X
   2,'EST SIGMA=',F15.8/68X,'EXACT SIGMA=',F15.8,' OR',F15.8)
   WRITE(7,56)
56 FORMAT(/15X,'SECOND RESULT APPLIES IF MEAN SQUARE WEIGHTED
   1DEVIATES > 1')
   WRITE(7,70)XBAR,YBAR,ITER
70 FORMAT(/10X,6HXBAR= ,F15.8,5X,6HYBAR= ,F15.8,10X,'ITER=',I5)
   A2=100000*ALOG(1+SLOPE2)/1.42
   IF(TEMP.GT.1.0) ERRAB=E5
   A3=100000*ALOG(1+ERRAB)/1.42
   WRITE(7,71)A2,A3
71 FORMAT(/'Rb-Sr date=',F10.5,'+/-',F10.5,'Ma')
   IF(TEMP.GT.1.0) ERRAA=E6
   WRITE(7,72)CINT,ERRAA
72 FORMAT('INITIAL 87Sr/86Sr=',F10.5,'+/-',F10.5)
   WRITE(7,65)
   WRITE(7,66)(CH1(I),CH2(I),CH3(I),X(I),EX(I),P(I),RESX(I),Y(I),
   1EY(I),Q(I),RESY(I),I=1,N)
65 FORMAT(///17X,'Rb87/Sr86 +/- WEIGHTS RESIDUALS',
   1 ' Sr87/Sr86 +/- WEIGHTS RESIDUALS')
66 FORMAT(A4,1X,A4,1X,A4,2F10.5,E15.5,3F10.5,E15.5,F10.5)
   GO TO 200
101 WRITE(7,95)
95 FORMAT(25X,22HDATA DID NOT CONVERGE.//)
200 GO TO 100
300 STOP
   END

```

APPENDIX 6-b PROGRAM "PLRBSR"

C PROGRAM PLRBSR. WRITTEN BY MIN SUN, 1984.
 C THIS PROGRAM PLOTS RB-SR ISOCHRON BY INPUTTING
 C 2=(OUTPUT 9 OF PROG. "RBSR")

```

    DIMENSION X(3),Y(3)
    K=0
    WRITE(6,10)
10   FORMAT('INPUT #(I2) OF POINTS,MAX OF RB87/SR86,
1   MAX OF SR87/86')
    READ(5,20)NPOINT,RSMAX,SSMAX
20   FORMAT(I2,1X,2F10.5)
    DO 100 I=1,NPOINT
    READ(2,30)A2,B,A1,C
30   FORMAT(64X,2F10.5,10X,2F10.5)
    X(1)=A1-C
    X(2)=A1
    X(3)=A1+C
    Y(1)=A2
    Y(2)=A2
    Y(3)=A2
    CALL POINTS(X,Y,K,RSMAX,SSMAX)
    K=1
    X(1)=A1
    X(2)=A1
    X(3)=A1
    Y(1)=A2-B
    Y(2)=A2
    Y(3)=A2+B
    CALL POINTS(X,Y,K,RSMAX,SSMAX)
100  CONTINUE
13   WRITE(6,11)
11   FORMAT('INPUT INTERCEPT(F15.8) & SLOPE(F15.8), IF NO',
1   'ISOCHRON IS PLOTEd, PUT 0.0,0.0')
    READ(5,12)CINT,SLOPE
12   FORMAT(2F15.8)
    IF(CINT.EQ.0.0)GOTO 120
    X(1)=0.0
    Y(1)=CINT
    X(2)=0.5*RSMAX
    Y(2)=0.5*RSMAX*SLOPE+CINT
    X(3)=RSMAX
    Y(3)=RSMAX*SLOPE+CINT
    CALL POINTS(X,Y,K,RSMAX,SSMAX)
    GOTO 13
120  CALL PLOTND
    STOP
    END

```

```
C *****PLOT POINTS*****
  SUBROUTINE POINTS(X,Y,K,RSMAX,SSMAX)
  DIMENSION X(3),Y(3)
  IF(K.NE.0)GOTO 100
  CALL ALSCAL(0.0,RSMAX,0.700,SSMAX)
  CALL ALSIZE(10.0,10.0)
  CALL ALAXIS('RB87/SR86',9,'SR87/SR86',9)
100 CALL ALGRAF(X,Y,-3,0)
  RETURN
  END
```

APPENDIX 7 DUPLICATED RB-SR DATA

Sample	Rb ppm +/-	Sr ppm +/-	Sr87/86 +/-	Rb87/Sr86 +/-
BM55 BAST	45.5	2.8	1276	33
			0.70258	0.00005
			0.70310	0.00018
average			0.70272	0.00006
BM55 WR	0.332	0.013	12.1	0.05
	0.324	0.003	11.3	0.08
average	0.326	0.010	11.7	0.33
BM55 DIOP			33.3	0.11
	0.142	0.001	33.1	0.10
	0.138	0.001	34.9	0.15
average	0.140	0.001	33.5	0.07
BM55 OLIV	0.070	0.0006	0.229	0.007
	0.069	0.0007	0.260	0.008
	0.071	0.0007	0.291	0.008
average	0.070	0.0004	0.260	0.005
BM55 OPX	0.251	0.002	0.735	0.007
	0.254	0.002	0.762	0.006
	0.254	0.002		
average	0.252	0.001	0.749	0.005
BM11 WR	1.14	0.02	25.2	0.6
	1.12	0.02	25.7	0.1
average	1.13	0.01	25.6	0.2
JL18 WR	0.252	0.002	38.7	0.1
	0.252	0.002	37.0	0.7
average	0.252	0.001	38.5	0.3
JL14 WR	0.181	0.001	8.37	0.08
	0.176	0.001	8.47	0.03
average	0.179	0.001	8.44	0.04
JL14 OLIV	0.094	0.001	0.617	0.008
	0.115	0.001	0.630	0.007
average	0.104	0.001	0.624	0.005
JL1 DIOP			77.1	0.7
	0.125	0.002	76.0	0.5
average			76.5	0.4
JL15 OPX	0.260	0.002	2.76	0.01
			0.70392	0.00231
			0.70524	0.00038
average			0.70505	0.00086
JL15 OLIV	0.084	0.001	0.325	0.007
			0.70791	0.00095
			0.70876	0.00020
average			0.70859	0.00037

LL14 WR	0.774	0.008	9.05	0.07	0.70388	0.00013	0.247	0.003
	0.765	0.007	8.70	0.03	0.70347	0.00010	0.254	0.002
average	0.767	0.008	8.55	0.04	0.70362	0.00010	0.259	0.003
	0.769	0.007	8.77	0.04	0.70366	0.00010	0.254	0.002
LL14 DIOP	0.233	0.002	16.9	0.06	0.70422	0.00029	0.0398	0.0004
					0.70402	0.00015		
average					0.70409	0.00017		
KR35 DIOP	0.278	0.002	55.6	0.2	0.70113	0.00049	0.0144	0.0001
KR35 DIOP					0.70255	0.00017		
average					0.70220	0.00025		
KR35 OLIV	0.101	0.001	0.369	0.008	0.71969	0.00036	0.795	0.0178
	0.099	0.001						
average	0.100	0.001						
KR1 WR	0.385	0.005	4.26	0.03	0.70358	0.00030	0.261	0.004
			4.39	0.03	0.70407	0.00041		
average			4.33	0.03	0.70416	0.00015		
					0.70399	0.00020		
KR2 OPX	0.122	0.001	0.416	0.009	0.71253	0.00175	0.848	0.0196
					0.71228	0.00026		
average					0.71232	0.00059		
JM14 DIOP	0.078	0.001	0.593	0.033	0.70631	0.00117	0.381	0.022
	0.074	0.002	0.571	0.040	0.70577	0.00347	0.376	0.027
average	0.076	0.001	0.582	0.028	0.70628	0.00150	0.379	0.014
JM14 OPX	0.073	0.001	0.825	0.024	0.70609	0.00241	0.257	0.008
					0.70513	0.00050		
average					0.70529	0.00080		
JM2 OPX	0.032	0.0004	0.171	0.008	0.70845	0.00199		
			0.099	0.020				
average	0.032	0.0003	0.119	0.005	0.70903	0.00133	0.784	0.032
	0.032	0.0003	0.130	0.008	0.70874	0.00150		
JM15 OLIV			0.154	0.02				
	0.091	0.0013	0.153	0.01	0.71330	0.00081	1.73	0.16
average			0.153	0.01				
JM15 OPX	0.031	0.001	0.130	0.025			0.683	0.13
	0.028	0.001	0.121	0.015	0.70792	0.00352	0.670	0.087
					0.70564	0.00142		
average	0.029	0.001	0.126	0.015	0.70640	0.00200	0.676	0.082
JM5 DIOP			0.449	0.019	0.70642	0.00247		
	0.056	0.001	0.463	0.010	0.70551	0.00039	0.348	0.012
average			0.456	0.015	0.70563	0.00050		

* -- unspiked run